NASA Tech Briefs

National Aeronautics and Space Administration

February 1987
Volume 11 Number 2

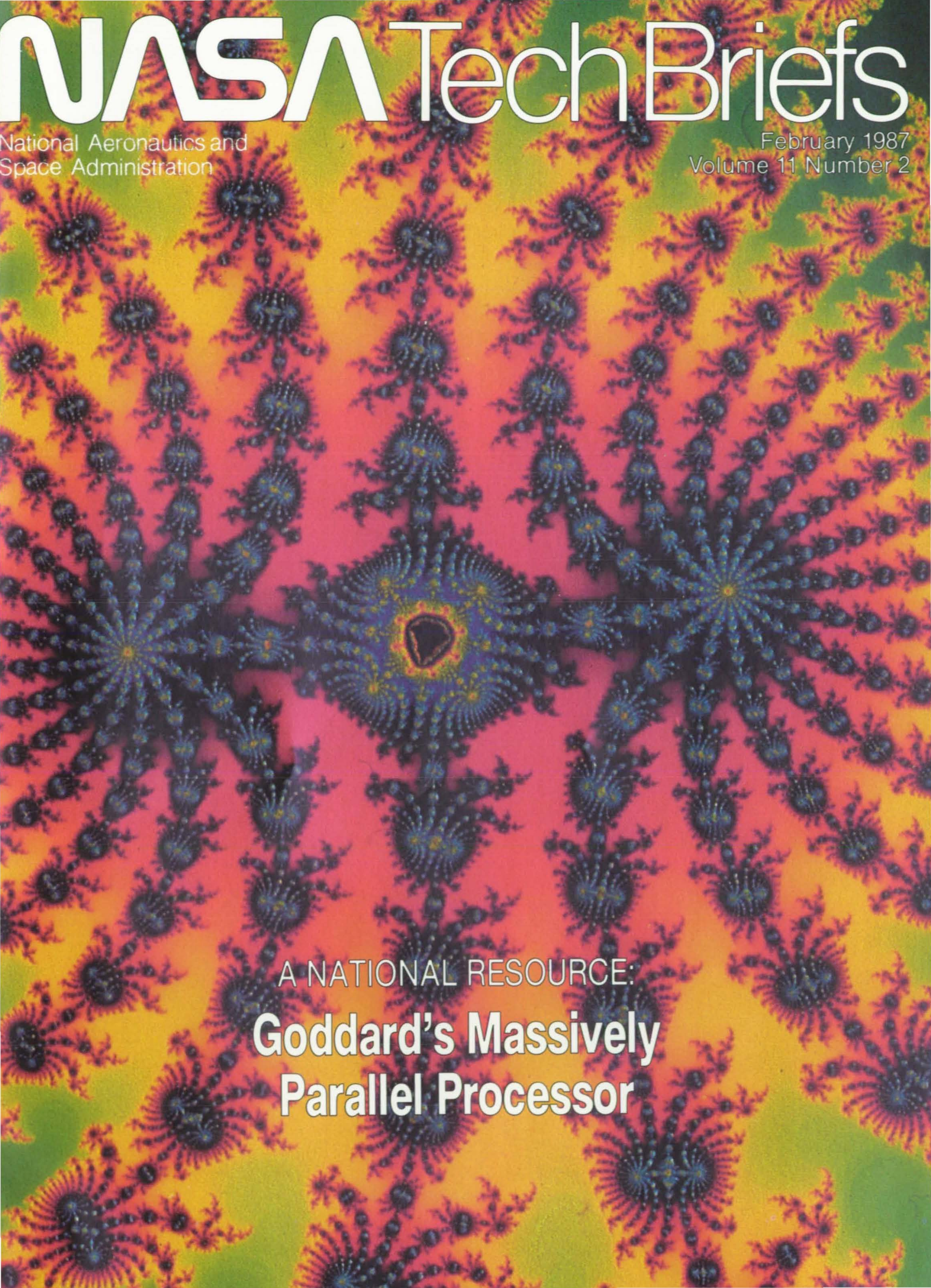

A NATIONAL RESOURCE:

Goddard's Massively Parallel Processor

Artificial intelligence and robotics: giving machines the ability to sense, reason and act.

Much as it may hurt to think so, many things might be done better by independently functioning machines than by humans. Certain tasks may require superhuman precision or speed, or need to be done where humans can't go. Martin Marietta is creating systems that combine the ability to sense, reason and take action — to function autonomously and intelligently. And we are exploring ways to put them to work on a variety of tasks.

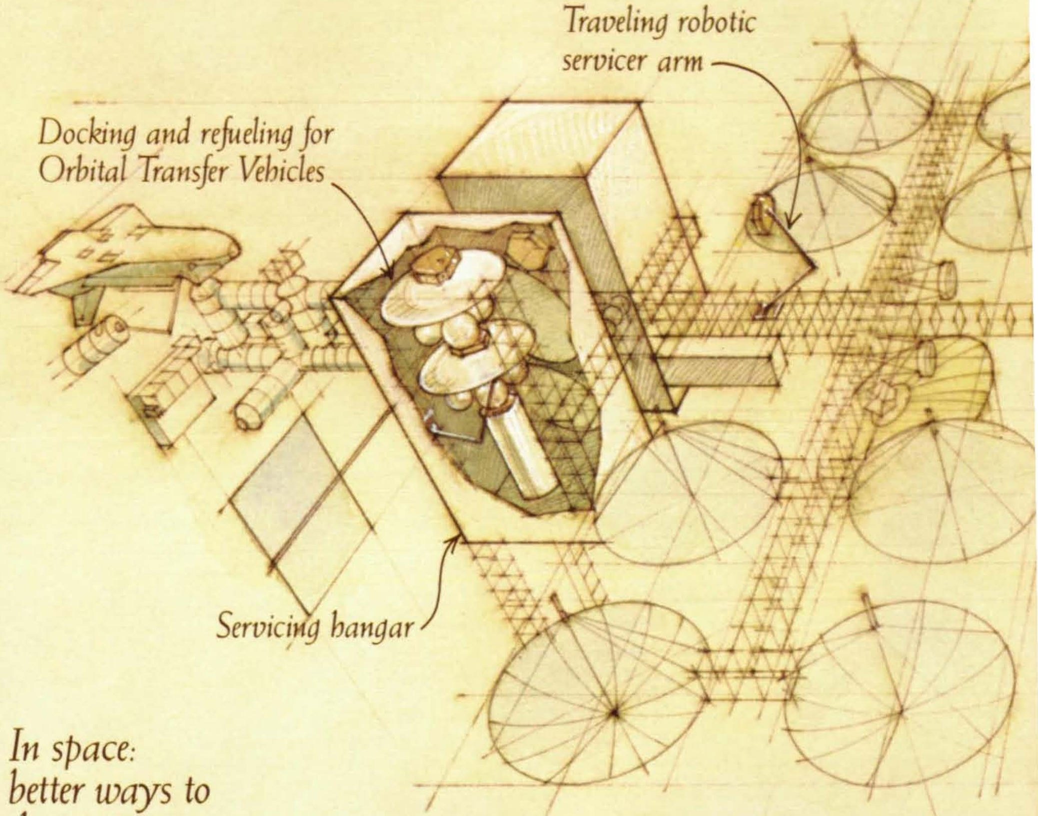

In space: better ways to do servicing.

NASA's manned space station and orbiting satellites will require the use of many robotic devices driven by artificial intelligence.

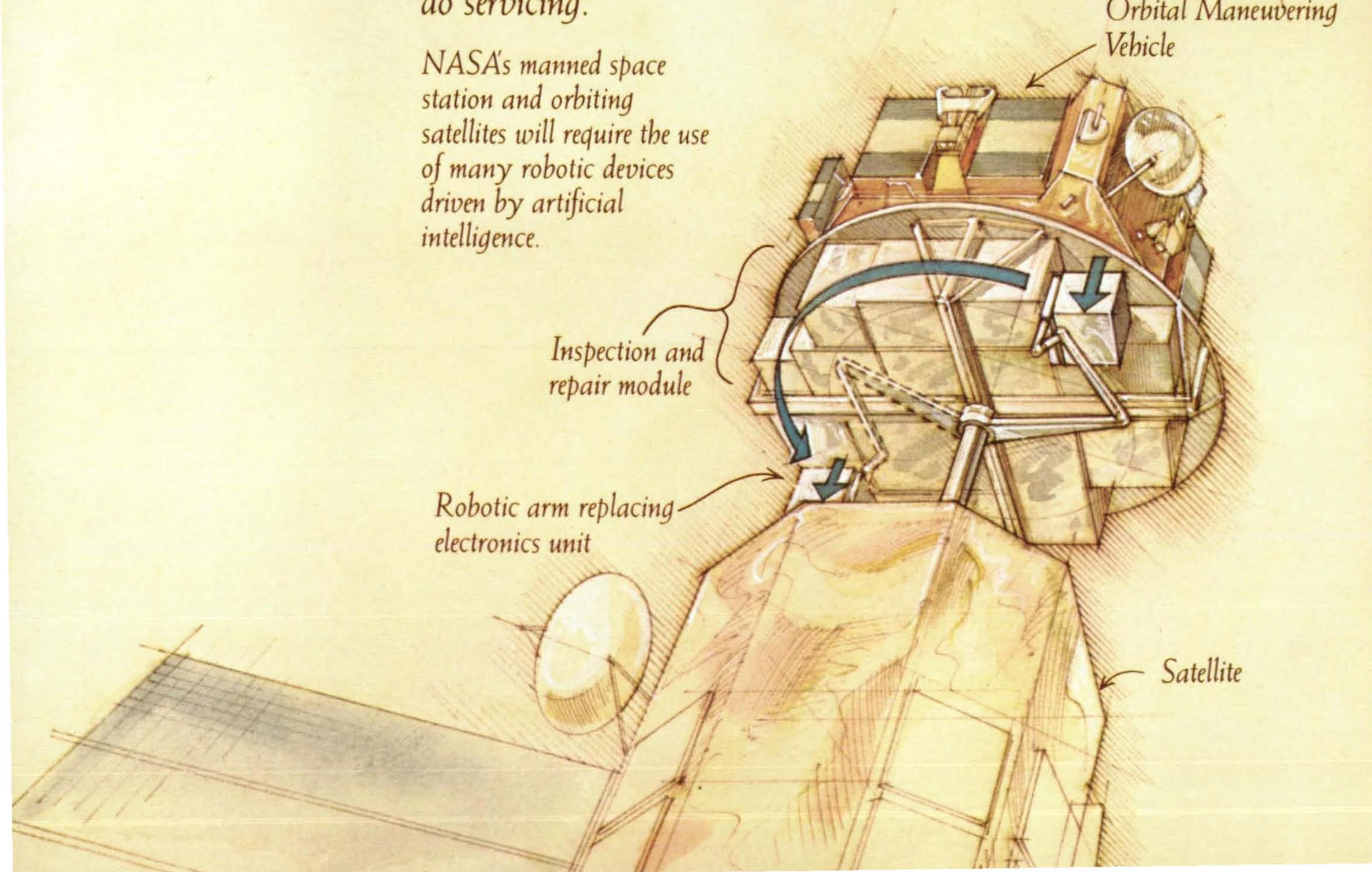

NASA Tech Briefs

National Aeronautics and
Space Administration

FEBRUARY 1987
Volume 11 Number 2

ABP BPA

Special Features and Departments

Goddard's Massively
8.....Parallel Processor

85.....Feedback

85.....Advertiser's Index

84.....Mission Accomplished

86.....About This Publication

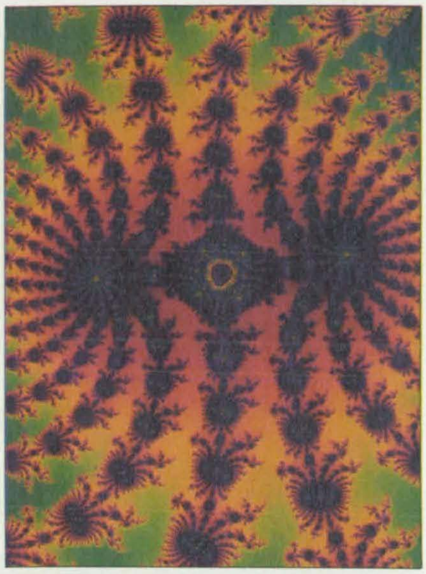

This month's cover shows a 4096 × 4096 pixel region of a Mandelbrot set, generated in 250 seconds of computation time on the Massively Parallel Processor (MPP) at NASA's Goddard Space Flight Center. For more information on the MPP, see page 8.

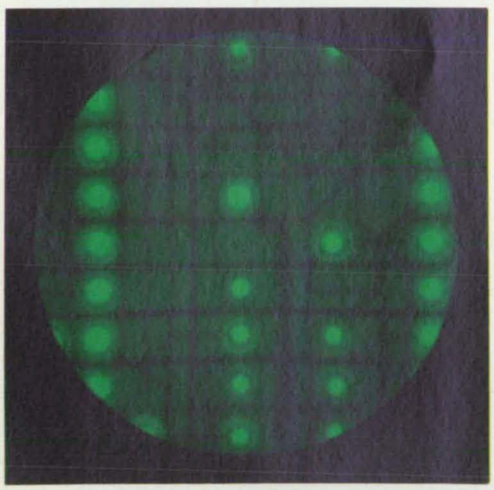

Lixi, Inc.'s x-ray system produced this image of a multi-layer printed circuit board. The 6½ pound handheld system, described in "Mission Accomplished," started out as a Goddard invention for astronomical research.

Technical Section Thumb Index

16......NASA TU Services

12.........New Product Ideas

18... Electronic Components and Circuits

28......Electronic Systems

32......Physical Sciences

40.....Materials

56.....Computer Programs

60....Mechanics

66....Machinery

72....Fabrication Technology

76......Mathematics and Information Sciences

80......Life Sciences

82.........Subject Index

Thumb Index Technical Section

NASA Tech Briefs, ISSN 0145-319X, copyright © 1987 in U.S., is published monthly except July/August and November/December (10x per year) by Associated Business Publications Co., 41 E. 42nd St., New York, NY 10017-5391. The copyrighted information does not include the individual Tech Briefs which are supplied by NASA. Editorial, sales, production and circulation offices at 41 E. 42nd Street, New York, NY 10017-5391. Subscriptions for non-qualified subscribers in the U.S., Panama Canal Zone, and Puerto Rico, $75.00 for 1 year; $125.00 for 2 years; $200 for 3 years. Single copies $15.00. Remit by check, draft, postal or express orders. Other remittances at sender's risk. Address all communications for subscriptions or circulation to NASA Tech Briefs, 41 E. 42nd Street, New York, NY 10017-5391. Application to mail at second-class postage rates is pending at New York, NY 10017 and additional mailing offices.

POSTMASTER: please send address changes to NASA Tech Briefs, 41 E. 42nd Street, Suite 921, New York, NY 10017-5391.

NASA Tech Briefs

National Aeronautics and Space Administration

NASA Tech Briefs:

Published by .... **Associated Business Publications**
Editor-in-Chief/Publisher ..... **Bill Schnirring**
Associate Publisher .... **Frank Nothaft**
Managing Editor .... **R. J. Laer**
Associate Editor .... **Leo Kluger**
Technical Advisor ... **Dr. Robert E. Waterman**
Art Director .... **Melanie Gottlieb**
Associate Art Director ..... **Michelle Schmitz**
Production Manager .... **Rita Nothaft**
Traffic Manager .... **J. T. Pramberger**
Circulation Manager .... **Anita Weissman**
Controller .... **Neil B. Rose**

Technical Staff:

Briefs prepared for National Aeronautics and Space Administration by **Logical Technical Services Corp.**
Technical Editor .... **Ted Selinsky**
Art Director .... **Ernest Gillespie**
Managing Editor .... **Theron Cole, Jr.**
Administrator .... **Elizabeth Texeira**
Chief Copy Editor .... **Joe Renzler**
Staff Editors .... **James Boyd, Larry Grunberger, Jordan Randjelovich, George Watson**
Graphics ..... **Luis Martinez, Huburn Profitt**
Editorial & Production .... **Lorne Bullen, Bill Little, Frank Ponce, Ivonne Valdes**

NASA:

NASA Tech Briefs are provided by the National Aeronautics and Space Administration, Technology Transfer Division, Washington, DC:
Administrator .... **Dr. James C. Fletcher**
Assistant Administrator for Commercial Programs .... **Isaac T. Gillam IV**
Director Technology Utilization Division .... **Henry J. Clarks**
Publications Manager .... **Leonard A. Ault**

Advertising:

New York Office: (212) 490-3999
Sales Manager .... **Robin DuCharme**
Account Executive .... **Dick Soule**
Account Executive .... **Carol-Lynne Cox**
Advertising Assistant .... **Erving Dockery, Jr.**

Los Angeles Office: (213) 477-5866

Associated Business Publications
41 East 42nd Street, Suite 921
New York, NY 10017-5391
(212) 490-3999

President .... **Bill Schnirring**
Executive Vice President ..... **Frank Nothaft**
Vice President .... **John K. Abely**

ABP BPA

Goddard's Massively Parallel Processor

Ten million years ago, light from spiral galaxy M101 started on its journey to our part of the universe. As an orbiting telescopic camera records its faint light, a slightly unstable pointing system blurs the shot, all but eliminating the usefulness of the image. In an earthly lab, the blurred spiral takes shape once again with crystalline clarity.

Elsewhere, a pilot flies his training simulator, surrounded by three-dimensional scenes as realistic and immediate as if he were actually in the air.

Skimming the surface of Mars, an automatic craft unerringly guides itself around a mountain plateau, following geographical contours as if steered by a human hand.

A deaf child struggles to understand others speaking around him—and succeeds. He's aided by a lip-reading computer that simulates his condition.

These solutions are some of the 39 experiments being developed on the Massively Parallel Processor (MPP) at NASA's Goddard Space Flight Center. Called "single instruction stream, multiple data stream (SIMD)," the MPP architecture represents a new class of computer hardware, with the potential for tremendous computing power at low cost. The Massively Parallel Pro-

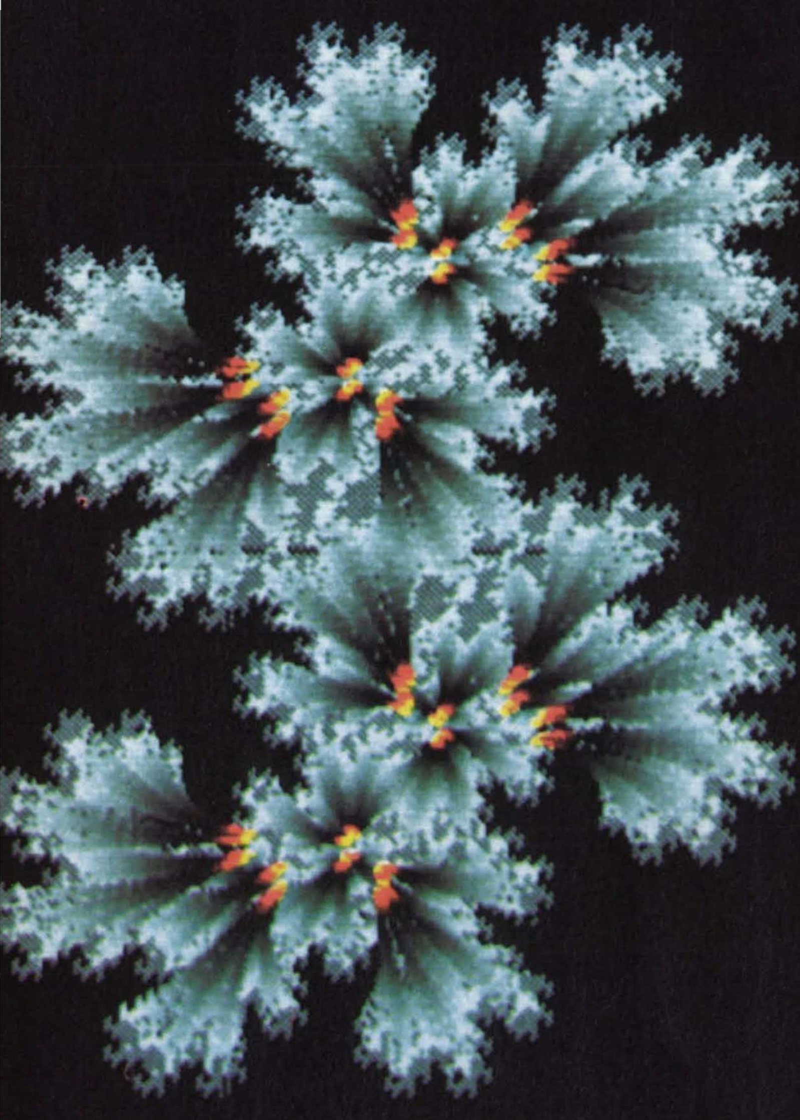

cessor derives its name from its 16384 1-bit parallel processing elements. In an array 128 processors square, each element stores 1024 bits of local random access memory (RAM), and connects to its four nearest neighbors. An array control unit manages the processors, broadcasting instructions every machine cycle.

A staging memory provides additional storage for the MPP. Enhancing the processors' RAM with an additional 32 megabytes of data storage, it reconfigures data, transferring it to and from the array at a rate of 80 megabytes per second. The MPP serves as the back end processor for a Digital Equipment Corporation VAX-11/780 host, which supports program development and peripherals. Though the MPP has a cycle time of 100 nanoseconds, it doesn't need special cooling, as does a Cray, and doesn't require expensive, exotic hardware. "The MPP offers inexpensive megaflops," says James R. Fisher, who heads the Image Analysis Facility at Goddard.

Built for Goddard by the Goodyear Aerospace Corporation, the MPP was originally intended to process the 10^8 bit-per-second data rates from the Landsat satellites. The MPP designers wanted an onboard machine that would have a digital processor for every point on a satellite image, with all data points input in parallel through a large, high bandwidth, analog to digital converter. "This was quite visionary in the early seventies," mentions Fisher.

New Ways of Looking at Things

A parallel approach to designing computer hardware becomes increasingly relevant as physical laws limit the speed serial computers can reach. A user can reap a number of benefits from the MPP after adopting this approach. "It's a matter of how imaginative you can be," says John Dorband, a Goddard computer scientist. "Programming the MPP is slightly different, as you learn how to divide your problem up. The nice thing about this is that if a researcher takes the time to utilize a problem's inherent parallelism, he ends up with a more elegant algorithm, one that runs better on serial machines as well."

On the far left, the "dragon curve" graphic shows superimposed solutions to a linear complex equation, with the coefficient changing 19 times in stepwise fashion. Goddard's Massively Parallel Processor simultaneously calculated 16,384 points for each solution. The MPP generated the scene on the right from a limited amount of information. Initial squares, defined only by their corners, were subdivided into four smaller patches, using random elements to interpolate the center detail. Seven repetitions on increasingly smaller squares gave pixel-level definition.

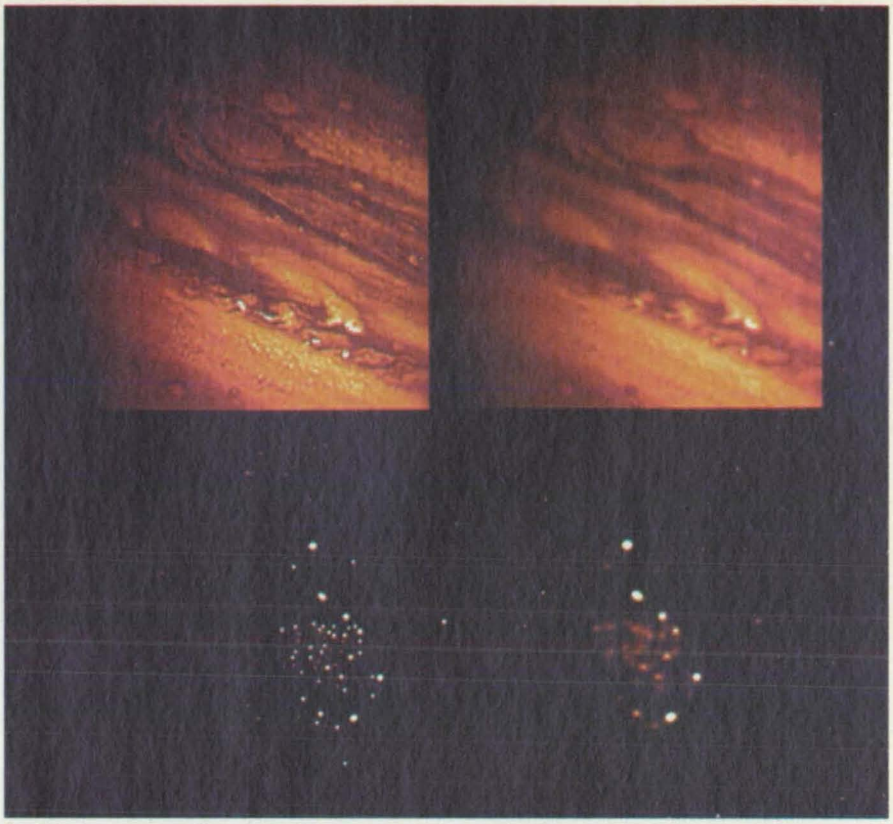

MPP image restoration techniques correct blurred images on the right to the improved ones on the left. Jupiter and spiral galaxy M101 are shown here.

The Mouse That Roared

The computer's power comes from a deceptively simple technique: a high number of processors work in concert on simple tasks, one step at a time. As the large number of processor's are connected to each other, the MPP structure emulates one theory of how the human brain works, with a large network of neurons connected by synapses. This similarity makes the MPP an ideal experimental tool for programs based on the "neural net" concept. Researchers based at Johns Hopkins University are taking advantage of this similarity to help the deaf understand others. By using a computer to realistically model a deaf person, the scientists at Johns Hopkins can investigate different ways to enhance communication.

Neural nets are able to reconfigure themselves in response to input, in effect, learning from stimuli. The stimuli used at Hopkins takes two forms: a laser-disk video recording of talking heads, centering on the lips, and audio input of what the lips are saying. Given the correct algorithms, the MPP will become a working example of HAL, the lip-reading computer in *2001, A Space Odyssey*.

When the MPP can read lips with accuracy, it will be weaned from the complementary audio input. "Eventually we'll be able to give it an image and ask: 'what sound is being produced?' and it should be able to produce it," explains Ben Yuhas, one of the researchers working on the project. At that point, the computer will be ready to act as a model for a deaf person. The Hopkins researchers will experiment with the model, trying different segments of speech that a deaf person could conceivably detect, such as pitch variation converted into a tactile stimulus. "Once we've built up the model, we want to find out what will help the deaf the most. The neural net seems to be the most powerful artificial intelligence tool applied to the problem," Yuhas adds.

Scanning the Scene

In Washington state, Dr. Y. Paul Chiang will use the Massively Parallel Processor to recognize familiar patterns. Chiang's algorithm will convert Landsat images into character strings, analyzing a scene at a time. In typical image analysis applications, the computer would need to search through a tremendous amount of data to find desired surface features such as highways or airports. The MPP will compare the entire scene against its library, looking for juxtipositions. Matchups occur when the processor recognizes a character string. Chiang explains the benefit of the MPP for this application: "If you have a sequential type operation, you have to go over the whole frame, piece by piece. With the ►

MPP, you're looking at entire 128 by 128 windows simultaneously." This significantly decreases the time needed for pattern recognition, paving the way for real-time robotic control.

At the other end of the U.S., Edward W. Davis, at North Carolina State University, works on a different type of graphics application. Davis plans to use the MPP's immense computational ability to realistically simulate topography. When completed, his project will allow real-time interactions such as panning over or zooming into a scene. For example, walking around a simulated mountain will show a continually changing, realistic geography, no propped-up Hollywood fronts. Such realism would vastly improve flight simulators, giving a three-dimensional reality to the cockpit. Natural and man-made features would combine to accurately portray a flight—while staying on the ground. This application calls for nonconventional computing power. "We're concerned with manipulating an image of thousands of pixels, so we would like to take advantage of the low-level parallelism inherent in the MPP," Davis explains. "Our initial results are pretty favorable," he adds.

Reconstructing astronomical images occupies much of Don Lindler and Sara Heap's time at Goddard's Laboratory for Astronomy and Solar Physics. They use the MPP to calculate algebraic solutions to a problem that confounds many a sky-watcher: blurred or distorted images. Heap and Lindler use a point spread function to solve the problem. Comparing a star's appearance on the image to its known value yields the point spread function, which can be applied to every part of the image. The entire picture can be mathematically refocussed, but it's not always easy.

Typical blurred images, 500 pixels square, if solved directly, would require solving 250,000 equations with 250,000 variables each. Even with the most powerful computers available, a direct solution to a problem of this magnitude would be all but impossible. By using a block iterative approach—dividing the 500 pixel image into slightly overlapping regions of 11 pixels by 11 pixels and restoring them separately—the problem reduces to 4900 sets of 121 equations, each with 121 variables. The MPP easily meets this challenge, taking a mere 11 minutes per frame. This compares favorably to the estimated 72 hours a VAX 11/750 would require for the same problem. Each pixel has a new value once the equations are solved. The small blocks are then reconstructed into a clearer and sharper full-sized image.

A National Resource

The MPP is now available for U.S. researchers to test and implement their computational algorithms. "We emphasize both those areas of direct application to disciplines NASA supports, and also the fallout that benefits other disciplines," says Milton Halem, Chief of Goddard's Space Data and Computing Division.

Though originally designed for Landsat data interpretation, Goddard's Massively Parallel Processor serves well in alternative applications. Through a variety of diverse projects underway across the U.S., the MPP proves its worth as a versatile tool for scientific applications. As Ed Davis observes, "There are not many resources like the MPP that we have available for our research. I'm glad that NASA opened access to it for our working group." □

To obtain an Applications Notice Book for Goddard's Massively Parallel Processor, contact the MPP User Support Office, Code 635, NASA/Goddard Space Flight Center, Greenbelt, MD, 20771, (301) 286-9412. For a description of a proposed "front end" for the MPP, one that digitizes x-ray sensor data in a satellite, see NASA Tech Brief GSC-12898, appearing on page 28 in this issue.


Brave New Vision In PC/AT-Based Imaging Systems.
For the Indian brave, each dab of paint was a plea for power, vision and greater understanding. In your quest for greater understanding, each keystroke taps the vast PC/AT-based image processing power of VisionLab II, from Comtal/3M.
VisionLab II is the perfect synthesis of processing power and system economy. It provides real time, flicker-free, true color computer imaging that outperforms many minicomputer and mainframe-based systems — at a fraction of the cost.
The unique dual bus architecture of VisionLab II boosts processing speed, so you can continuously zoom, minify and roam, analyze, edit, alter contrast and more in real time. Even with true color images.
And you do all this with a user-friendly, inexpensive IBM PC AT* or 100% compatible, which makes VisionLab II the ideal image processing workstation for a wide array of aerospace, military, earth science, medical and research applications.
VisionLab II — just the kind of brave new vision you would expect from Comtal/3M. We've scouted the frontier of computer imaging technology since the dawn of the industry.
VisionLab II
Expanding the Powers of Perception
Comtal/3M
For information call today: (800) 423-4166
Circle Reader Action No. 319
*IBM PC AT is a registered trademark of International Business Machines Corporation.
3M

New Product Ideas

New Product Ideas are just a few of the many innovations described in this issue of *NASA Tech Briefs* and having promising commercial applications. Each is discussed further on the referenced page in the appropriate section in this issue. If you are interested in developing a product from these or other NASA innovations, you can receive further technical information by requesting the TSP referenced at the end of the full-length article or by writing the Technology Utilization Office of the sponsoring NASA center (see page 17). NASA's patent-licensing program to encourage commercial development is described on page 17.

Sliding Capacitive Displacement Transducer

A sliding capacitive displacement transducer, the capacitance of which varies linearly with displacement, enables the use of a simple circuit based on an operational amplifier instead of a more complicated capacitance bridge. With the new circuit, transducers as small as 0.05 in. (1.3 mm) square and 0.004 in. (0.1 mm) thick have produced output-voltage changes of about 200 mV per 0.005 in. (0.13 mm) of displacement. Displacement measurements repeatable to 1 percent have been achieved. The output is insensitive to the capacitances of the connecting cables.
(See page 20).

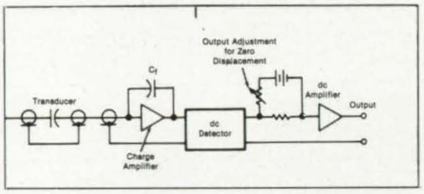

Spring-Loaded Inscribing Tool

A spring-loaded, roller-type inscribing tool marks flat or nearly flat panels. Devised to apply grid lines to gore panels, the tool can also be used to mark plastics, soft metals, and the like under numerical or manual control or can be used manually in applications that do not require precision. Because the inscribing roller is spring loaded, it follows the surface variations on the workpiece. Consequently, the workpiece does not have to be clamped extremely flat.
(See page 74).

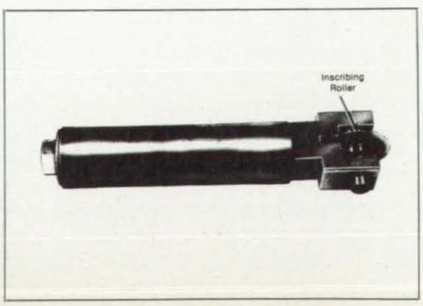

Portable, Controlled-Load-Rate Tension Tester

A tensile-testing machine for ceramic and foam materials has a self-contained air supply with a built-in-airflow controller. The prechargeable cylinder chambers make it unnecessary to attach the machine to an air line. The machine is therefore mobile and more convenient for users. The exhaust-speed control unit ensures a consistent loading rate. The control unit also prevents the piston from flying upward when a specimen breaks. The machine can be adapted to compression testing by attaching the exhaust-control valve to the bottom cylinder instead of the top.
(See page 60).

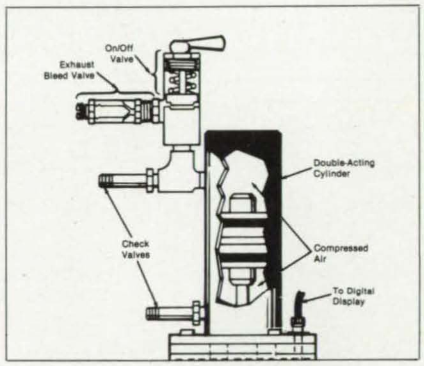

A Surface-Controlled Solar Cell

A proposed technique for controlling the recombination velocity on solar-cell surfaces could provide cells of increased efficiency and open-circuit voltage. In a

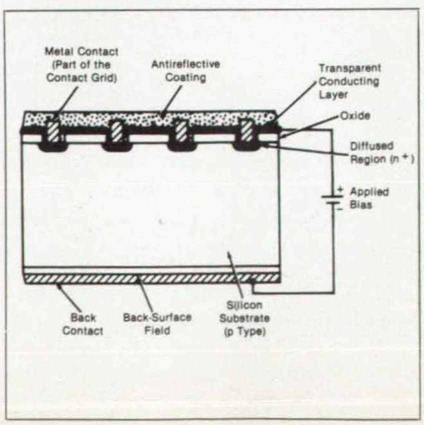

TEK MICROCIRCUITS

The QuickCustom™ approach to bipolar ICs.

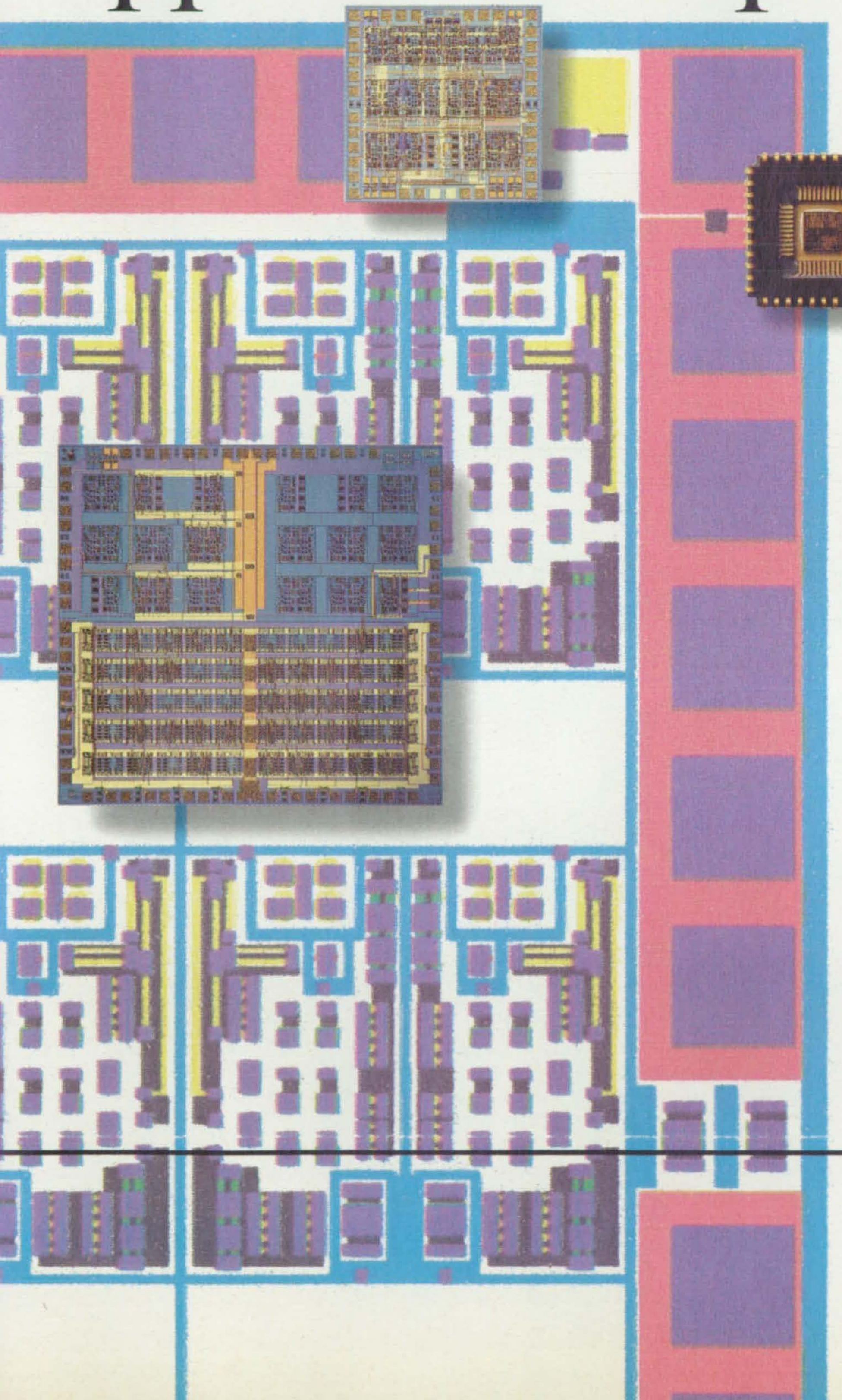

Now, it's all yours.

Tektronix has developed a way to design semi-custom analog ICs that will greatly reduce your development time and cost.

The QuickCustom approach uses a series of QuickChips™ prefabricated with "core" arrays of capacitors, resistors and up to 1800 transistors configured for easy interconnection. Analog QuickChip designs use NPN transistors with f_T typical to 6.5 GHz at 15V or 2.5 GHz at 95V. Analog-digital combination QuickChip arrays offer a gate propagation delay of 400 ps with digital functions including OR/NOR/AND/NAND, flip-flops, latches, buffers and inverters.

We'll provide the training, graphic layout and simulation tools for your design, and one of our experienced IC designers will be available to consult with you.

Following design approval, we'll deliver two untested wafers within three weeks. Guaranteed. Or, 25 untested packaged parts within four weeks.

This is the fastest semi-custom process in the industry. And it's dedicated to meeting your exact ASIC requirements at a reasonable price. So, if you're interested in turning Tektronix' unsurpassed IC advantage into yours, call us. We're ready to talk with you about your semi-custom and full custom needs.

Tektronix Integrated Circuits Operation
P.O. Box 500, M/S 59-420
Beaverton, OR 97077
Phone: 800-262-4374
503-627-2515 within Oregon or for technical assistance.

Tektronix®
COMMITTED TO EXCELLENCE

Circle Reader Action No. 468

cell using the proposed technique, a transparent conducting layer, insulated from the cell contacts, would be biased to enable the variable control of the surface recombination velocities. By the application of a suitable voltage with very little power consumption, the surface can be put in the enhancement mode to repel the minority carriers from the surface. This should enhance carrier collection at the junctions and increase the open-circuit voltage and the efficiency of the solar cell.
(See page 22).

More Efficient Solar Thermal-Energy Receiver

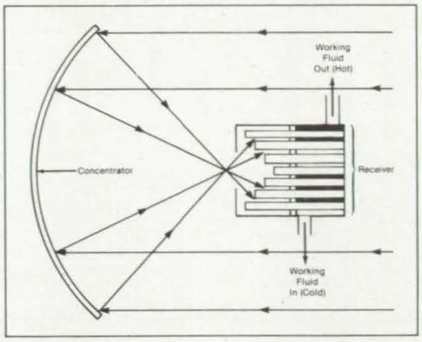

An improved design for a solar thermal-energy receiver features two chambers: a radiation section and a storage section. The radiation section receives the solar energy from the concentrator. The boiling ends of numerous heat pipes thermally connect the radiation section with the heat-storage section. The condensing end of each heat pipe delivers heat to the thermal energy-storage material (TSM), which is located coaxially around the heat pipes. Heat is passed through the TSM to the outer walls of the TSM container and into the working fluid. The improved design minimizes reflection losses, reradiation losses, and thermal stresses in the TSM.
(See page 37).

Electronic Power Switch for Fault-Tolerant Networks

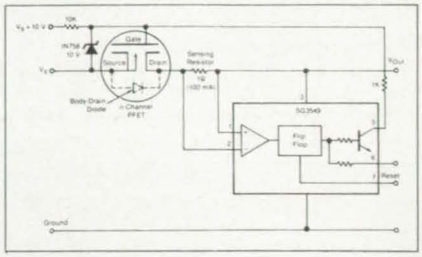

A current switch containing a power field-effect transistor (PFET) is placed in series with each load in a fault-tolerant power-distribution system. PFET's reduce energy waste and simplify interconnections. If the system includes several loads and supplies, the switches are placed in series with adjacent loads and supplies. The system of switches protects against overloads and losses of individual power sources.
(See page 18).

Polyimide Prepregs With Improved Tack

In a recent study, PMR-15 (or equivalent) resin compositions, designated "PMR-15IT," were identified that provide improved tack and drape retention for graphite-fiber/PMR-15 (or equivalent) prepreg materials without adversely affecting processability or composite mechanical properties. The improved tack system identified to provide the best overall processability, along with excellent composite properties, was obtained by utilizing methyl ester monomers and a solvent containing methanol/1-propanol in a 3:1 weight ratio. Graphite-fiber/PMR-15 (or equivalent) prepreg prepared from the above PMR-15IT resin and exposed to ambient conditions exhibits excellent tack retention for at least 10 days — approximately four times longer than current-technology PMR-15 (or equivalent) prepreg exposed under the same conditions.
(See page 40).

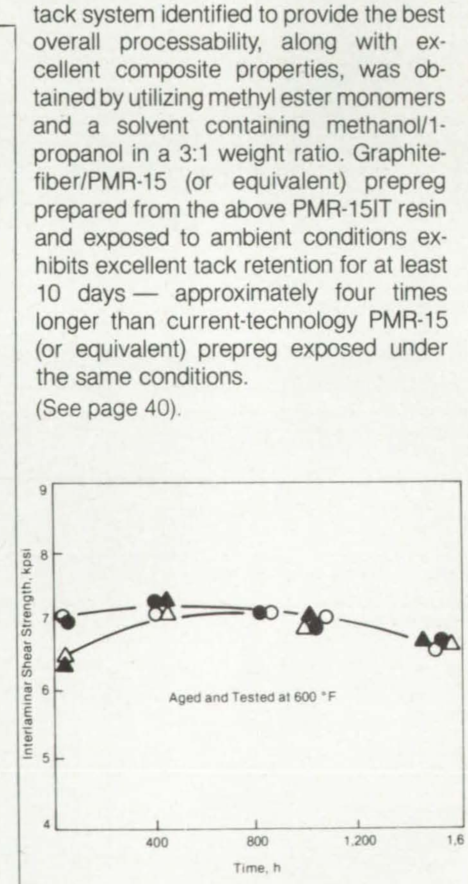

HOW YOU CAN BENEFIT FROM NASA's TECHNOLOGY UTILIZATION SERVICES

If you're a regular reader of TECH BRIEFS, then you're already making use of one of the low- and no-cost services provided by NASA's Technology Utilization (TU) Network. But a TECH BRIEFS subscription represents only a fraction of the technical information and applications/engineering services offered by the TU Network as a whole. In fact, when all of the components of NASA's Technology Utilization Network are considered, TECH BRIEFS represents the proverbial tip of the iceberg.

On the following pages, we've outlined NASA's TU Network—named the participants, described their services, and listed the individuals you can contact for more information relating to your specific needs. We encourage you to make use of the information, access, and applications services offered by NASA's Technology Utilization Network. You can save time and money by doing so.

HOW YOU CAN UTILIZE NASA'S

Industrial Applications Centers

A nationwide network offering a broad range of technical services, including computerized access to over 100 million documents worldwide.

You can contact NASA's network of Industrial Applications Centers (IACs) for assistance in solving a specific technical problem or meeting your information needs. The "user friendly" IACs are staffed by technology transfer experts who provide computerized information retrieval from one of the world's largest banks of technical data. Nearly 500 computerized data bases, ranging from NASA's own data base to Chemical Abstracts and INSPEC, are accessible through the nine IACs, which are located throughout the nation. The IACs also offer technical consultation services and/or linkage with other experts in the field.

You can obtain more information about these services by calling or writing the nearest IAC. User fees are charged for IAC information services.

Aerospace Research Applications Center (ARAC)
Indianapolis Center for Advanced Research
611 N. Capitol Avenue
Indianapolis, IN 46204
Dr. F. Timothy Janis, Director
(317) 262-5003

Kerr Industrial Applications Center (KIAC)
Southeastern Oklahoma State University
Station A, Box 2584
Durant, OK 74701
Tom J. McRorey, Director
(405) 924-6822

NASA Industrial Applications Center
823 William Pitt Union
University of Pittsburgh
Pittsburgh, PA 15260
Paul A. McWilliams, Executive Director
(412) 648-7000

NASA/Southern Technology Applications Center
State University System of Florida
307 Weil Hall
Gainesville, FL 32611
J. Ronald Thornton, Director
(904) 392-6760

NASA/UK Technology Applications Center
University of Kentucky
109 Kinkead Hall
Lexington, KY 40506-0057
William R. Strong, Director
(606) 257-6322

NERAC, Inc.
Mansfield Professional Park
Storrs, CT 06268
Daniel U. Wilde, President
(203) 429-3000

North Carolina Science and Technology Research Center (NC/STRC)
Post Office Box 12235
Research Triangle Park, NC 27709
J. Graves Vann, Jr., Director
(919) 549-0671

Technology Application Center (TAC)
University of New Mexico
Albuquerque, NM 87131
Stanley A. Morain, Director
(505) 277-3622

NASA Industrial Applications Center (WESRAC)
University of Southern California
Research Annex
3716 South Hope Street
Room 200
Los Angeles, CA 90007
Radford G. King, Acting Director
(213) 743-6132
(800) 642-2872 (CA only)
(800) 872-7477 (toll-free US)

If you represent a public sector organization with a particular need, you can contact NASA's Application Team for technology matching and problem solving assistance. Staffed by professional engineers from a variety of disciplines, the Application Team works with public sector organizations to identify and solve critical problems with existing NASA technology.

Technology Application Team
Research Triangle Institute
P.O. Box 12194
Research Triangle Park, NC 27709
Doris Rouse, Director
(919) 541-6980

A SHORTCUT TO SOFTWARE:

COSMIC®

An economical source of computer programs developed by NASA & other gov't. agencies.

Software developed by the U.S. government may be applicable to your needs. To tap this valuable resource, contact COSMIC, NASA's Computer Software Management and Information Center. Approximately 1400 computer programs and related documentation comprise the current library. New and updated programs are announced regularly in NASA Tech Briefs' Computer Programs section, and COSMIC publishes an annual software catalog.

More information about COSMIC's services can be obtained by calling or writing:

COSMIC®
Computer Services Annex
University of Georgia
Athens, GA 30602
John A. Gibson, Director
(404) 542-3265

HOW YOU CAN ACCESS TECHNOLOGY TRANSFER SERVICES AT NASA FIELD CENTERS:

Technology Utilization Officers & Patent Counsels

Each NASA Field Center has designated a Technology Utilization Officer and a Patent Counsel to facilitate technology transfer between NASA and the private sector.

If you need further information about new technologies presented in NASA Tech Briefs, you should request the Technical Support Package (TSP) that accompanies the brief. In the event that a TSP is not available, you can contact the Technology Utilization Officer at the NASA Field Center that sponsored the research. He can arrange for expert assistance in applying the technology by putting you in touch with the people who developed it.

If you want additional information about the patent status of a particular technology or are interested in licensing a NASA invention, contact the Patent Counsel at the NASA Field Center that sponsored the research. Be sure to refer to the NASA reference number at the end of the tech brief.

Ames Research Center
Technology Utilization Officer:
Laurance A. Milov
Mail Code 204-10
Moffett Field, CA 94035
(415) 694-5761
Patent Counsel:
Darrell G. Brekke
Mail Code 200-11
Moffett Field, CA 94035
(415) 694-5104

Goddard Space Flight Center
Technology Utilization Officer:
Donald S. Friedman
Mail Code 702-1
Greenbelt, MD 20771
(301) 286-6242
Patent Counsel:
John O. Tresansky
Mail Code 204
Greenbelt, MD 20771
(301) 286-7351

Lyndon B. Johnson Space Center
Technology Utilization Officer:
Dean C. Glenn
Mail Code EA4
Houston, TX 77058
(713) 483-3809
Patent Counsel:
Edward K. Fein
Mail Code AL3
Houston, TX 77058
(713) 483-4871

John F. Kennedy Space Center
Technology Utilization Officer:
Thomas M. Hammond
Mail Stop PT-TPO-A
Kennedy Space Center, FL 32899
(305) 867-3017
Patent Counsel:
James O. Harrell
Mail Code PT-PAT
Kennedy Space Center, FL 32899
(305) 867-2544

Langley Research Center
Technology Utilization Officer:
John Samos
Mail Stop 139A
Hampton, VA 23665
(804) 865-3281
Patent Counsel:
Howard J. Osborn
Mail Code 279
Hampton, VA 23665
(804) 865-3725

Lewis Research Center
Technology Utilization Officer:
Daniel G. Soltis
Mail Stop 7-3
21000 Brookpark Road
Cleveland, OH 44135
(216) 433-5567
Patent Counsel:
Gene E. Shook
Mail Code 60-2
21000 Brookpark Road
Cleveland, OH 44135
(216) 433-5753

Jet Propulsion Laboratory
Technology Utilization Manager:
Norman L. Chalfin
Mail Stop 201-110
4800 Oak Grove Drive
Pasadena, CA 91109
(818) 354-2240

NASA Resident Office-JPL
Technology Utilization Officer:
Gordon S. Chapman
Mail Stop 180-801
4800 Oak Grove Drive
Pasadena, CA 91109
(818) 354-4849
Patent Counsel:
Paul F. McCaul
Mail Code 180-801
4800 Oak Grove Drive
Pasadena, CA 91109
(818) 354-2734

George C. Marshall Space Flight Center
Technology Utilization Officer:
Ismail Akbay
Code AT01
Marshall Space Flight Center, AL 35812
(205) 544-2223
Patent Counsel:
Leon D. Wofford, Jr.
Mail Code CC01
Marshall Space Flight Center, AL 35812
(205) 544-0024

National Space Technology Laboratories
Technology Utilization Officer:
Robert M. Barlow
Code GA-10
NSTL Station, MS 39529
(601) 688-1929

NASA Headquarters
Technology Utilization Officer:
Leonard A. Ault
Code IU
Washington, DC 20546
(202) 453-1920
Assistant General Counsel for Patent Matters: Robert F. Kempf
Code GP
Washington, DC 20546
(202) 453-2424

IF YOU HAVE A QUESTION . . .

NASA Scientific & Technical Information Facility

If you have a general or specific question about NASA's Technology Utilization Network or its services and documents, you can contact the STI facility for assistance. The STI staff can answer your questions, supply documents and provide referrals to meet your needs. You can use the feedback card in this issue to contact STI directly.

NASA Scientific and Technical Information Facility

Technology Utilization Office
P.O. Box 8757
BWI Airport, MD 21240
Walter M. Heiland, Manager
(301) 859-5300, Ext. 242, 243

Electronic Components & Circuits

Hardware, Techniques, and Processes

18 Electronic Power Switch for Fault-Tolerant Networks
20 Sliding Capacitive Displacement Transducer
22 A Surface-Controlled Solar Cell
22 Monolithic Isolated Single-Mode Ring Laser
24 Calculating Effects of Reflector-Antenna Distortions
27 Controller for Fast-Acting Furnaces

Electronic Power Switch for Fault-Tolerant Networks

Power field-effect transistors reduce energy waste and simplify interconnections.

Lyndon B. Johnson Space Center, Houston, Texas

A current switch containing a power field-effect transistor (PFET) is placed in series with each load in a fault-tolerant power-distribution system. If the system includes several loads and supplies, switches are placed in series with adjacent loads and supplies (see figure). The system of switches protects against overloads and losses of individual power sources.

If a power supply fails, current flows to the affected loads through the switches that connect them to the remaining power supplies. On the other hand, when a sensor associated with each PFET measures excessive current drain (senses an overload), the switch automatically disconnects the load from the supply. If the load is receiving power from more than one supply, the switches to all connecting

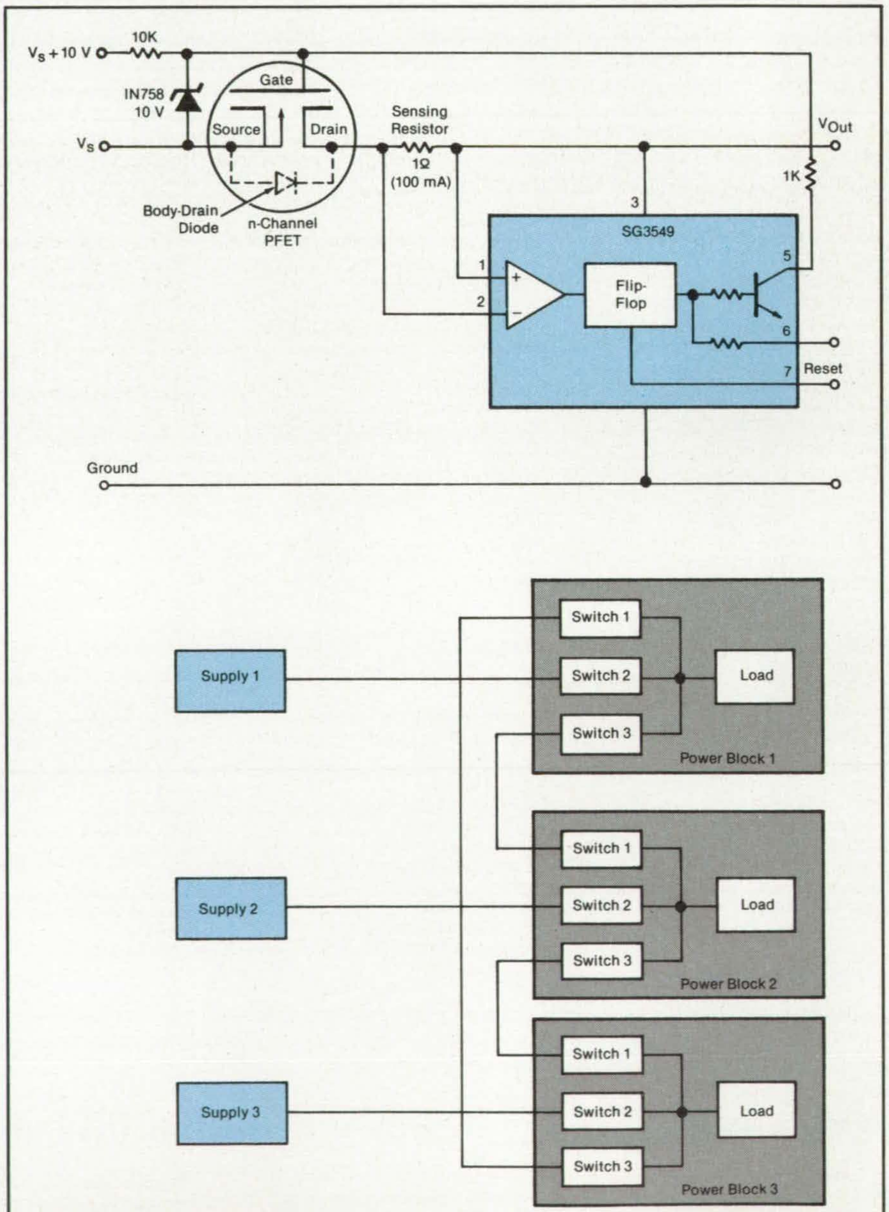

A **Current Switch Is Formed** by a power field-effect transistor and a current sensor. For three power supplies and three loads in a fault-tolerant system, three switches are placed in each power block.

supplies will turn off if all the currents to that load are excessive. Thus, current is automatically routed around a fault.

When power is initially applied to a power block through its current switch, current passes through the body-drain diode of the PFET. When the load comes up to power, the PFET is turned on. The voltage across it drops to a low value, which reduces the waste of power.

This work was done by Jeffrey Volp of The Charles Stark Draper Laboratory, Inc. for **Johnson Space Center**. *For further information, Circle 5 on the TSP Request Card.*

In accordance with Public Law 96-517, the contractor has elected to retain title to this invention. Inquiries concerning rights for its commercial use should be addressed to:

The Charles Stark Draper Laboratory, Inc.
555 Technology Square
Cambridge, MA 02139

Refer to MSC-20874, volume and number of this NASA Tech Briefs issue, and the page number.

Sliding Capacitive Displacement Transducer

A simple circuit replaces a bridge circuit.

Marshall Space Flight Center, Alabama

A sliding capacitive displacement transducer, the capacitance of which varies linearly with displacement, enables the use of a simple circuit based on an operational amplifier instead of a more complicated capacitance bridge. With the new circuit, transducers as small as 0.05 in. (1.3 mm) square and 0.004 in. (0.1 mm) thick have produced output-voltage changes of about 200 mV per 0.005 in. (0.13 mm) of displacement.

Examples of transducers and the circuit are shown in the figure. The flat-plate transducer is sensitive only to motion in the x direction, since motion in the y direction does not change the area of overlap. The piston-type transducer can be made quite small for installation in confined spaces.

The circuit includes a charge amplifier, consisting of an operational amplifier with a stable fixed capacitor in its feedback loop. When an alternating voltage of fixed amplitude is applied to the capacitive transducer, the amplitude of the output of the charge amplifier changes by an amount proportional to the change of capacitance produced by the motion of the displacement transducer. The detector rectifies the amplifier output, producing a voltage that changes by an amount proportional to the change in capacitance and, therefore, to the displacement.

To adjust the final output signal to zero for some selected reference displacement, a steady voltage equal to the signal voltage at that displacement is subtracted from the signal. Once that has been done, the final output voltage will be proportional to the displacement from the reference position. A dc amplifier is used to provide a buffered output.

To obtain accurate, repeatable results, the transducers must be designed so that the spacing between the plates remains constant. This is ordinarily done by placing the plates directly in contact with a

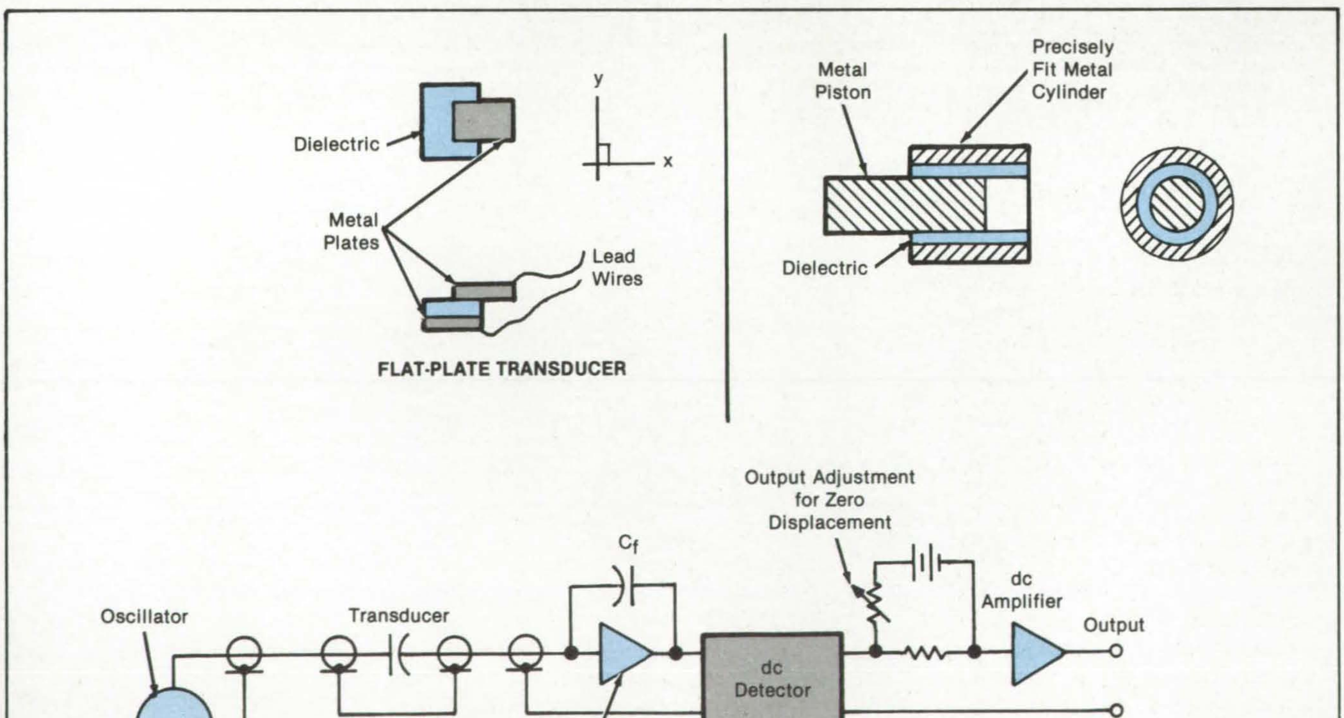

Capacitive Displacement Transducers are used to monitor small displacements. Each plate of the transducer capacitor is attached to one of the two objects, the relative motion of which is to be monitored. The relative motion of the two objects changes the area of plate overlap and hence the capacitance of the transducer.

rigid dielectric layer. With the circuit and transducers described, displacement measurements repeatable to 1 percent have been achieved. The output is insensitive to the capacitances of the connecting cables.

This work was done by Boyd D. Bryner and Alan L. Godfrey of Thiokol Corp. for **Marshall Space Flight Center**. *No further documentation is available.*

Inquiries concerning rights for the commercial use of this invention should be addressed to the Patent Counsel, Marshall Space Flight Center [see page 17]. Refer to MFS-28017.

A Surface-Controlled Solar Cell

The open-circuit voltage and the cell efficiency may be increased.

NASA's Jet Propulsion Laboratory, Pasadena, California

A proposed technique for controlling the recombination velocity on solar-cell surfaces could provide cells of increased efficiency and open-circuit voltage. In present cells, uncontrolled surface recombination velocity degrades the open-circuit voltage and the efficiency. In a cell using the proposed technique, a transparent conducting layer, insulated from the cell contacts, would be biased (see figure) to enable variable control of the surface recombination velocity.

The fabrication process for one of the new solar cells includes the following two steps:

1. A solar cell with isolated junctions is made by use of oxide-masking and photolithographic techniques. Contacts to the junctions are made by the usual photolithographic metallization.
2. A thin, passivating oxide is grown at the surface (everywhere except at the junctions). On this oxide layer is superimposed a very thin, slightly absorbing layer of metal or of transparent and conducting oxide or polymer. This transparent conducting layer serves as an antireflective coating and also can be biased to alter the surface properties of the cell.

By the application of a suitable voltage with very little power consumption, the surface can be put in the enhancement mode to repel the minority carriers from the surface. This should enhance carrier collection at the junctions and increase the open-circuit voltage and the efficiency of the solar cell.

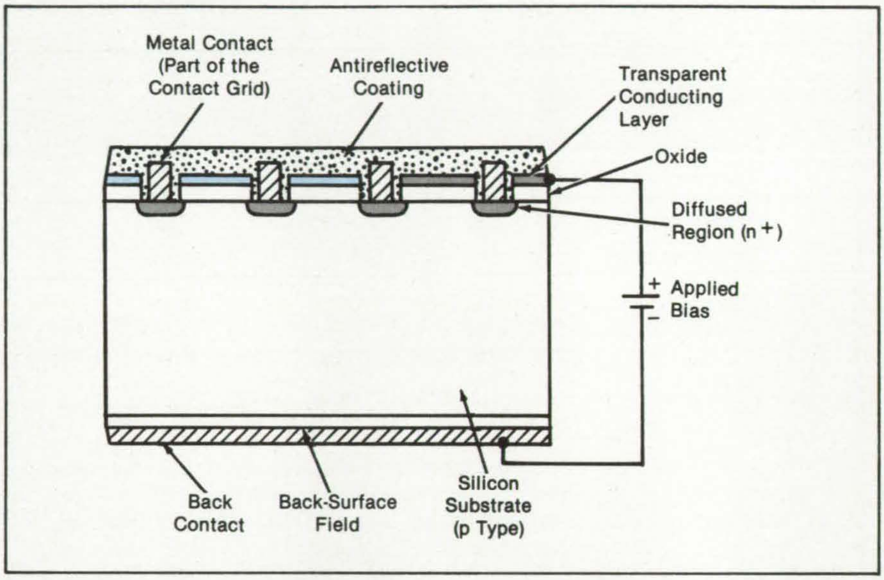

Biasing a Thin, Transparent Coating on a solar cell could enhance carrier collection at the junctions, increasing the open-circuit voltage and the efficiency.

This work was done by Taher Daud and Gerald T. Crotty of Caltech for **NASA's Jet Propulsion Laboratory.** *For further information, Circle 125 on the TSP Request Card.*
NPO-16430

Monolithic Isolated Single-Mode Ring Laser

The MISER uses a four-sided ring to lase nonreciprocally.

Langley Research Center, Hampton, Virginia

Lasers of a single, very-stable frequency are desirable for a number of purposes. Frequency stability makes possible coherent detection of laser radiation with a low-bandwidth detector, which is useful for communications. It also allows very-high-resolution spectroscopy. Any application where it is desired to use a laser in the way microwaves have been used traditionally can be enhanced if the frequency is very stable. This laser concept should provide a very-compact, efficient, and stable source of coherent radiation.

Laser materials that are homogeneously broadened, such as Nd:YAG, should lase easily in a single mode, at least when pumped continuously. In a conventional linear resonator, Nd:YAG lases in five or more modes due to a phenomenon known as spatial hole burning. Spatial hole burning occurs when there is a standing wave in the resonator with a sinusoidal intensity pattern. At points of low intensity, there is poor saturation of the gain, and the other modes will be above threshold.

One successful technique for achieving single-longitudinal-mode operation in materials such as Nd:YAG is to build the laser resonator as a nonreciprocal ring.

Wyle at work.

Helping make Space Station a reality.

Wyle Laboratories is playing an important role in the development of the Space Station. As a team member with Martin Marietta, we are responsible for payload accommodations analysis and mission modeling for the U.S. Laboratory.

We are defining requirements and developing conceptual designs for experiment apparatus and production-scale materials processing facilities. We're also developing materials processing furnaces to support Microgravity Science research.

Wyle has in-depth experience in defining and assessing user requirements and developing functional hardware and systems to meet user needs. Our translation of research objectives into workable integrated systems represents a valuable asset in the successful development of the Space Station.

For over 20 years, Wyle has been working with NASA and prime contractors on virtually every major space system development program.

Wyle is also contributing Mission Support for National Transonic Wind Tunnel and JPL Environmental Testing Facilities. For more information, call collect: Don McAvin in Huntsville, AL, (205) 837-4411.

WYLE LABORATORIES SCIENTIFIC SERVICES & SYSTEMS GROUP

Huntsville, AL
Lanham, MD
Los Angeles, CA
Arlington, VA
El Segundo, CA
Santa Clara, CA
Colorado Springs, CO
Norco, CA
Hampton, VA
Houston, TX

When there is a traveling wave instead of a standing wave, there is uniform saturation of the gain, and only one mode should lase. What is needed is a ring resonator that has a slightly greater loss in one direction than in the other.

The Monolithic (no external mirrors) Isolated (from external reflections) Single-Mode End-Pumped Ring Laser (MISER) consists of a single piece of solid-state laser material with a ring path for the laser beam. The simplest ring would be three sided. However, the two possible directions for lasing in a single-crystal triangle ring will be equivalent. Nonreciprocity is impossible, and the laser will lase in both directions. For nonreciprocity to exist, it is necessary for the ray path to be in two different planes.

The MISER design is a four-sided ring. Three of the corners utilize total internal reflection, while the fourth is the output coupler. The output coupler is at nonnormal incidence, so it acts as a polarizer. The corners at which total internal reflection takes place act as birefringent elements. There is a magnetic field that causes magneto-optic rotation of the direction of polarization.

Because the planes of incidence for the four faces are not all the same, there is some nonmagnetic rotation of the polarization. The strength of the magnetic field and the orientation of the total-internal-reflection faces are such that light traveling in one direction "sees" each face in the proper orientation for no birefringence to take place, while light traveling in the other direction is fairly strongly polarized. Since the output coupling will be substantially greater for the P-polarization than for the S-polarization, the laser will operate in the S-polarization. Only for one direction of travel will a ray leaving the coupler in the S-polarization return in that polarization. This is the direction in which the laser will operate.

Because the laser will be a nonreciprocal ring, it will lase in a single-axial mode. The ring also isolates it from outside reflection, because light entering the output coupler parallel to the output beam will travel the wrong way through the ring and thus will not be amplified. Matching the pump radiation (from a mostly-coherent diode laser array) into the mode volume will result in easy single-transverse-mode operation. Frequency stability is possible, because the natural acoustic modes of the crystal are at very high frequencies, which cannot propagate through the mounting hardware into the crystal. Thermal stability is also possible, since the diode pumping results in little waste heat, and cooling may be done by conduction or thermoelectrically.

This work was done by Thomas J. Kane and Robert L. Byer of Stanford University for **Langley Research Center**. *No further documentation is available.*

In accordance with Public Law 96-517, the contractor has elected to retain title to this invention. Inquiries concerning rights for its commercial use should be addressed to:

Office of Technology Licensing
Stanford University
Stanford, CA 94305
(ref. invention S83-081).

Refer to LAR-13191, volume and number of this NASA Tech Briefs issue, and the page number.

Calculating Effects of Reflector-Antenna Distortions

Changes in radiation patterns are predicted from surface-displacement measurements.

NASA's Jet Propulsion Laboratory, Pasadena, California

A mathematical numerical model accurately predicts the effects of systematic (that is, nonrandom) distortions on the radiation pattern of a reflector antenna. Techniques for predicting radiation patterns were developed previously for reflectors with perfect surfaces and for surfaces with random deviations from perfection. The new model treats reflectors distorted by thermal, gravitational, and dynamic effects.

The steps in the analysis of a distorted reflector are illustrated schematically in Figure 1. The model incorporates physical optics via vector diffraction analysis to obtain the co- and cross-polar components of the electric field. The reflector-surface shape is specified in terms of the undistorted part of the displacement from a reference surface (for example, a best-fit paraboloid), plus the distortion. Assuming an incident radiation field from a feed horn or other source, the integral for the far radiation field is taken over the surface and evaluated using a Jacobi-Bessel expansion.

In principle, the radiation integral requires the specification of the surface distortion and orientation at every point. The distortion, in practice, may be known from measurements at a limited number of points or from a finite-element calculation of thermal or dynamic distortions. Therefore, the model includes an interpolation scheme that describes the distortion with relatively high accuracy in the spaces between the known points.

The choice of interpolation scheme or combination of schemes depends on the specific problem. In global interpolation, the surface is described in a two-dimensional polynomial or an expansion

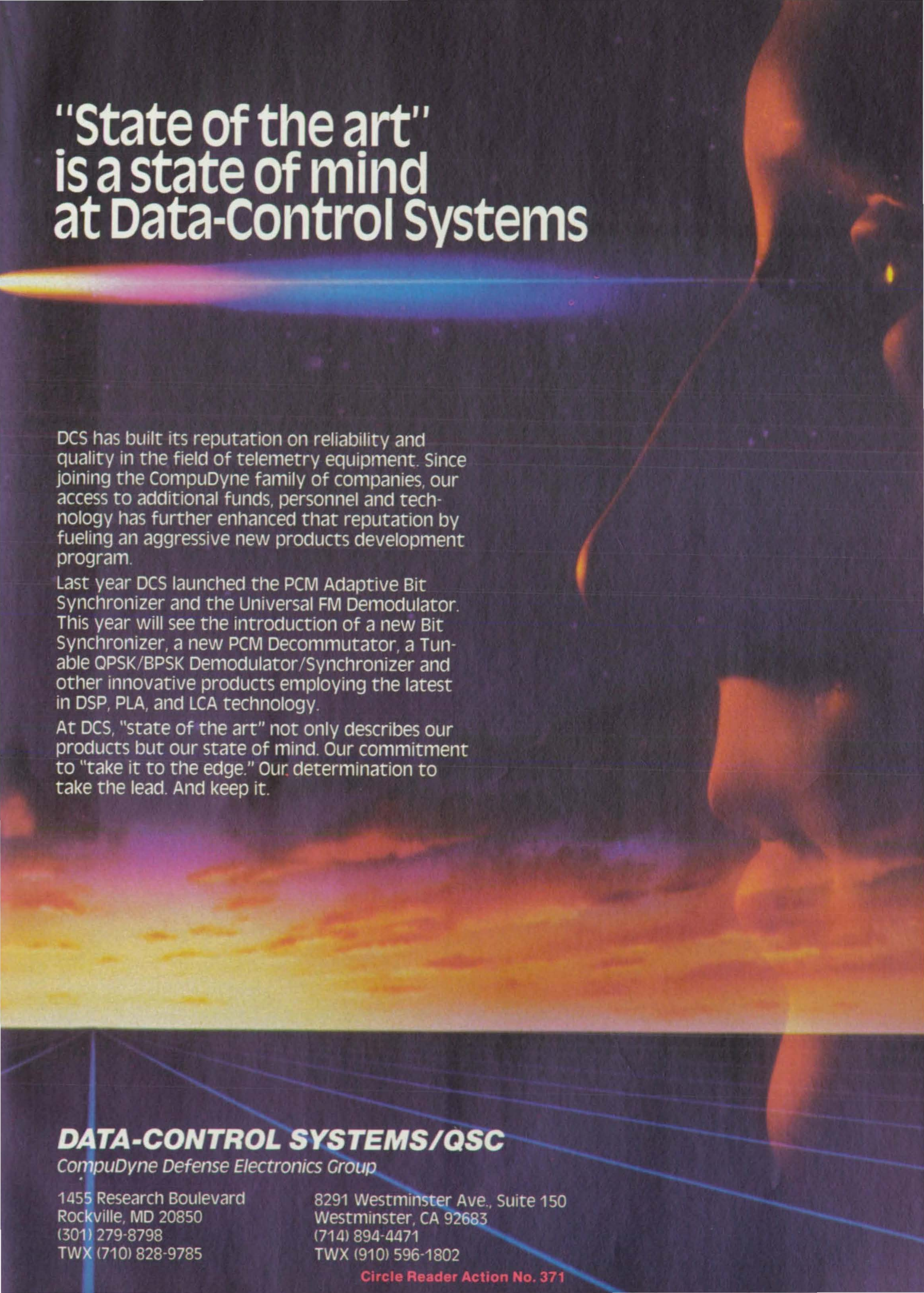
"State of the art"
is a state of mind
at Data-Control Systems
DCS has built its reputation on reliability and quality in the field of telemetry equipment. Since joining the CompuDyne family of companies, our access to additional funds, personnel and technology has further enhanced that reputation by fueling an aggressive new products development program.
Last year DCS launched the PCM Adaptive Bit Synchronizer and the Universal FM Demodulator. This year will see the introduction of a new Bit Synchronizer, a new PCM Decommutator, a Tunable QPSK/BPSK Demodulator/Synchronizer and other innovative products employing the latest in DSP, PLA, and LCA technology.
At DCS, "state of the art" not only describes our products but our state of mind. Our commitment to "take it to the edge." Our determination to take the lead. And keep it.
DATA-CONTROL SYSTEMS/QSC
CompuDyne Defense Electronics Group
1455 Research Boulevard
Rockville, MD 20850
(301) 279-8798
TWX (710) 828-9785
8291 Westminster Ave., Suite 150
Westminster, CA 92683
(714) 894-4471
TWX (910) 596-1802
Circle Reader Action No. 371

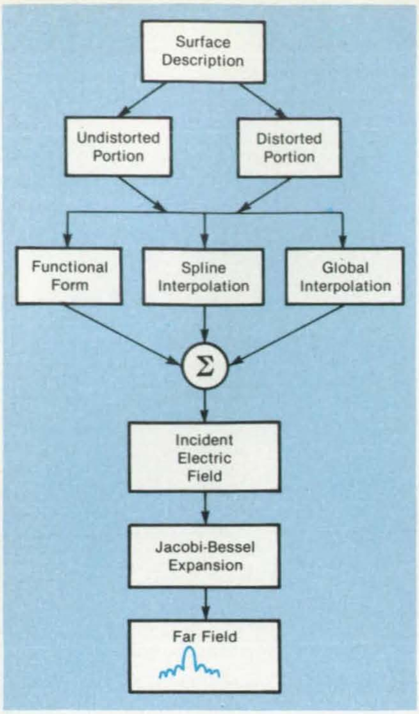

Figure 1. The **Diffraction Analysis** of a reflector antenna depends on an interpolation of the surface description for the far-field radiation integral.

in orthogonal functions: The task in such a case is to determine the coefficients of the polynomial or expansion. In local interpolation, a spline patch provides a smooth surface connecting adjacent known points, subject to the requirement that the interpolation function and its derivatives be continuous.

The local interpolation (see Figure 2) expresses the z distortion coordinate of a desired surface point as a bicubic or higher order polynomial in the x and y coordinates of that point. The coefficients of the bicubic polynomial are obtained from the 10 or more neighboring known points, which are found by a binary search algorithm that identifies the number of prescribed points in a rectangular search area. If the number of such points exceeds 10, the system of linear equations for the coefficients is overdetermined, and the coefficients are calculated by the method of least squares.

Many numerical examples have demonstrated the accuracy of the interpolation scheme. A notable success was achieved in predicting the radiation pattern of a distorted offset parabolic reflector. The far-field predictions for both functionally and discretely prescribed

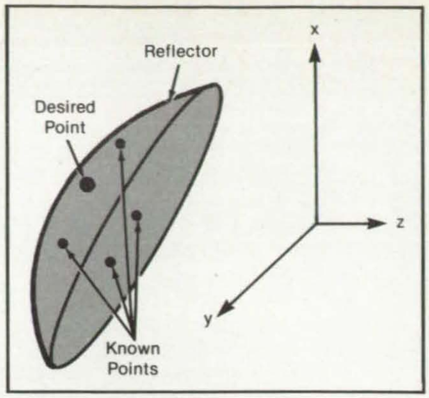

Figure 2. The **Local Interpolation Scheme** uses a bicubic or higher order polynomial approximation of the surface to express a desired surface point in terms of nearby known surface points.

surface shapes have been compared with far-field measurements. In all cases, very good agreement was obtained on the main beam and over several sidelobes away from the main beam.

This work was done by Yahya Rahmat-Samii of Caltech for **NASA's Jet Propulsion Laboratory**. *For further information, Circle 122 on the TSP Request Card. NPO-16641*

Controller for Fast-Acting Furnaces

Circuit slows the responses of certain furnace types.

Lyndon B. Johnson Space Center, Houston, Texas

The temperature-control circuit shown in the figure suppresses temperature oscillations in rapidly responding laboratory furnaces. Ordinarily, such furnaces are difficult to control because their temperatures change very rapidly with changes in delivered electric power. Ordinary commercial controllers are not designed to handle this kind of response.

The circuit output actuates an external power supply, which furnishes heater power to the furnace in response to the furnace temperature sensed by a thermocouple. Variable resistor R_{29} is adjusted so that the power supply provides whatever percentage of full power is needed to maintain temperature. Operational amplifier A_6, diode D_1, and capacitor C_3 form a feedback network that introduces a delay that changes as the capacitor charges or discharges. Rotary switch SW_2 is used to select R_{10}, R_{11}, R_{12}, or R_{13} to set the gain of A_3, which determines the response time of A_6.

Switch SW_1 is used to select the input range. Two ranges (0 to 10 mV and 0 to 50 mV) are provided so that almost any type of thermocouple can be used. The switch selects R_4 or R_5 to change the gain of A_1 and thus the thermocouple range. The input temperature signal is indicated by a commercial readout device that can, if desired, be connected to a different thermocouple or to the same thermocouple.

R_{31} is adjusted so that, with no input from the thermocouple, transistor Q_1 conducts, short-circuiting the controller output to ground and turning off the furnace power supply. Therefore, if the thermocouple fails, the furnace will simply shut down. If overheating should occur, SW_8, a panic button, can be used. When SW_8 is pressed, C_3 discharges rapidly and the controller output drops to zero. When SW_8 is released, the output increases slowly as C_3 recharges.

To start the controller, the operator increases R_{30} while pressing SW_7 until the readout indicates that the preselected minimum temperature has been reached. The operator releases SW_7 and observes the readout for about 20 minutes. If there is any temperature cycling during this period, the operator changes the position of SW_2 to adjust the response time. When cycling has been eliminated, the operator adjusts R_{30} in small steps until the required temperature is reached precisely. If the temperature cannot be reached with R_{30} at full scale, the operator adjusts R_{29} to add power to the heater.

This work was done by Richard J. Williams of **Johnson Space Center** *and Oscar Mullins and Frank Gaudiano of Lockheed Engineering and Management Services Co. Further information may be found in NASA TM-58250 [N83-19000/NSP], "A Slow Response Temperature Controller."*

Copies may be purchased [prepayment required] from the National Technical Information Service, Springfield, Virginia 22161, Telephone No. (703) 487-4650. Rush orders may be placed for an extra fee by calling (800) 336-4700. MSC-20624

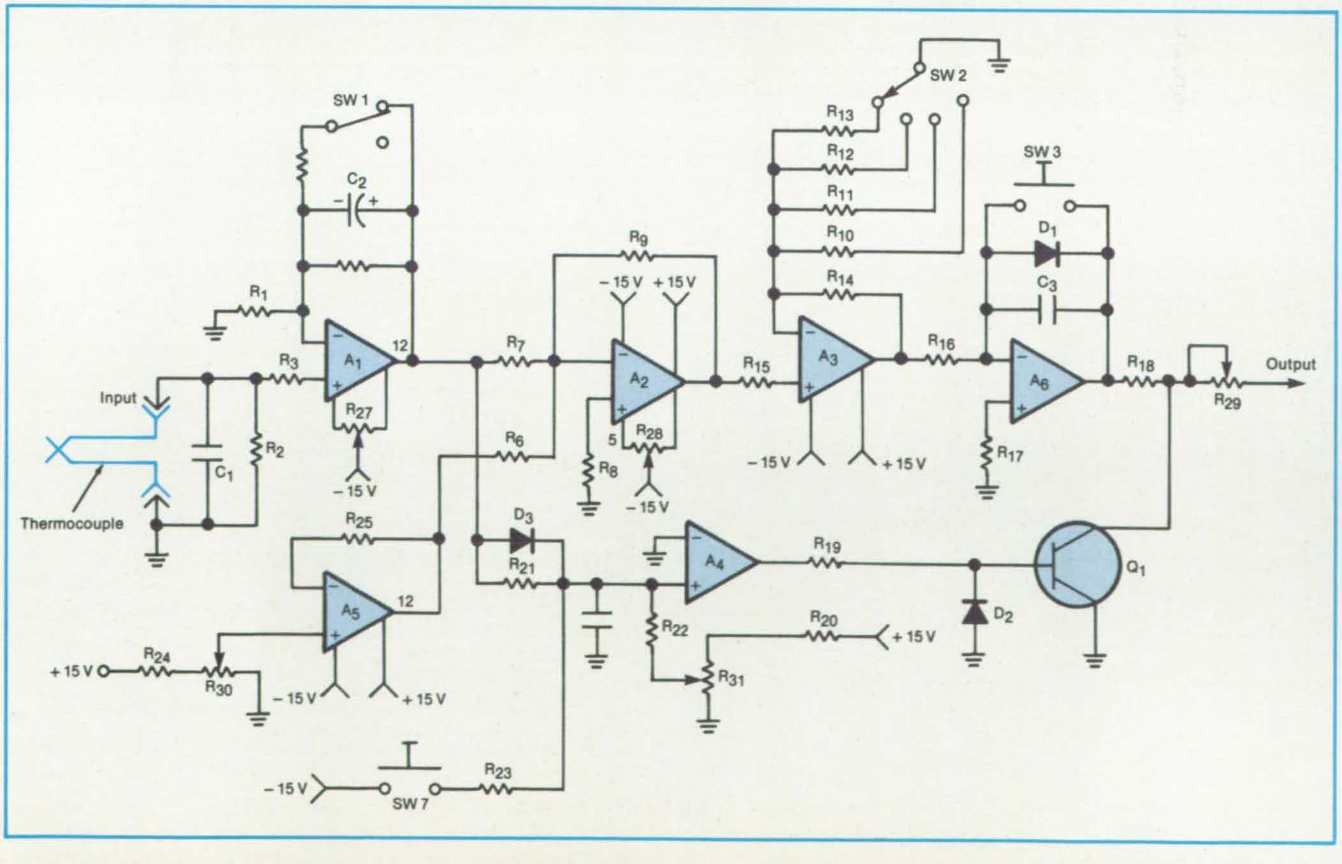

This **Control Circuit** has been used to maintain the temperature of a furnace within 2 °C over a period of 12 hours or more.

Electronic Systems

Hardware, Techniques, and Processes

28 Parallel Analog-to-Digital Image Processor
29 Local Data Processing for a Robot Hand
30 Optoelectronic Docking System

Parallel Analog-to-Digital Image Processor *

Compact circuitry performs conversions.

Goddard Space Flight Center, Greenbelt, Maryland

A proposed integrated-circuit network of many identical units would convert the analog outputs of imaging arrays of x-ray or infrared detectors to digital outputs. The converter would be located near the imaging detectors, within the cryogenic detector package. Because the converter output would be digital, it would lend itself well to multiplexing and to postprocessing for correction of the gain and offset errors peculiar to each picture element and its sampling and conversion circuits.

The conceptual processor (see figure) could include a primitive amplifier for the detector of each picture element. Alternatively, groups of detectors could be multiplexed to a smaller number of amplifiers to reduce the size of the processor. In either case, each amplified detector output is fed to an associated track-and-hold circuit, which charges a capacitor to a voltage representing the detector signal.

The analog-to-digital conversion is performed by using one digital-to-analog converter (D/A) common to all of the processors and external to the cryogenic chamber. A goal is to make each pixel converter as simple and small in integrated-circuit space as possible near the focal plane. Using high-speed silicon-gate CMOS technology operating at multimegacycle rates for digital counters, voltage-to-time conversions are performed for each detector or group of detectors. The sample is held as a voltage on a capacitor referenced to the most negative voltage in the range of the converter. Then the capacitor is ramped from the most positive voltage linearly downward using the D/A, and each pixel counter counts time until the pixel comparator stops the counting. These digital results are read out serially. A megahertz

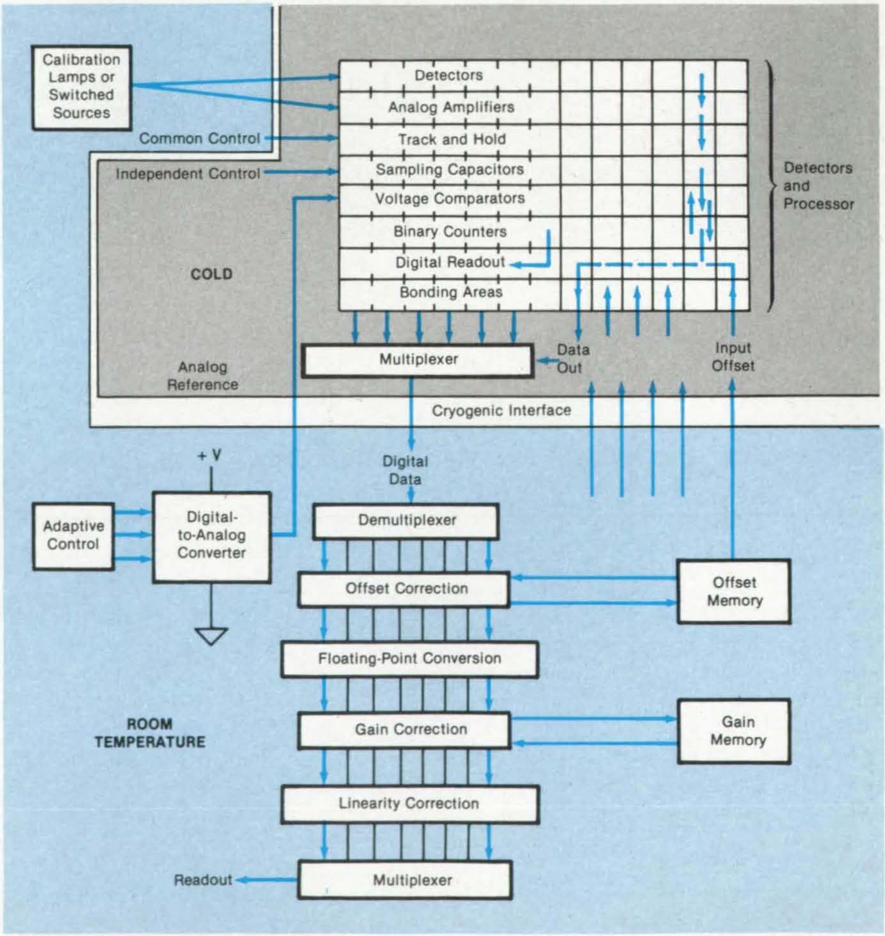

The **Analog-to-Digital Image Processor** is a massively parallel system for processing data from an array of photodetectors. The system could be built as a compact integrated circuit located near the focal plane. The buffer amplifier for each picture element can have a different offset.

clock rate could perform 8-bit conversions in about 0.3 ms and 16-bit conversions in 75 ms. The ramp technique minimizes differential nonlinearity that is important to many detectors such as x-ray and infrared imaging.

Because such detectors have large voltage "read noise" offsets, previously estimated offset corrections can be preset into the counters by shifting offset values into the digital registers as readouts are being shifted out of the focal plane. The dynamic range required of the digital logic can then be reduced.

The combined offset and gain errors for each picture element and its following circuits can be measured in a calibration run, stored in digital memories, then applied as corrections to the raw converter outputs. Input offsets and adaptive control signals can also be fed directly into the detector array.

This work was done by Donald C. Lokerson of **Goddard Space Flight Center**. *For further information, Circle 138 on the TSP Request Card.*
GSC-12898

***For more information on the Massively Parallel Processor, see out feature story beginning on page 8 in this issue.**

Local Data Processing for a Robot Hand

Integrated-circuit microcomputers process signals among sensors, external controls, and the end-effector motor.

NASA's Jet Propulsion Laboratory, Pasadena, California

A multiple-microprocessor system within the end effector of a remote manipulator accepts data from sensors in the end effector, communicates with the external control system, and controls the end-effector motor. The external system includes a central control computer (which interacts with the operator) and a display.

The electronic system in the end effector (see figure) is based on a distributed-microcomputer architecture, using high-level, multifunctional, monolithic integrated circuits. The architecture minimizes the chip count. A single-chip data-acquisition system accepts the analog signals from sensors, amplifies them, samples and holds them, and finally converts them to digital form. A pair of single-chip microcomputers equipped with input/output ports for serial data constitutes the heart of the communication subsystem. A third microcomputer chip controls the hand motor and turns the sensors on and off.

The chips are on three printed-circuit cards — one disk-shaped to fit behind the end-effector motor and the others annular to fit around the motor. Seven sliprings at the wrist connect the hand electronics with the rest of the manipulator system. Four sliprings carry power at 24 Vdc and 50 Vac. One ring is for bidirectional sensor data-communication. One is for bidirectional control-data communication. The remaining ring is for the system ground.

The communication microprocessor and the motor-control microprocessor constitute the end-effector subsystem. In addition to accepting serial input and providing serial output, the communication chip checks for transmission errors.

External commands from the central computer pass through the communication chip to the motor-control chip. These commands specify the final position of the claws on the end effector, the maximum-allowable claw closing speed, and the desired claw-gripping force. The motor-control chip uses sensor data and closed-loop feedback from the force, position, and speed sensors to ensure that the end effector follows the commands accurately. Once every millisecond, the chip calculates the proper width of the power pulses, which are then sent to the motor.

The chip in the sensor subsystem includes a 16-channel commercial data-acquisition system. A separate multiplexer provides access to the proximity-detector readings and feeds them to the data-acquisition chip, allowing it to accommodate a total of 27 analog channels of torque, proximity, force, and position data. It sends the sensor readings as 12-parallel-bit data to the external control system.

This work was done by Antal K. Bejczy of Caltech for **NASA's Jet Propulsion Laboratory**. *For further information, Circle 52 on the TSP Request Card.*
NPO-16695

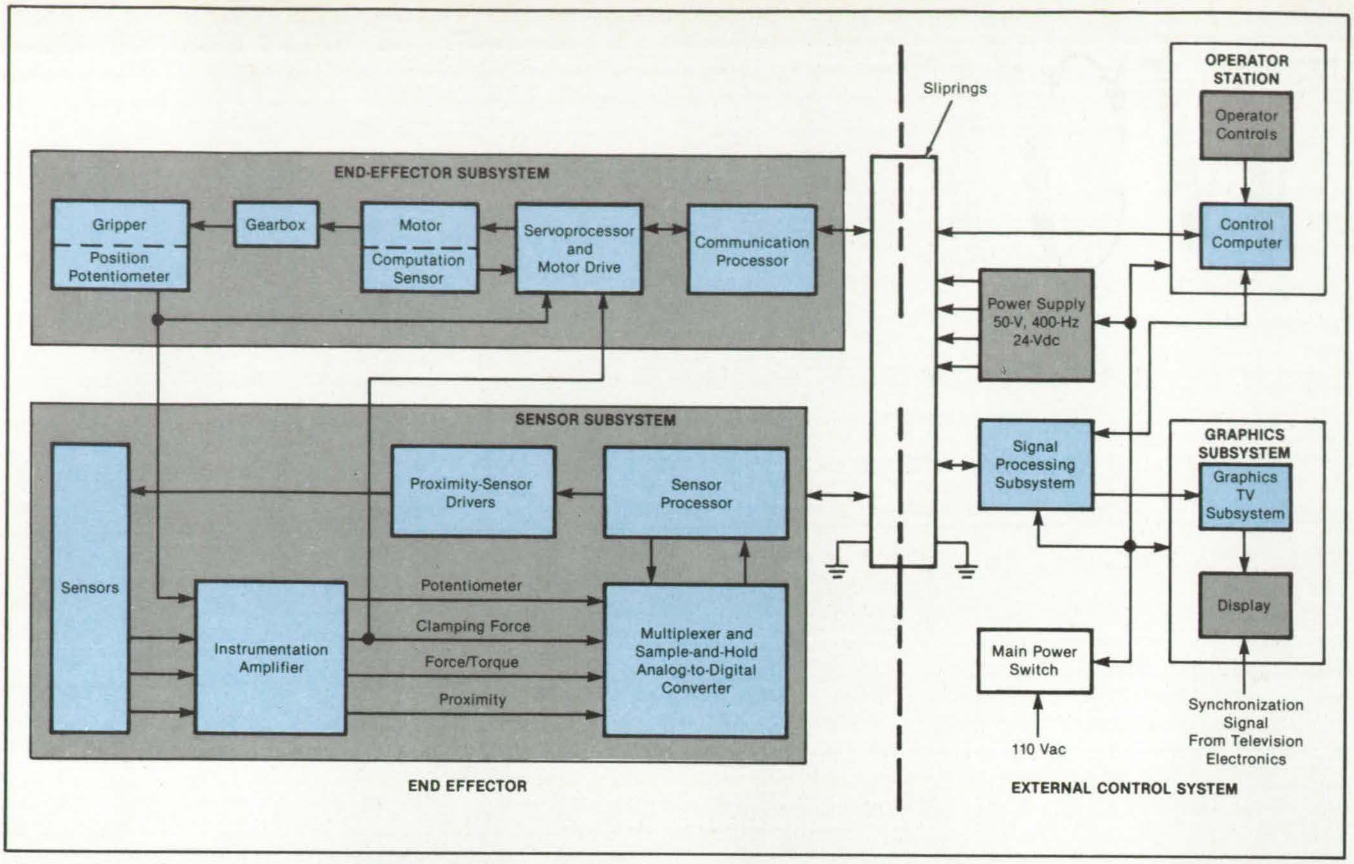

The **Local Data-Processing System in the End Effector** (left) relieves the external control system (right) of some of its computational load and minimizes data communication load with the external higher level controller.

Optoelectronic Docking System

Sensors and computers control approach and coupling.

Lyndon B. Johnson Space Center, Houston, Texas

A proposed optoelectronic system with no moving parts would automatically control the approach of two spacecraft as they closed from a distance of about 1 km to within a few cm. The system concept could probably be modified for use on Earth in robotic assembly, to control the docking of large ships, or to guide the placement of large structural components.

Through light emitters, sensors, and microcomputers on the approaching vehicle, the control system detects and computes the relative position, orientation, and velocity of target retroreflectors on the approached vehicle (see figure). The velocity and roll (spin along the docking axis) of the approaching vehicle are set in response to these computed quantities, starting with a rapid approach at long range along a direction that may be several degrees off target and ending with a slow, precise approach at close range as the two vehicles become aligned in both position and angle.

When the spacecraft are 1 km apart, the central processing unit of the optoelectronic system turns on a pulsed-laser ranging subsystem. The light from each of 20 GaAs laser diodes is formed by a cylindrical lens into a fan-shaped beam of 1° by 20°. The light reflected by the retroreflectors back to the sensor array is channeled into an array of 20 photodiode detectors by cylindrical lenses, along fan-shaped beams of 1° by 20° that are perpendicular to the transmitted beams. The emitting and detecting diodes are switched on in sequence so that the entire 20° by 20° field of view is sampled in the sequence of 1° by 1° overlaps of the transmitted and received beams. The direction to the target is thus determined to within the 1° by 1° sector that contains the target reflection, while the distance to the target is determined from the time of flight of the light pulses; the approach speed is calculated from the rate of change of the distance.

At a distance of 30 m, the approach-control task is handed to a continuous-wave-laser tracking subsystem, which distinguishes among the return signals from the three retroreflectors. In this case, the 20° by 20° field of view is still scanned by driving 20 transmitting and 20 receiving diodes in sequence, but the three target returns are detected in separate diodes, and the distance (within about ±3 cm) to each retroreflector is computed by measurement of the relative phase, in the return signal, of a 3-MHz modulation imposed on the transmitted signal.

From the three range signals, the system computes the average target distance and the orientation of the target relative to the line of sight. The coordinates of the return signals are also processed to compute both the direction to the target and the target roll angle and roll rate.

A charge-coupled-device-television/pulse-ranging system takes over at distances of less than 3 m: from 3 m to 1 m, the system processes the outline of the reflective docking plate in the television image to determine the target pitch and yaw; at 1 m, the docking-plate image exceeds the camera field of view and the system begins to seek alignment between four laser beams and the converging edges of the dark pattern in the docking plate; at a distance of 35 cm, the docking probe enters the docking port; and at 20 cm, the probe closes a hard-docking indicator switch, which deactivates the system.

This work was done by Steven M. Ward of Energy Optics, Inc., for **Johnson Space Center**. *For further information, Circle 69 on the TSP Request Card.*
MSC-21159

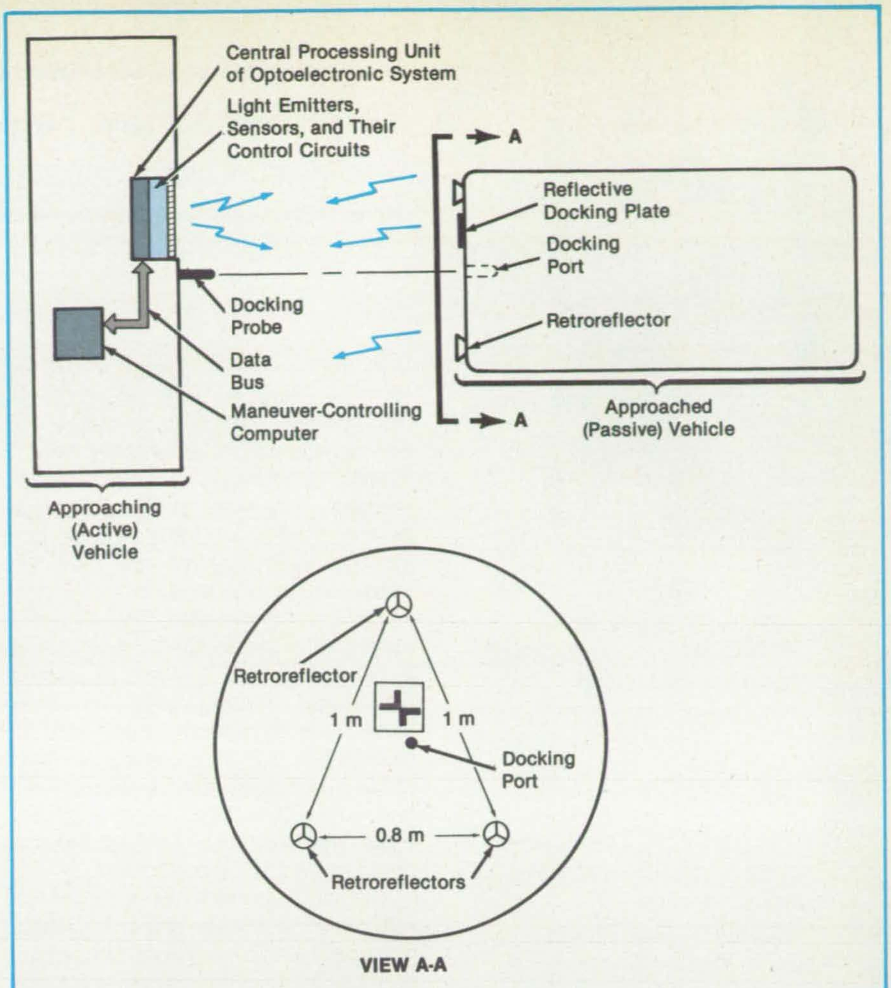

The **Optoelectronic Docking System** automatically controls the approach of an active vehicle or mechanism to a passive vehicle or object. The maneuvers of the approaching vehicle are controlled in response to the optoelectronically sensed relative position of the approached vehicle.

Physical Sciences

Hardware, Techniques, and Processes

32 Versatile X-Ray Telescope
35 Determining Optical Axes of Uniaxial Crystals
36 Wide-Angle, Flat-Field Telescope
37 More Efficient Solar Thermal-Energy Receiver
38 Calibration of Germanium Resistance Thermometers

Versatile X-Ray Telescope

Spatial and spectral resolutions are increased.

A proposed telescope for x-rays and extreme ultraviolet rays would feature high spectral and spatial resolution. Like previous telescopes of its class, it would include a glancing-incidence primary reflector. However, unlike its predecessors it would include a concave, nonglancing secondary reflector more like those used in telescopes for visible light.

The primary reflector (see Figure 1) consists of adjacent annular segments of a paraboloid and a confocal, coaxial hyperboloid. Paraxial rays that strike these surfaces produce an image at the primary focus, F_1. The secondary reflector is a concave, off-axis ellipsoid with one of its focuses at F_1 and the other at F_2. A high-resolution x-ray detector or photographic film is placed at F_2.

The secondary reflector functions well with x-rays at or near normal incidence because it is coated with alternating thin layers of two different materials (usually, metals) that support Bragg reflection at the wavelengths of interest. Such coatings, called synthetic layered microstructures, are described more fully in "Computation of Bragg Reflection for Layered Microstructures" (NPO-15880), page 41, *NASA Tech Briefs,* Vol. 8, No. 1 (Fall 1983).

Figure 2 illustrates some variations of the new telescope concept. At the top, several off-axis secondary reflectors of identical curvature are mounted on a cylinder. Any of these reflectors can be selected by simply rotating the cylinder to bring it into the focal position. Because a synthetic layered microstructure reflects primarily in a narrow wavelength band at a given angle of incidence, each reflector can be given a different coating so that it will produce an image at a different part of the x-ray spectrum.

The middle of Figure 2 shows two secondary mirrors and two detectors in use with the same primary mirror. The image produced by mirror A is larger than that produced by mirror B. The lower magnification of B is selected by moving mirror A out of the focused x-ray beam. If the synthetic layered microstructure of B is the same as that of A, then mirror B can be used to image a band of wavelengths slightly shorter than those of A, because B has a slightly lower glancing angle.

A normal-incidence concave ellipsoidal reflector with a synthetic layered microstructure can be used to reflect the x-rays back along the optical axis (see Figure 2, bottom). In this case, a pair of nested primary reflectors is used.

This work was done by Richard B. Hoover of **Marshall Space Flight Center.** *For further information, Circle 146 on the TSP Request Card.*

Inquiries concerning rights for the

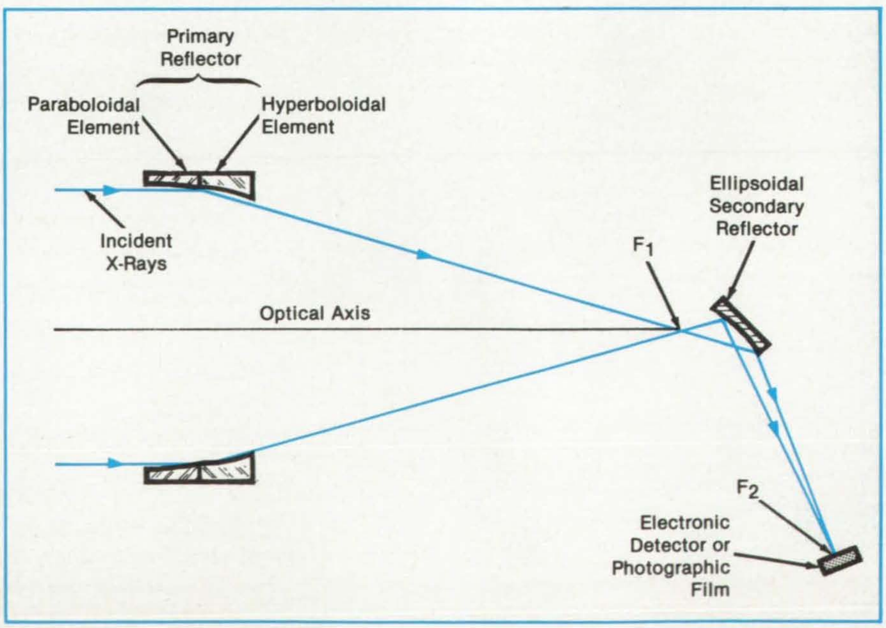

Figure 1. The Basic **X-Ray Telescope** includes a glancing-incidence, two-element primary reflector and a concave, off-axis ellipsoidal secondary reflector.

THINK SMART.

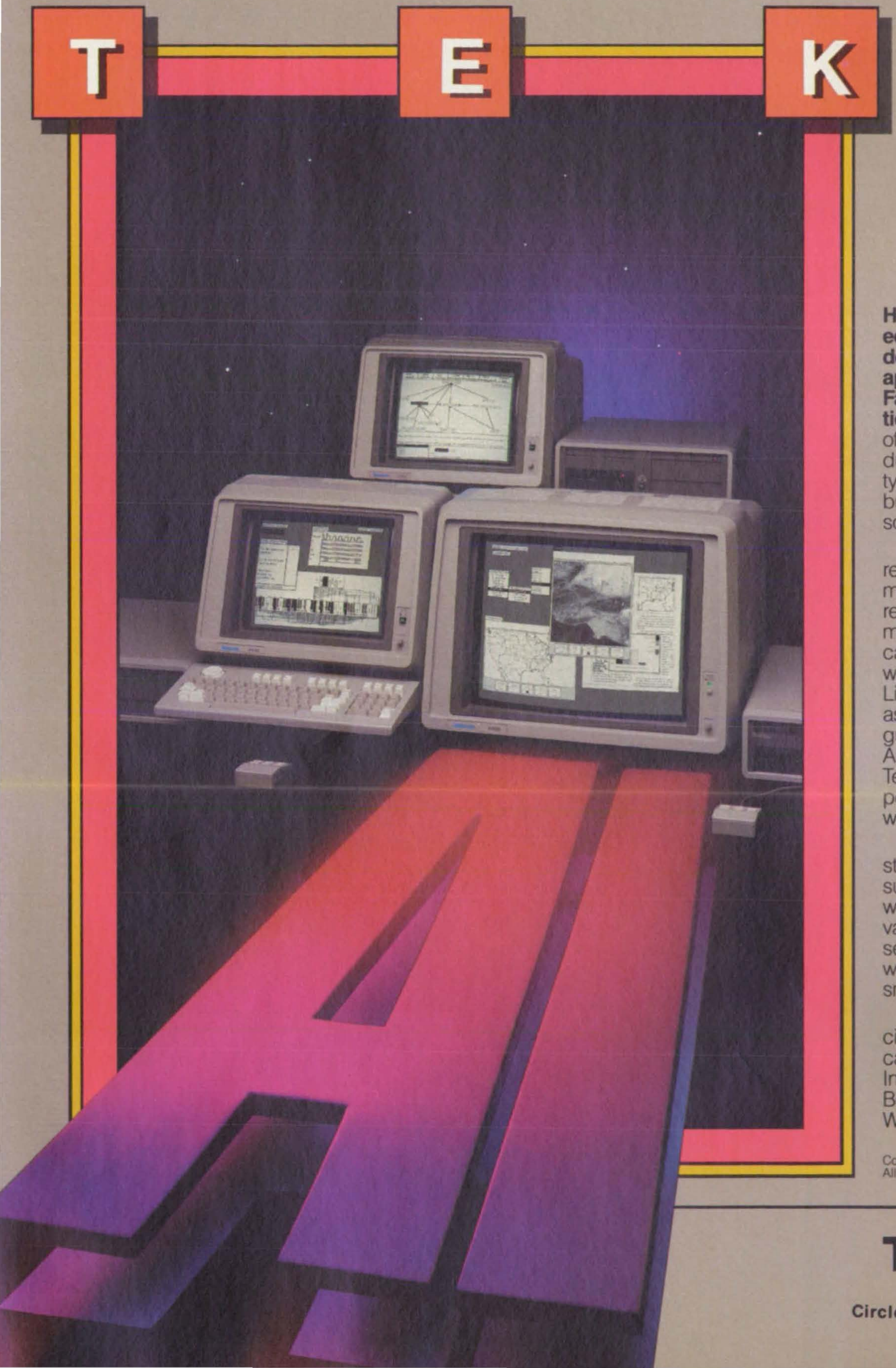

Hundreds of leading edge organizations develop practical applications using Tek's Family of AI Workstations. The 4400 Series offers you excellent productivity for rapid prototyping, expert systems building and advanced software development.

This productivity results from Tek's commitment to practical research and development goals. Goals we can help you achieve with tools like Common Lisp and Prolog as well as object-oriented languages like Smalltalk. All optimized to run on Tek's low-cost, high-performance 32-bit workstations.

Add to this the outstanding training and support, and you know why more and more innovative developers are selecting Tek AI systems when they want to think smart.

For more information, circle the reader service card or write to: Tektronix, Inc., AI Marketing, P.O. Box 1000, M.S. 63-635, Wilsonville, OR 97070.

Tektronix
COMMITTED TO EXCELLENCE

Circle Reader Action No. 462

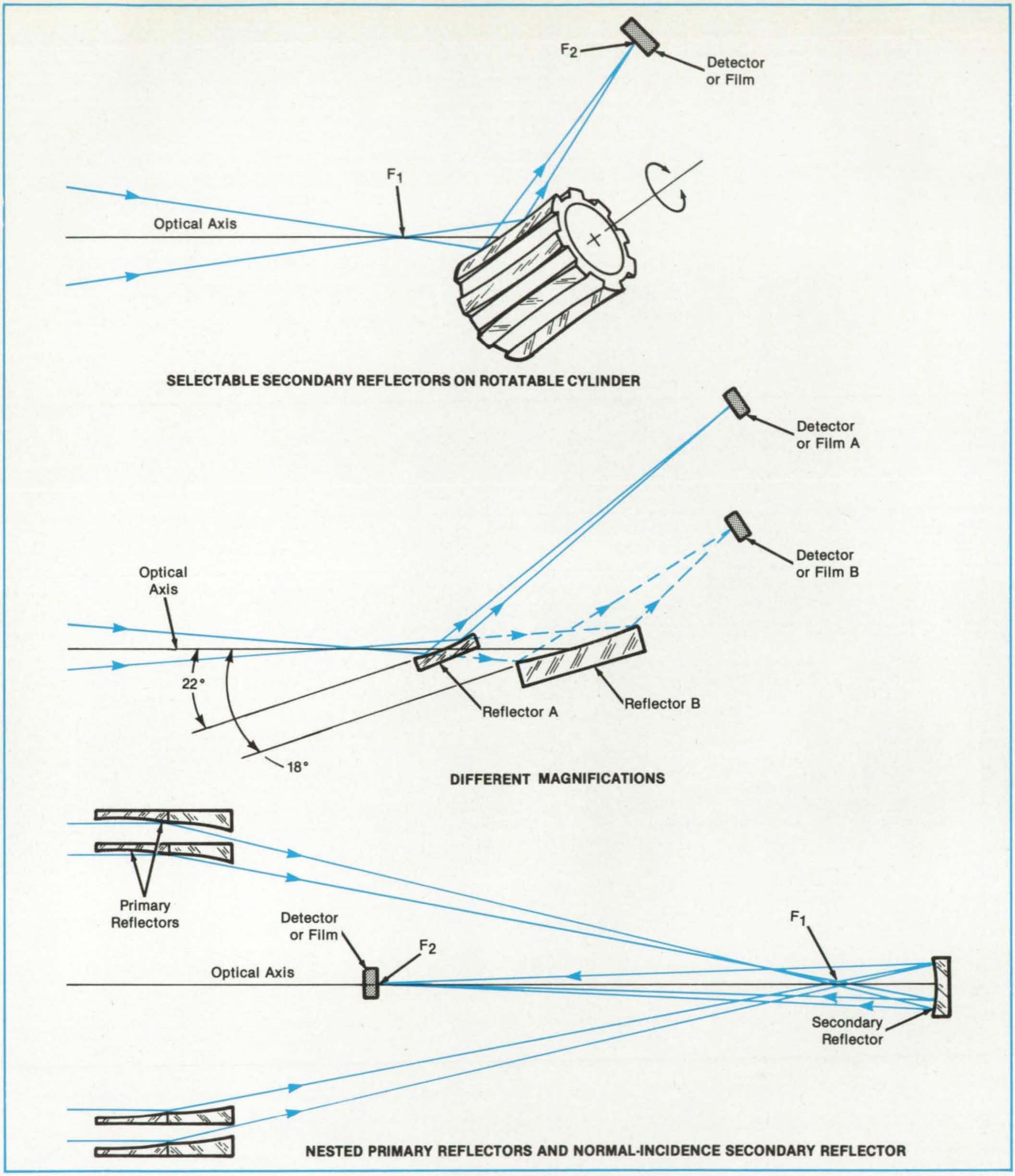

Figure 2. **Different Versions of the Telescope** are obtained by the use of different reflector and detector configurations.

commercial use of this invention should be addressed to the Patent Counsel, Marshall Space Flight Center [see page 17]. Refer to MFS-28013.

Determining Optical Axes of Uniaxial Crystals

The polarizing-microscope concept is adapted for thick samples.

Lewis Research Center, Cleveland, Ohio

Uniaxial crystals such as sapphire, quartz, calcite, and ice exhibit the property known as birefringence. A single laser beam entering such a material is generally split into two beams, each having a different polarization. Single-beam transmission is possible if the optical axis of the crystal is perpendicular to the direction of the beam propagation or if the polarization of the incoming beam is identical to that of either of the outgoing beams. These polarization directions can be calculated if the directions of the incident beam and the optical axis are known.

The optical axis of a crystal is usually found by examining a sample thinner than 1 mm between crossed polarizing plates. Because it is frequently impractical to cut off a small sample of a crystal for testing, the technique was modified to accommodate large crystals.

A vertically polarized, expanded laser beam is first passed through the crystal under study and then through a horizontally polarizing plate. The crystal is rotated until light ceases to be transmitted through the final polarizing plate. This places the optical axis in the plane containing the initial beam and the axis of rotation of the crystal. The crystal is then rotated 90°, and the initial polarization is rotated until transmission again ceases. This polarization is now parallel or perpendicular to the optical axis. The correct orientation is chosen by observing the interference pattern created by light passing through the final polarizing plate.

The ability to circumvent the effect of birefringence has applications where laser beams must be transmitted through uniaxial crystals, as in laser diagnostics of contained flows in systems requiring windows for optical access.

This work was done by Harold J. Schock and Carolyn A. Regan of **Lewis Research Center** *and James A. Lock of Cleveland State University. Further information may be found in NASA TM-86892 [N86-22915/NSP], "The Determination of the Direction of the Optic Axis of Uniaxial Crystalline Materials."*

Copies may be purchased [prepayment required] from the National Technical Information Service, Springfield, Virginia 22161, Telephone No. (703) 487-4650. Rush orders may be placed for an extra fee by calling (800) 336-4700. LEW-14452

Wide-Angle, Flat-Field Telescope

An all-reflective system is unvignetted.

Goddard Space Flight Center, Greenbelt, Maryland

A wide-angle telescope uses unobstructed reflecting elements to produce a flat image. Because there are no refracting elements, there is no chromatic aberration, and the telescope operates over the spectral range from infrared to far ultraviolet. The telescope can be used with such image detectors as photographic film, vidicons, and solid-state image arrays.

The telescope (see figure) includes three reflectors: A spherical primary mirror, M_1; an ellipsoidal secondary mirror, M_2; and a spherical tertiary mirror, M_3. The centers of curvature of the spheres and the foci of the ellipsoid lie on the common optical (Z) axis. Practical values of the effective focal length of the three-mirror system could range from 20 to 100 mm.

To eliminate vignetting, the mirrors are offset portions of the parent reflector surfaces. An input baffle helps define the field of view, which is 20° about the X axis and 30° about the Y axis. Additional masks and baffles define further the field of view and suppress stray light.

The incoming light beam first strikes M_1 and is reflected to M_2. After M_2, the beam narrows to a waist where it crosses the common optical axis. An iris diaphragm placed there serves as an aperture stop, with its center on the common optical axis. None of the rays that pass through the iris is obscured by any of the mirror segments. The iris is adjusted to produce any desired focal ratio between f/4 and f/22.

The curvatures of M_1, M_2, and M_3 are balanced so that their combined spherical aberration is nearly zero. Coma is corrected by balancing the contribution of M_1 and M_3 against that of M_2. Astigmatism is corrected by balancing the contribution of M_1 against that of M_3, leaving a small residue from M_2. The curvatures of M_1, M_2, and M_3 are selected so that a distant object produces a flat image.

After passing through the iris, the light is reflected and focused by M_3 onto the detector. Because the image is flat, the detector can be flat. The image on the detector plane has about 10 percent barrel distortion, which in most cases would be acceptable as the price of maintaining high resolution throughout the entire image field, and can be corrected with automatic processing of the image data.

This work was done by Kenneth L. Hallam, Barton J. Howell, and Mark E. Wilson of ***Goddard Space Flight Center****. For further information, Circle 23 on the TSP Request Card.*

This invention is owned by NASA, and a patent application has been filed. Inquiries concerning nonexclusive or exclusive license for its commercial development should be addressed to the Patent Counsel, Goddard Space Flight Center [see page 17]. Refer to GSC-12825.

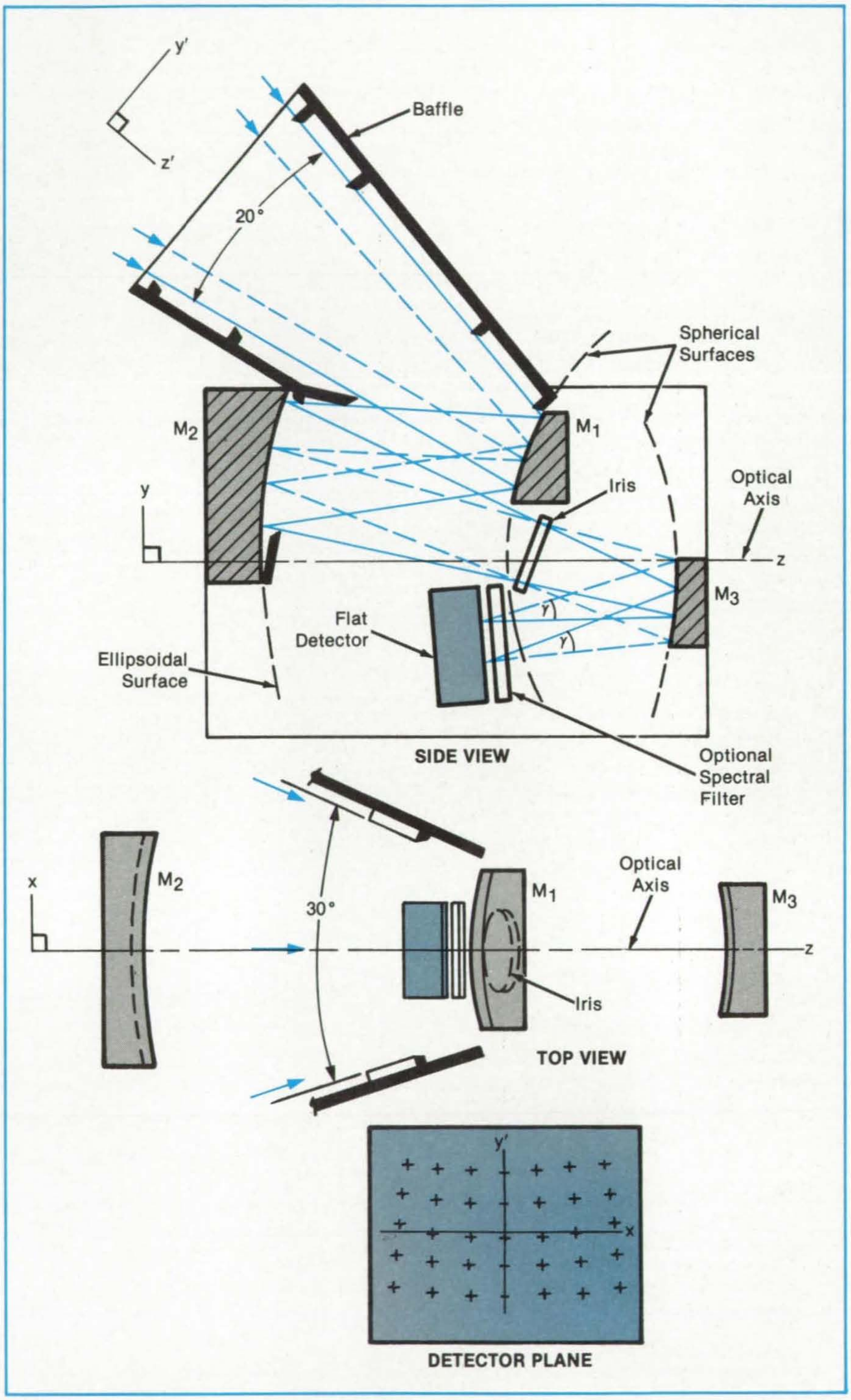

The **Wide-Angle Telescope** includes offset mirrors to achieve an unobstructed field of view. The mirror curvatures are chosen to produce a flat image on the detector.

More Efficient Solar Thermal-Energy Receiver

Thermal stresses and reradiation are reduced.

Lewis Research Center, Cleveland, Ohio

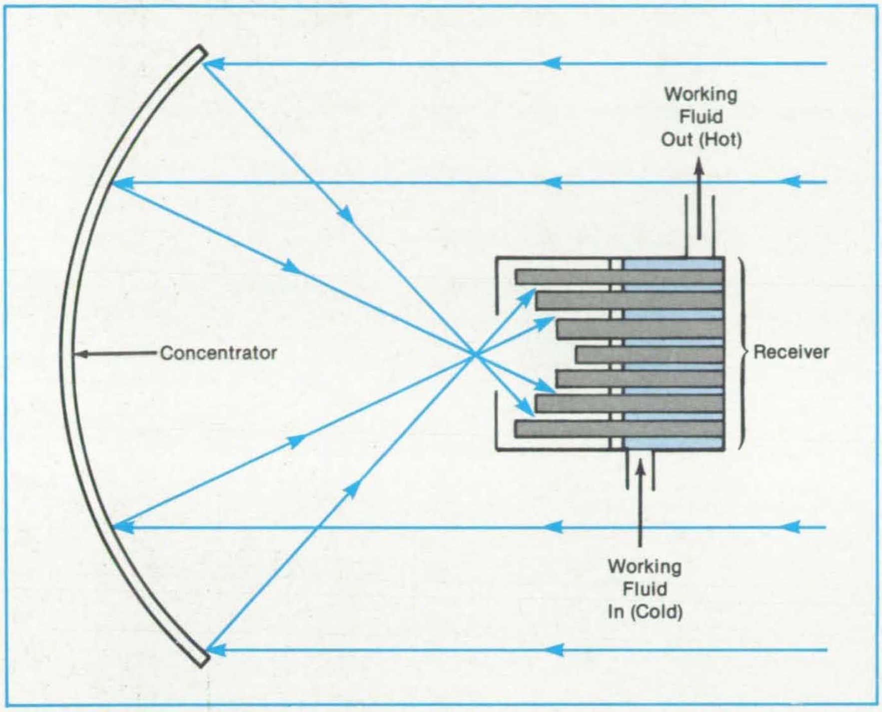

Figure 1. The **Concentrator and Receiver** are part of a solar-thermal-energy system.

An improved design for a solar thermal-energy receiver overcomes three major deficiencies of the solar dynamic receivers described in literature. These deficiencies are as follows:

1. Present receiver designs allow reradiation losses from the thermal-energy-storage material (TSM) during the shade period.
2. Most of the present receiver designs do not prevent the stressing of the TSM container due to expansion and contraction of the TSM as it freezes and melts.
3. When the solar energy enters such receivers, the rays can be easily reflected back out of the cavities, resulting in high reflection losses. To minimize these reflection losses, the rays must undergo several reflections from high-absorbtivity surfaces within the cavity.

In the proposed receiver (see Figure 1), solar energy is reflected by the surface of the concentrator into a small aperture. A working fluid, which can be liquid or gas, circulating through the receiver is heated by this energy and then ducted to a dynamic heat engine — for example, Brayton, Rankine, or Stirling — or to any other system requiring a high-temperature fluid.

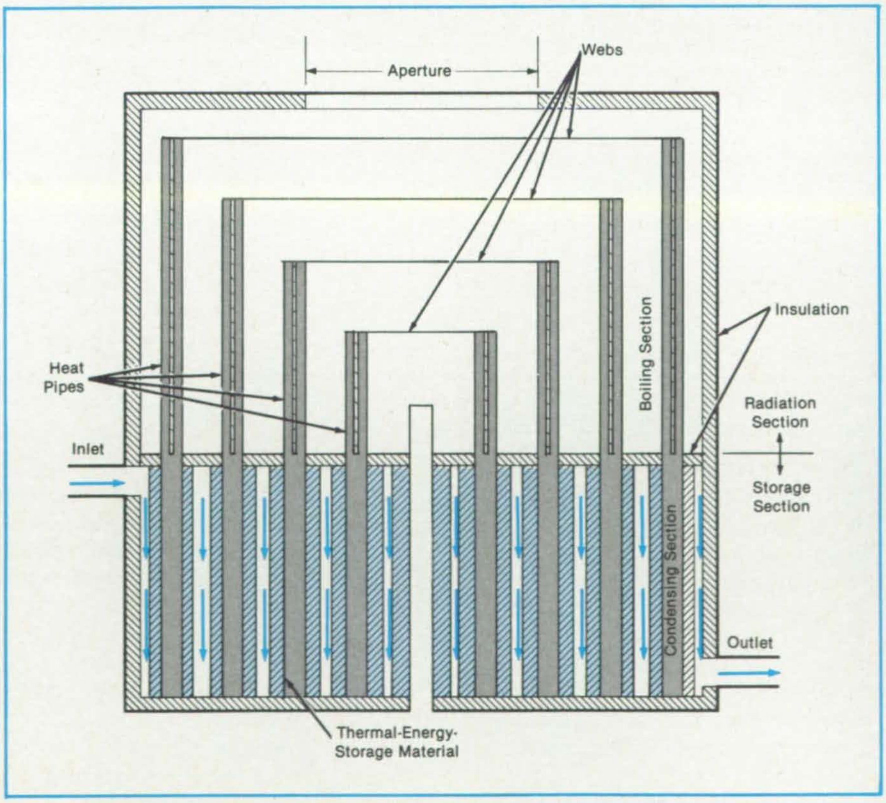

Figure 2. The **Receiver** is divided into a radiation section (top) and a storage section (bottom). Concentrated solar radiation falls on the boiling ends of heat pipes, which transmit the heat to the thermal-energy-storage medium.

The receiver, shown in Figure 2, is divided by an insulated partition into two chambers; a radiation section and a storage section. The radiation section receives the solar energy from the concentrator. The boiling ends of numerous heat pipes thermally connect the radiation section with the heat-storage section. The condensing end of each heat pipe delivers heat to the TSM, which is located coaxially around the heat pipes. Heat is passed through the TSM to the outer walls of the TSM container and into the working fluid. Fins on the outer wall of the container provide good heat transfer into the working fluid. The fins are not shown on the figure for clarity.

The improved receiver performance is attributed to three factors:

1. It minimizes reflection losses: The heat pipes in the radiation section of the receiver are connected with webs. The webs conduct heat circumferentially around the receiver to maintain an even temperature distribution, provide a

large heat-transfer surface, and cause the solar rays coming into the aperture to be reflected internally many times. Each of these reflections allows more of the solar energy to be absorbed, thereby minimizing the energy losses from the aperture.

2. It minimizes reradiation losses: Another feature is that the heat pipe can be constructed to pass heat in one direction only so that in the shade portion of the cycle the radiation section of the receiver is cold, thereby preventing heat from being lost by reradiation.
3. It minimizes thermal stresses in the thermal-storage-material container: Stresses in the TSM container are minimized by controlling the manner in which the TSM freezes and melts as the system goes through Sun and shade cycles.

The receiver can be used in a number of applications to produce thermal energy directly for use or to store thermal energy for subsequent use in a heat engine.

This work was done by Miles O. Dustin of **Lewis Research Center**. *For further information, Circle 120 on the TSP Request Card.*

Inquiries concerning rights for the commercial use of this invention should be addressed to the Patent Counsel, Lewis Research Center [see page 17]. Refer to LEW-14309.

Calibration of Germanium Resistance Thermometers

Six thermometers can be calibrated at once in the range below 2.17 K.

Marshall Space Flight Center, Alabama

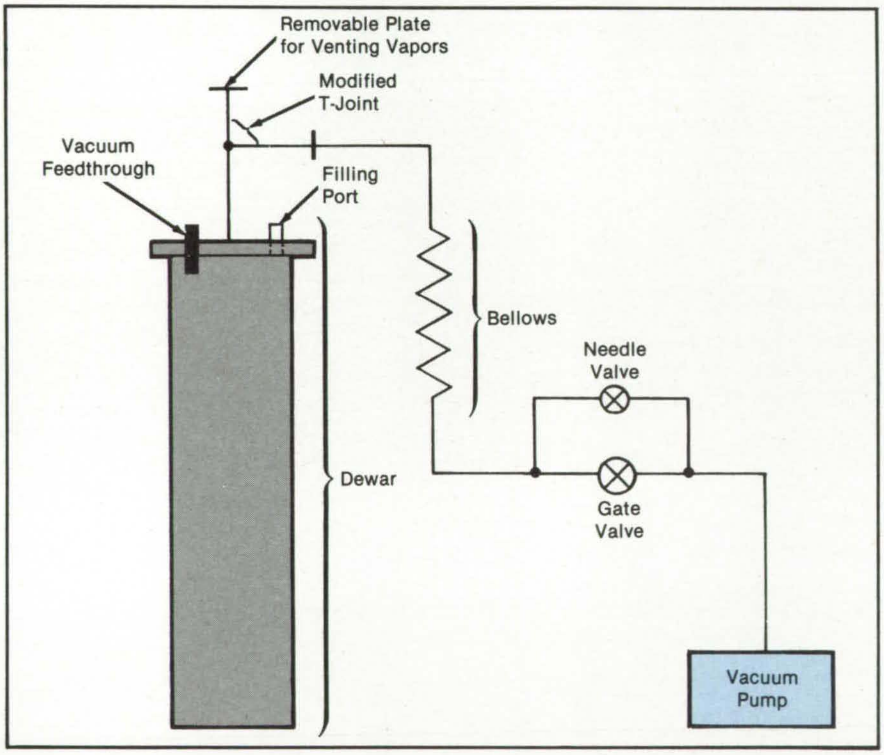

Figure 1. The **Cryostat** maintains a temperature less than 2.17 K through the controlled evaporation and removal of liquid helium from the Dewar.

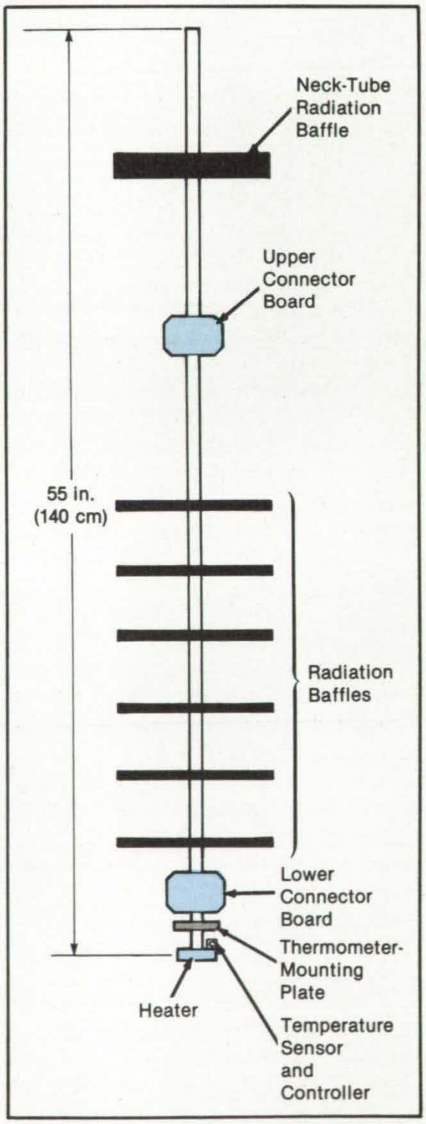

Figure 2. The **Probe** holds the thermometers to be calibrated and applies a small amount of heat as needed to maintain a precise temperature below 2.17 K.

A largely completed thermometer-calibration cryostat and probe will allow six germanium resistance thermometers to be calibrated at one time at superfluid-helium temperatures. In experiments involving several such thermometers, the use of this calibration apparatus could result in substantial cost savings: An uncalibrated germanium thermometer costs approximately $100 (1984 prices), whereas a calibrated thermometer, approximately $600.

Germanium thermometers are well suited for temperatures below 4.2 K because in this range their electrical resistances increase rapidly with decreasing temperature and because of the high reproducibility of the temperature dependence of resistance when the thermometers are cycled between liquid-helium temperatures and room temperature. In contrast, ordinary metallic resistance thermometers have low sensitivities in this range, while the temperature dependences of the resistances of carbon resistors are not reproducible under temperature cycling.

The cryostat (see Figure 1) includes a helium Dewar in which the helium space is enclosed by a cylindrical, 25-l aluminum-alloy can. The pumping line contains valves to regulate the pumping speed and a section of vacuum bellows tube to suppress the effect of pump vibrations on the calibration process.

The Dewar is connected to the pumping line by a modified "T" joint in a flange at the top. The joint has an inside adapter that supports the probe. Also on top of the flange is a plate that is removed to allow the escape of vapors when helium is being added to the Dewar through the filling port. A 37-pin connector serves as the vacuum feedthrough for connecting the various probe components to the electronics.

The probe (see Figure 2) is a 55-in. (140-cm) long stainless-steel tube fitted with radiation baffles and supporting both the thermometer-mounting plate and a temperature sensor and controller with its associated temperature-regulating resistance heater. The heater wires are wound in a bifilar coil to minimize the production of magnetic fields, which could affect the resistances of the thermometers to be calibrated. The four wires from each of seven resistance thermometers (one calibrated, six to be calibrated), the three wires from the sensor of the temperature controller, and the two from the regulator heater are consolidated at the lower connector board and pass through rubber-grommeted holes in the radiation baffles to the upper connector board.

To determine the resistances of the uncalibrated thermometers as a function of temperature, their conductances are measured under a constant voltage, using a potentiometric conductance bridge. A rotary wafer switch permits each of the six uncalibrated resistors to be switched into the bridge, with the calibrated resistor being switched into the bridge after resistors 1, 4, and 6 in a cyclic manner. This allows for a quick, multiple measurement of the calibrated resistor at each temperature during a calibration run.

Since the calibrating temperature range lies between 2.17 and 1.5 K or lower, approximately one-third of the starting 25 liters of helium in the Dewar is pumped away to accomplish the λ transition at 2.17 K. After this temperature has been attained, the pumping speed is set by adjusting the valves in the pumping line until the approximate temperature of a calibration point is reached. The temperature is then maintained at the desired value by the regulator. A variety of temperatures can be maintained in this manner, allowing a resistance-versus-temperature calibration curve to be established for each of the uncalibrated thermometers.

This work was done by Dan Ladner and Eugene Urban of **Marshall Space Flight Center** *and Franklin Curtis Mason of Middle Tennessee University. For further information, Circle 107 on the TSP Request Card.* *MFS-27107*

Materials

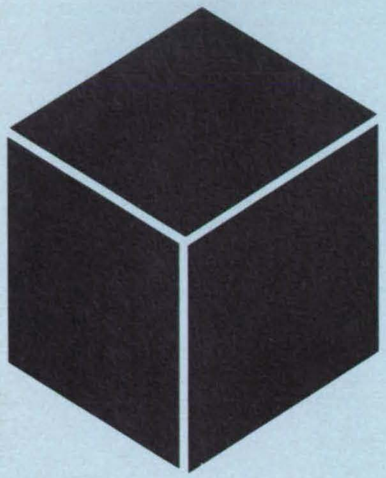

Hardware, Techniques, and Processes

40 Polyimide Prepregs With Improved Tack
42 Negative-Electrode Catalysts for Fe/Cr Redox Cells
43 Desulfurizing Coal With an Alkali Treatment
44 Semi-Interpenetrating Polymer Networks
45 Noble Metals Would Prevent Hydrogen Embrittlement
45 Progress Toward Monolithic Peritectic Solidification

Books and Reports

46 Flexural Properties of Aramid-Reinforced Pultrusions
48 High-Strength Glass for Solar Applications
48 Transparent Analogs for Alloy Phase Studies

Computer Programs

56 Computer Simulation of Ablator Charring

Polyimide Prepregs With Improved Tack

Drape and tack are improved without loss of strength.

Lewis Research Center, Cleveland, Ohio

Composites made with PMR-15 (or equivalent) polyimides have gained acceptance as viable engineering materials for high-use-temperature applications. This acceptance is due to both the thermo-oxidative stability of PMR-15 (or equivalent) and the ease with which PMR-15 (or equivalent) prepreg materials can be processed into composite structures. An important factor contributing to the processability of PMR-15 (or equivalent) is the volatility of the alcoholic solvents used in preparing prepregging solutions. These low-boiling-point solvents (methanol or ethanol) are easily removed during fabrication, making it possible to obtain void-free or low-void composites. However, the volatility of these solvents does limit the tack and drape retention of PMR-15 (or equivalent) prepreg exposed to the ambient. Retention of these two important material-handling properties is essential for consistent performance during layup of composite structures, particularly large composite structures that require long layup times.

In a recent study, PMR-15 (or equivalent) resin compositions, designated "PMR-15IT," were identified that provide improved tack and drape retention for graphite-fiber/PMR-15 (or equivalent) prepreg materials without adversely affecting processability or composite mechanical properties (see figure). The improved tack system identified to provide the best overall processability, along with excellent composite properties, was obtained by utilizing methyl ester monomers and a solvent containing methanol/1-propanol in a 3:1 weight ratio. Graphite-fiber/PMR-15 (or equivalent) prepreg prepared from the above PMR-15IT (or equivalent) resin and exposed to ambient conditions exhibits excellent tack retention for at least 10 days — approximately four times longer than current-technology PMR-15 (or equivalent) prepreg exposed under the same conditions. The figure shows that the 600 °F (320 °C) mechanical properties of composites fabricated from the PMR-15IT (or equivalent), by either compression- or autoclave-molding methods, are equivalent to those exhibited by the composites fabricated from state-of-the-art PMR-15 (or equivalent) prepreg.

This work was done by R. D. Vanucci of **Lewis Research Center.** *Further information may be found in:*

NASA TM-82951 [N83-12175/NSP], "PMR-15 Polyimide Modification for Improved Prepreg Tack" and

NASA TN-D-7257 [N72-29598/NSP], "Addition Type Polyimides from Solutions of Monomer Reactants."

Copies may be purchased [prepayment required] from the National Technical Information Service, Springfield, Virginia 22161, Telephone No. (703) 487-4650. Rush orders may be placed for an extra fee by calling (800) 336-4700. LEW-14198

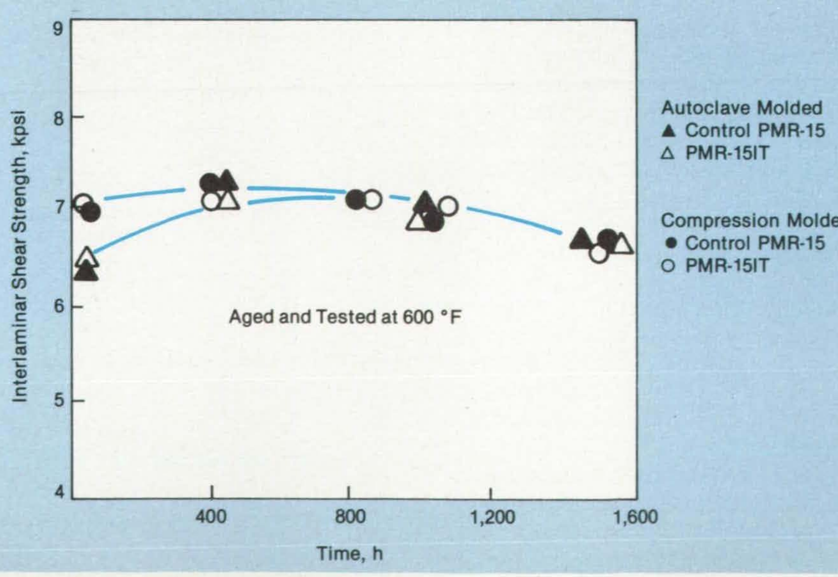

The **Interlaminar Shear Strength** of composites made with the improved polyimide nearly matches that of its predecessor.

Negative-Electrode Catalysts for Fe/Cr Redox Cells

Electrodes perform more consistently and are less expensive.

Lewis Research Center, Cleveland, Ohio

Surfaces catalyzed by bismuth (Bi) and bismuth/lead (Bi/Pb) have been developed for application on the chromium electrode in the iron/chromium (Fe/Cr) redox electrochemical energy storage system. The NASA Fe/Cr storage system incorporates two soluble electrodes consisting of acidified solutions of iron chloride ($FeCl_3$ and $FeCl_2$) and chromium chloride ($CrCl_3$ and $CrCl_2$), which are oxidized and reduced in a power-conversion unit to store and produce electricity. Electrolytes are circulated with pumps and stored in external tanks.

Reactant solutions are separated in the power-conversion unit by a semipermeable membrane or a microporous separator. The iron electrode consists of an uncatalyzed carbon felt where the Fe^{+2}/Fe^{+3} reaction occurs. However, carbon felt is not an electrochemically reversible surface for the Cr^{+3}/Cr^{+2} couple. A catalyst is required to improve the electrochemical performance. The required catalyst must have high activity for reducing and oxidizing chromium between the (+2) and (+3) oxidation states, and it must also have a high hydrogen overvoltage.

The most successful catalyst surface used for the redox system in the past has been a combination of gold (Au) and lead (Pb). Excellent results have been obtained from systems using chromium electrodes catalyzed with Au/Pb. However, electrode fabrication has not been totally reproducible. Unexplained variations in the carbon-felt substrate have influenced the deposition of the gold catalyst. Apparently the effectiveness of the lead component of the catalyst is also controlled by the integrity of the gold deposit. Other disadvantages of the Au/Pb catalyst include the fabrication time and the loss of hydrogen overvoltage following the exposure of a functioning electrode to air.

The bismuth or bismuth/lead catalyst is applied to the carbon-felt substrate by in situ electrochemical deposition of trace quantities of Bi or of Bi and Pb dissolved in the chromium solution. The loading concentrations of the catalysts are nominally 110 $\mu g/cm^2$ of projected area for bismuth and 90 $\mu g/cm^2$ of projected area for lead.

The catalysts have been evaluated in two types of Fe/Cr redox systems: one using pure iron chloride as the catholyte and pure chromium chloride as the anolyte, the other using an equimolar mixture of iron chloride and chromium chloride for both the anode and cathode. In the mixed-solution concept, however, only the iron in the catholyte and the chromium in the anolyte are the electrochemically active species.

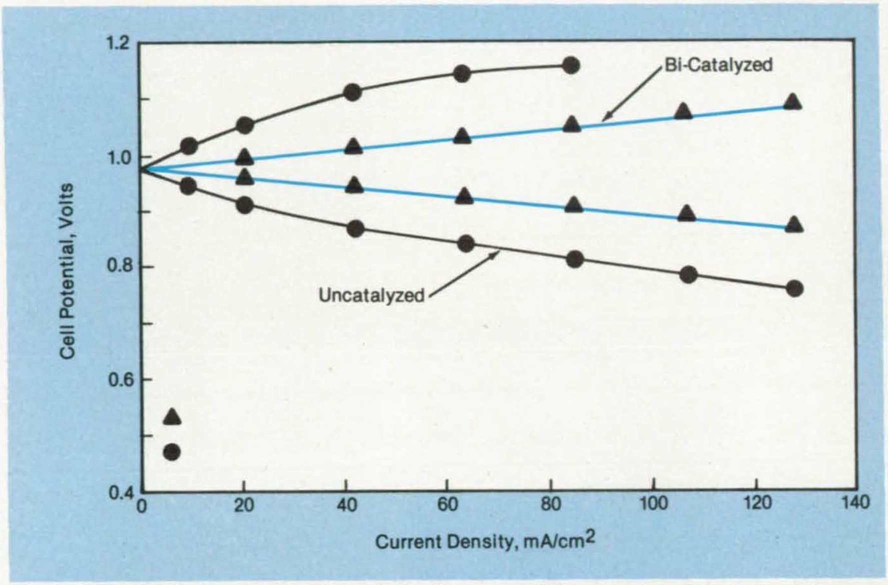

Figure 1. The **Performance of a Redox Cell** with an uncatalyzed carbon-felt electrode is compared to that of a cell with a bismuth-catalyzed carbon-felt electrode. These measurements were taken at 50 percent state of charge, with mixed reactants, at a temperature of 65 °C.

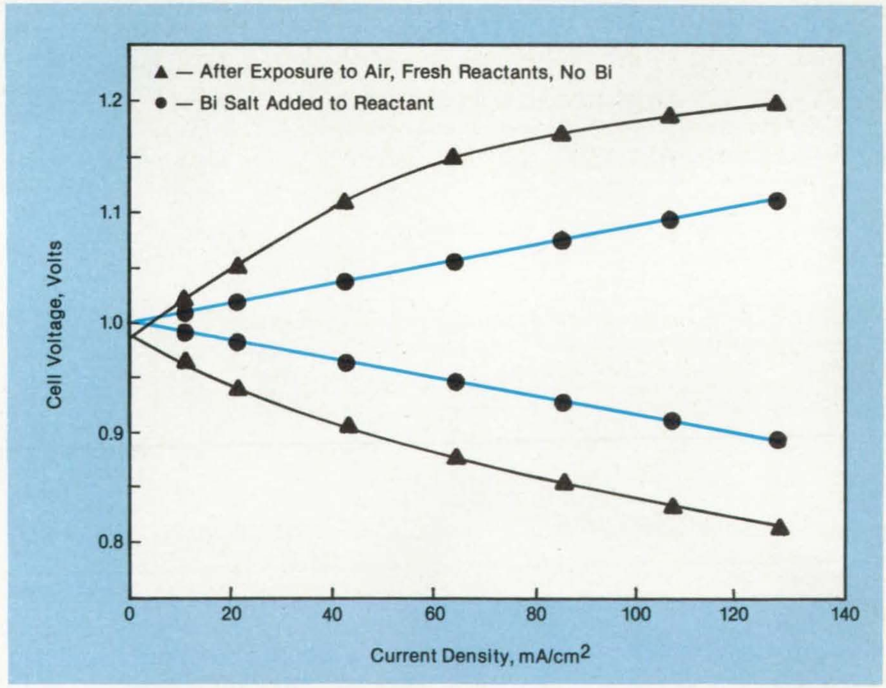

Figure 2. The **Effect of Recatalyzing the Chromium Electrode** after exposure to air is shown in this plot of cell performance. These measurements were taken at 50 percent state of charge, at a temperature of 65 °C.

Figure 1 compares the performance of a redox cell at 65 °C using a catalyzed chromium electrode to that of a cell with an uncatalyzed carbon surface. The voltage/current relationship for the uncatalyzed carbon surface shows significant kinetic polarization, whereas reversible performance is obtained following the addition of bismuth to the chromium solution. The energy efficiency for a constant-current cycle at 43 mA/cm^2 was 80 percent with the catalyzed electrode, compared to 66 percent with the uncatalyzed carbon surface.

An example of the flexibility of the bismuth-catalyzed electrode was demonstrated through the exposure of the electrode to air between cycles. (Typically, Au/Pb-catalyzed electrodes evolve greater quantities of hydrogen following exposure to air.) A system was cycled at 65 °C, the reactant solutions removed, and the system flushed with acid. The electrode was removed from the cell, dried in air at 100 °C and returned to the cell along with fresh reactants. Polarization results at 65 °C (see Figure 2), before the addition of bismuth to the anolyte, show the irreversible nature of the uncatalyzed surface. Following the addition of bismuth to the chromium solution, the reversible nature of the electrode was regained, indicating no apparent effect of the exposure to air.

The small changes in cell performance that occurred during extended cycling were corrected by completely discharging the reactants and replating the catalysts: the initial performance was restored. Remixing the anolyte and catholyte solutions to equalize the reactant volumes showed no detrimental effect.

The advantages of the bismuth catalyzed or bismuth/lead catalyzed carbon surfaces over the gold/lead catalyst system for the Cr(III)/Cr(II) couple include the following:

- Less variability in electrode performance;
- Simpler, less costly electrode fabrication; and
- Satisfactory performance following exposure to air.

It is anticipated that bismuth or bismuth/lead surfaces could also be effective for the reduction of other metal ions, e.g., manganese, vanadium, titanium, tin and copper ions.

This work was done by Randall F. Gahn and Norman Hagedorn of **Lewis Research Center**. *Further information may be found in NASA TM-87034 [N85-27387/NSP], "Cycling Performance of the Iron-Chromium Redox Energy Storage."*

Copies may be purchased [prepayment required] from the National Technical Information Service, Springfield, Virginia 22161, Telephone No. (703) 487-4650. Rush orders may be placed for an extra fee by calling (800) 336-4700.

This invention has been patented by NASA (U.S. Patent No. 4,543,302). Inquiries concerning nonexclusive or exclusive license for its commercial development should be addressed to the Patent Counsel, [see page 17]. Refer to LEW-14028.

Desulfurizing Coal With an Alkali Treatment

A simplified, fluidized-bed process removes most of the sulfur.

NASA's Jet Propulsion Laboratory, Pasadena, California

An experimental coal-desulfurization process uses alkalies and steam in a fluidized-bed reactor. With a highly volatile, high-sulfur bituminous coal, the process removed 98 percent of the pyritic sulfur and 47 percent of the organic sulfur. The process can be used in coal liquefaction and in production of clean solid fuels and synthetic liquid fuels.

The fluidized bed ensures good mixing and isothermal reaction. The process is based on the displacement of sulfur by alkalies and the conversion of sulfur to the sulfide form. Unlike other displacement processes, however, the new pro-

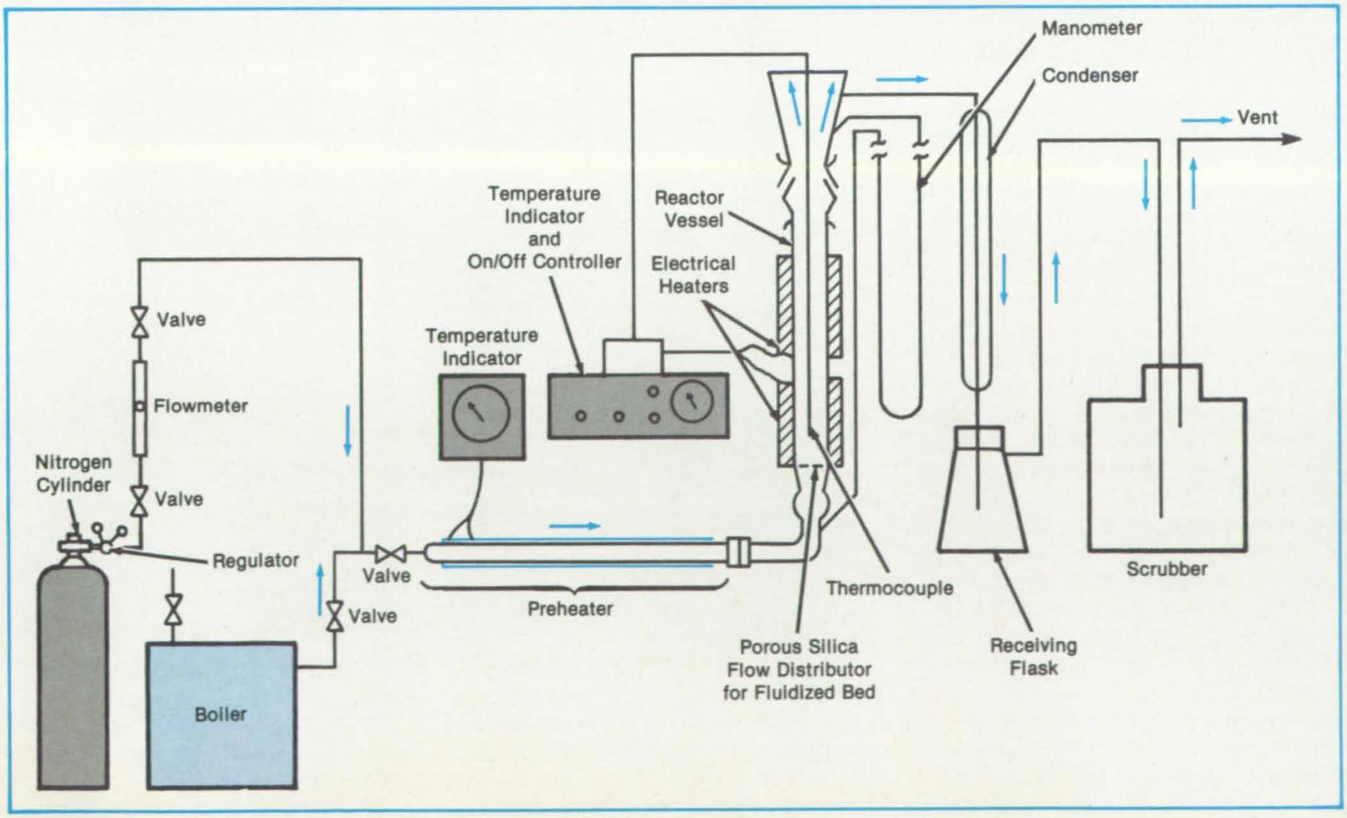

Nitrogen or Steam Flows Through a Bed of coal in a reactor. Alkalies react with sulfur, removing it from the coal. The nitrogen flow fluidizes the bed while it is heating or cooling; the steam is the fluidizing medium during the reaction.

cess adds the alkalies to the coal in water solution instead of as molten material; it is therefore simpler, safer, and more convenient and avoids excessive alkali use. The use of steam in the process helps to reduce the loss of volatile matter and to increase the extraction of mineral matter in addition to sulfur.

The process has been demonstrated in a laboratory (see figure). The apparatus included a quartz fluidized-bed reactor of 1-in. (2.5-cm) diameter and 30-in. (76.2-cm) length, a source of steam, a preheater, a reflux condenser, and a scrubber. The reactor and connecting lines were well insulated to prevent the steam from condensing in them.

In the experiment, 50 g of pulverized coal were added to 100 ml of a solution of equal amounts of sodium hydroxide and potassium hydroxide in water. The total alkali content was 20 weight percent of the solution. After the coal was soaked in the solution for 2 hours the water was allowed to evaporate. The coal was then dried in an oven at 100 °C for 4 hours.

The dry coal was loaded in the reactor and fluidized with nitrogen. After the reactor temperature reached a temperature between 250 and 500 °C, steam was substituted as the fluidizing medium. After 30 to 60 min of reaction time, the heaters were switched off, and the nitrogen flow was resumed while the reactor cooled.

The processed coal was removed and washed alternately with hot and cold distilled water until it was free of alkali. An intermediate acid wash with dilute hydrochloric acid expedited the washing process. Finally, the coal was dried in an oven and analyzed for sulfur content.

It is likely that sulfur removal can be increased further by optimizing such process variables as the concentration and composition of the alkali mixture, the coal characteristics, and the temperature and duration of the steam treatment. For example, the proportion of potassium hydroxide in the mixture seems to affect the extent of sulfur removal. Moreover, the reaction may proceed efficiently at temperatures below 250 °C, which was the nominal steam temperature available in the laboratory.

This work was done by Maddury Ravindram and John J. Kalvinskas of Caltech for **NASA's Jet Propulsion Laboratory**. *For further information Circle 152 on the TSP Request Card. NPO-16366*

Semi-Interpenetrating Polymer Networks

Desirable qualities are achieved by "networking" aromatic and addition polyimides.

Langley Research Center, Hampton, Virginia

A novel semi-interpenetrating network (semi-ipn) has been prepared at Langley Research Center from two types of polyimides (see figure). A semi-ipn results when a linear polymer is synthesized in the presence of a cross-linked polymer or vice-versa. The semi-ipn can attain certain properties that are better than those of either polymer alone.

The number of new classes of polymers discovered each year is declining. An area of increasing interest, therefore, is finding new ways of modifying existing polymer systems to obtain desired properties. For example, aromatic polyimides as a class are very attractive as structural materials for aircraft and space structures. They exhibit high thermal and thermo-oxidative stabilities and good solvent resistances over a wide temperature range. However, these systems are difficult to process. Addition polyimides, on the other hand, offer the advantage of improved processability.

Polyimidesulfone ($PISO_2$), a linear aromatic polyimide, is attractive because of its high thermal and thermo-oxidative stability, adhesion strength [2,500 to 3,000 psi (17 to 21 MPa)], and good solvent resistance. Processing, however, is difficult because there is not much flow above its glass-transition point of 275 °C. Acetylene-terminated imidesulfone ($ATPISO_2$), an addition polymer, is not quite as strong as $PISO_2$, but it maintains some strength at very high temperatures [500 to 800 psi (3.4 to 5.5 MPa) up to 593 °C]. The cross-linking acetylene end cap gives the polyimide excessive flow, however, and it can bleed during lamination. When these two polyimides are combined in various ratios to form the semi-ipn, the cross-linked $ATPISO_2$, plasticizes the linear thermoplastic while the latter adds toughness to the brittle cured $ATPISO_2$.

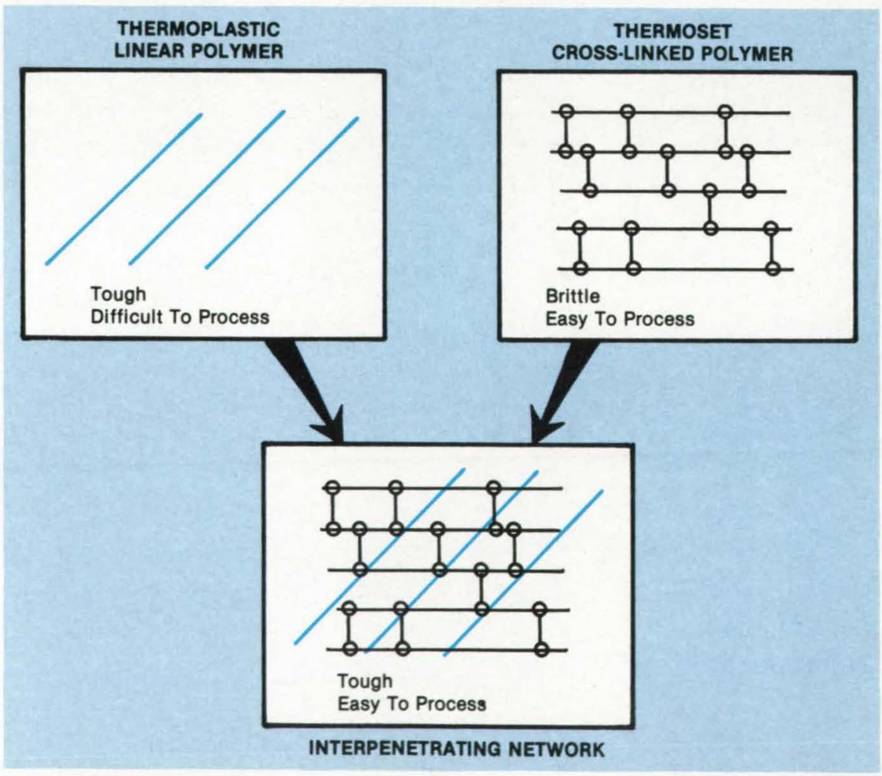

A **Semi-Interpenetrating Network** is formed to different polymers to combine the desirable properties of both.

This network has two other major advantages: First, the polyimides are mutually soluble, eliminating phase-separation problems typical of networks. Second, the flow properties of the network are midway between those of the two individual polymers, making processing easier. In addition, the characterization of these semi-ipn's indicates that several of them had improved thermo-oxidative stabilities and retained adhesive tensile strengths well above 2,000 psi (14 MPa), even after 1,000 hours of aging at 232 °C. Well-consolidated composites were also prepared from the semi-ipn's that yielded good initial mechanical strengths [flexural strength, 111.8 ksi (771.0 MPa), flexural modulus 8.9 Msi (61 GPa)] without optimization work.

These results indicate that semi-interpenetrating network formation is a way to enhance the properties of existing polymer systems. It is an avenue of investigation open to many polymer systems previously thought to have been fully developed.

This work was done by Terry L. St. Clair of **Langley Research Center** *and Annemarie O. Egli of PRC Kentron, Inc. For further information, Circle 156 on the TSP Request Card.*

This invention is owned by NASA, and a patent application has been filed. Inquiries concerning nonexclusive or exclusive license for its commercial development should be addressed to the Patent Counsel, Langley Research Center [see page 17]. Refer to LAR-13450.

Noble Metals Would Prevent Hydrogen Embrittlement

Hydrogen in solid solution is immobilized at palladium or platinum sites.

Marshall Space Flight Center, Alabama

According to a proposal, the addition of small amounts of noble metals would make iron- and nickel-based alloys less susceptible to embrittlement by hydrogen. Metallurgists have demonstrated that adding 0.6 to 1.0 percent by weight of Pd or Pt eliminates stress/corrosion cracking in type 4130 steel. The proposal is based on the assumption that similar levels (0.5 to 1.0 weight percent) of the same elements will be effective against hydrogen embrittlement.

The noble metal acts as a catalyst for the recombination of hydrogen atoms. A noble-metal site in the alloy lattice traps two hydrogen atoms (see figure) by causing them to recombine into a molecule of H_2 gas. This prevents the atoms from migrating in solid solution as protons toward the tip of a crack. Since this proton migration causes embrittlement, preventing it is expected to make the alloy more resistant to embrittlement.

This work was done by Neil E. Paton and Jon D. Frandsen of Rockwell International Corp. for **Marshall Space Flight Center**. *No further documentation is available.* MFS-29114

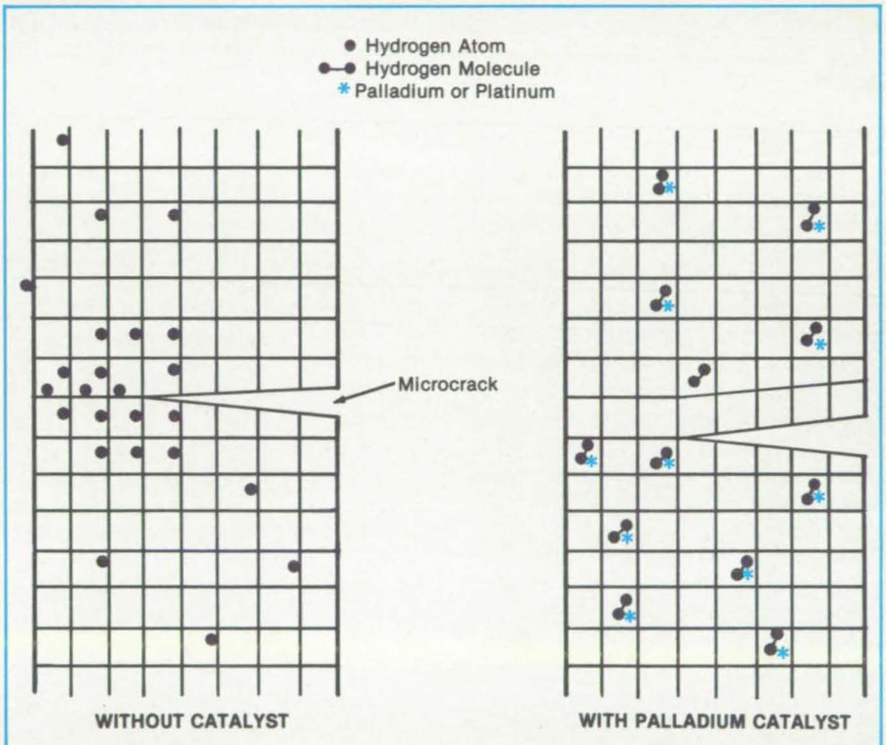

Without Pd or Pt Sites, protons drift toward the tip of a microcrack. With a Pd or Pt catalyst, however, hydrogen is trapped and is less likely to cause embrittlement.

Progress Toward Monolithic Peritectic Solidification

Reducing convection during plane-front, two-phase peritectic solidification reduces banding.

Marshall Space Flight Center, Alabama

Experiments show that reducing radial thermal gradients and flattening the solidification interface — which reduces the level of convection occurring at the interface — reduces the compositional banding associated with plane-front, two-phase peritectic solidification. Consequently, the possibility of coupled two-phase peritectic composite solidification still exists. Previously, it had been thought that banding was inevitable.

Many important materials, including most cobalt-base superalloys, rare-earth magnetic compounds, and A_3B superconductors, solidify via peritectic reactions. Although aligned two-phase composites are desirable forms of these materials, previously available processing techniques have not yielded aligned fibrous or lamellar two-phase composite structures.

Since plane-front directional solidifica-

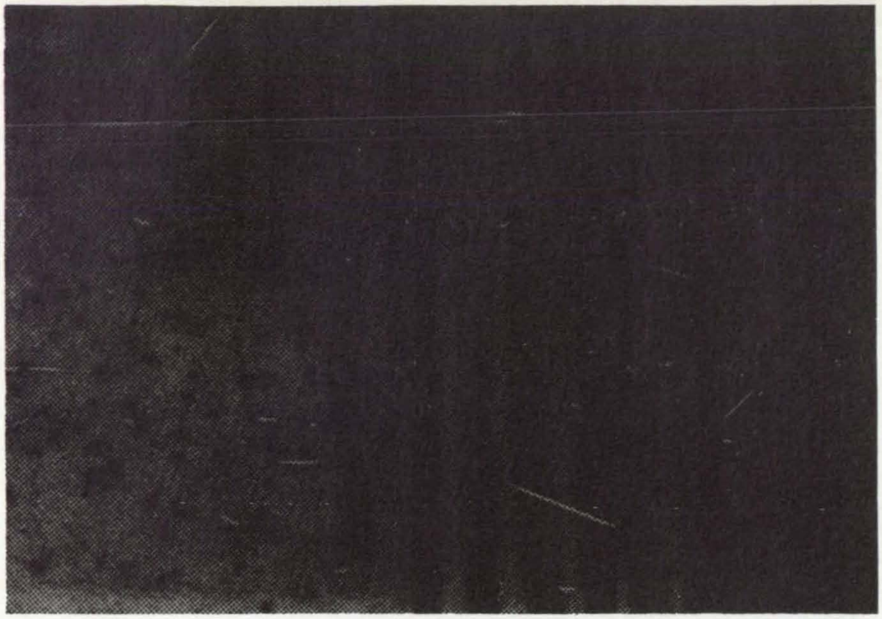

Figure 1. **Morphological Transition** from $\alpha + \beta$ to β showing banding in the presence of convection.

tion has been shown to produce aligned composites for eutectic, off-eutectic, and monotectic solidification reactions, the directional-solidification approach is an attractive candidate for processing peritectics. However, the anticipated peritectic two-phase composite microstructures have not been realized experimentally.

Applied to the case of the peritectic Sn/Cd system, constitutional-supercooling criteria successfully predicted an approximate ratio of thermal gradient to solidification velocity (G/V), above which nonplanar (dendritic or cellular) growth would not occur for hypoperitectic alloys. Experimentally, no coupled, eutecticlike, growth was observed; when the G/V ratio was in excess of that required by the constitutional-supercooling criteria, samples solidified with planar interfaces — but with a structure characterized by alternating bands of the α and β solid phases (having differing compositions) arrayed perpendicularly to the growth direction. In a related analysis of a two-phase lamellar peritectic system, the peritectic undercooling vs. velocity and lamellar spacing was found to differ greatly from the eutectic case; these differences implied growth instability and possibly precluded coupled growth in peritectic systems.

The accompanying figures illustrate morphological transitions from the α and β to peritectic β structure, showing the sensitivity of the morphology to the presence of convection.

Figure 1 shows the banded planar/planar α/β transition for the Pb/Bi peritectic system. Banding has been reported in both convectively-stabilized and destabilized peritectic-alloy systems.

However, reducing the level of convection by minimizing the radial thermal gradients in the vicinity of the solidification interface and by flattening the interface reduced the amount of banding (see Figure 2). This demonstrates that banding may not be inevitably associated with plane-front, two-phase peritectic solidification and allows hope for the possibility of coupled two-phase composite solidification.

This work was done by David J. Larson, Jr., William Poit, Jr., and Ron G. Pirich of Grumman Aerospace Corp. for **Marshall Space Flight Center**. *For further information, Circle 102 on the TSP Request Card.*
MFS-28079

Figure 2. **Morphological Transition** from $\alpha + \beta$ to β showing the absence of banding when convection is suppressed.

Books and Reports

These reports, studies, and handbooks are available from NASA as Technical Support Packages (TSP's) when a Request Card number is cited; otherwise they are available from the National Technical Information Service.

Flexural Properties of Aramid-Reinforced Pultrusions

Four resin systems show improved properties after postcuring.

A comparison of flexural properties has been made of pultrusions reinforced by Kevlar (or equivalent) aromatic polyamide and having constant fiber volume and varied matrices, pretreatments, and postcures. The objective of the study was to improve flexural properties of pultrusions reinforced with Kevlar (or equivalent). Advantages of using the pultrusion process, over conventional hand-layup methods include higher production rates, low facility and labor requirements, and reduced manufacturing costs of advanced composites.

Composite materials containing Kevlar 49 (or equivalent) reinforcement and having equal fiber volume and varied thermosetting-polymer matrices were pultruded and flexurally tested to failure. Pultrusions of both sized and unsized Kevlar were compared to determine the effects of sizing compounds and postthermal treatments on flexural strength as an indication of fiber wettability and fiber-to-resin interface bonding. The pultruded materials were flexurally tested in the "as-pultruded" condition and also after

THE FIRST NAME IN DIGITAL SCOPES

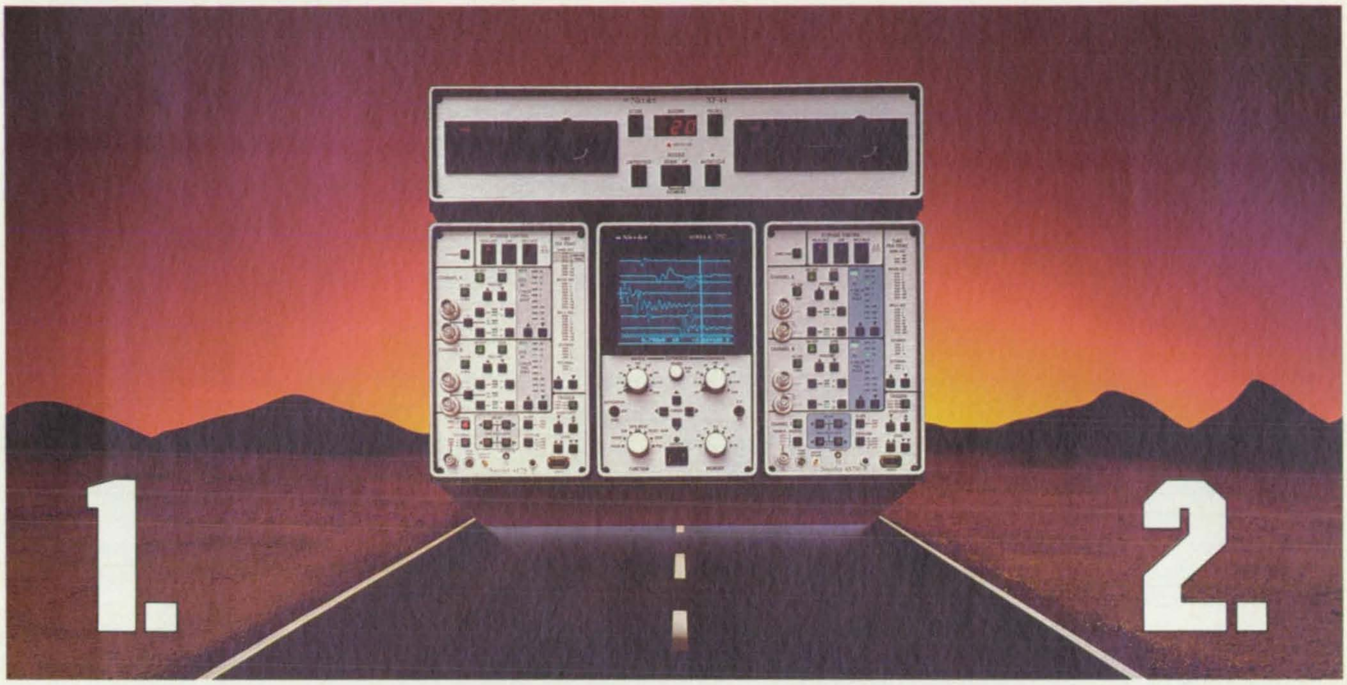

TWO DIGITAL SCOPES IN ONE.

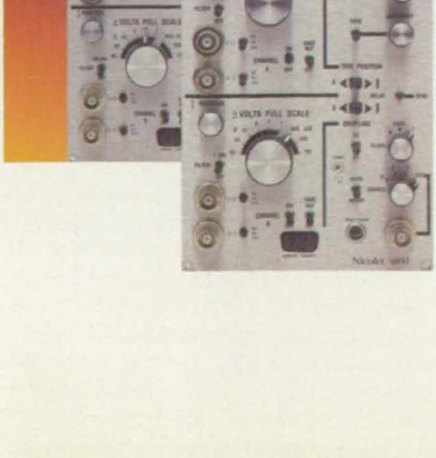

The Acquisition.

With sweep speeds from days to nanoseconds and resolution up to 15 bits, the 4094 digital 'scope can capture the most elusive signals. Every plug-in has 16K of memory, viewable trigger set-up and independent pre- or post-trigger delay on each channel. Signal averaging is standard and our latest 10 MHz/12-bit plug-in even offers real time manipulation of the incoming signals. With two plug-ins the 4094 can record four channels simultaneously. Or even monitor two slow signals and capture high speed glitches at the same time. All under computer control or via manual operation: whatever your application demands.

The Analysis.

Expand and examine any waveform feature in detail. Use the dual cursors and numerics to measure the time or voltage of any point. Compare live or stored waveforms with each other or with pre-recorded references. Store signals on disk manually or automatically. Use pushbutton programs to manipulate the data or send it to your computer via GPIB or RS232 interface. Complete your report with a hardcopy plot using the XY/YT recorder or digital plotter outputs.

First Time, Everytime.

Don't miss important data because of set-up errors. From the World's first in 1973 to the latest models, Nicolet 'scopes are easy to use. Find out how they can be the quickest solution to your signal problems. For more information call 608/273-5008, or write Nicolet Test Instruments Division, P.O. Box 4288, 5225 Verona Road, Madison, WI 53711-0288.

Nicolet

Circle Reader Action No. 350

various postcuring treatments. The ASTM Standard D790 three-point flexural test was used: This is a simple and economical method for comparing the results obtained by varying processing parameters for the purpose of improving strength properties. Its failure mode is a combination of compression, tension, and shear.

Four resin matrix systems were used. Improvements in flexural strength as a result of pretreatments with sizing solutions were marginal. The most significant improvements in flexural properties occurred as the result of postcuring treatments. The flexural strength of each pultrusion increased because of postcuring in the following order: (1) polyester matrix material, 87 percent; (2) vinyl ester, 50 percent; (3) first epoxy system, 19 percent; and (4) second epoxy system, 17 percent. The two conventional pultrusion matrices, polyester and vinyl ester, exhibited the greatest flexural-strength increases as the result of postcuring. The second epoxy pultrusion had the highest flexural strength in all conditions.

The fact that postthermal treatments improved flexural properties of all four pultrusions indicates that full cure did not occur in any resin system during the pultrusion process. Although the increased flexural strengths of the polyester and vinyl ester pultrusions were the most surprising, overall test results indicate that the most-promising resin system of the four is the second of the epoxy systems used. More tests need to be conducted to determine the thermo-oxidative stability at postcuring temperatures of sizing compounds and resin systems used in pultrusion.

This work was done by Maywood L. Wilson, Gary S. Johnson, and Ian O. MacConochie of **Langley Research Center**. *For further information, Circle 66 on the TSP Request Card.*
LAR-13442

High-Strength Glass for Solar Applications

Technology for strengthening thin sections is reviewed.

A report reviews the technology of high-strength glass for such solar applications as heat collectors, reflectors, and photovoltaic arrays. The report discusses the most feasible methods — heat strengthening and chemical strengthening — of increasing the strength of glass for solar-energy use. It also estimates the cost and availability of high-strength glass and considers physical characteristics, amenability to back-silvering, and the effects of atmospheric contamination.

Both glass-strengthening methods create residual compression in the glass surface. Brittle materials like glasses tend to fracture in tension at the surface. The precompression therefore makes thin glass less likely to fracture on impact — by impinging hailstones, for example.

In heat strengthening, the surface of the molten glass is quenched by a flow of air (sometimes water or oil) while the glass is still viscous. The surface is thus rapidly cooled to a temperature lower than that of the core. Since the core initially remains hot and viscous, it flows to accommodate the surface shrinkage, and no stress is introduced. Then, as the core cools, it attempts to contract between the unyielding surface layers, thereby setting up tension in the core and compression in the surface layers. The residual compression increases the strength to more than twice that of ordinary annealed glass.

Heat strengthening is easy and inexpensive. However, it is hard to control and may create nonuniform surface stress.

In chemical strengthening, surface compression is induced by replacing sodium ions with larger potassium ions. Usually the surface is treated with a molten potassium salt like potassium nitrate at about 400 °C. Although chemical strengthening is more expensive than heat strengthening, it gives higher strength — 10 to 20 times that of ordinary annealed glass. It also produces a uniform surface stress.

This work was done by Frank L. Bouquet of Caltech for **NASA's Jet Propulsion Laboratory**. *To obtain a copy of the report, "High Strength Glass for Solar Applications: A Technology Review," Circle 62 on the TSP Request Card.*
NPO-16536

Transparent Analogs for Alloy Phase Studies

Experiments are safer, easier, and cheaper than they are with metals.

A report describes experiments to add information to the data base supporting the use of transparent, partially miscible liquids and solids as analogs in studies of alloy solidification. The behavior of these materials can be observed directly while they undergo liquid/liquid and liquid/solid phase transformations. Light-scattering techniques can be used to determine phase boundaries. Thus the transparent

Multiple Pages Intentionally Left Blank

analogs allow the observation of both solidification patterns and the processes leading to those patterns, whereas metal alloys require tedious post-solidification metallographic analyses because the processes cannot be generally observed. Furthermore, experiments with the transparent substances are safer and cheaper because they are conducted at much lower temperatures; typically, at −50 to +150 °C.

The immediate objective of these experiments was to determine the monotectic phase diagrams of several binary and pseudobinary mixtures that had previously been identified as suitable analogs. These included succinonitrile (SN)/ethanol, SN/azeotropic ethanol and water, SN/benzene, SN/toluene, SN/cyclohexanol, and SN/ordinary and heavy water.

The SN/ethanol/water experiments helped to explain the disappearance of a phase interface at lower than the expected temperature in a previous experiment on SN and nominally pure ethanol. Pure ethanol is hygroscopic and continues to absorb water from the air when mixed with SN. As the water content increases, the monotectic point changes from a temperature of 14.775 °C and a composition of 25.8 weight percent ethanol to a temperature of 12.289 °C and a composition of 24.19 weight percent azeotropic ethanol and water.

The measurements on benzene yielded the monotectic point (11.45 °C, 36.90 weight percent benzene), the eutectic point (−2.14 °C, 93.30 weight percent benzene), and the critical point (39.83 °C, 66.83 weight percent benzene). Because of the carcinogenicity of benzene, toluene was investigated as a possible replacement. SN/toluene was found to have interesting properties, including a monotectic temperature of 30.46 °C, which is just far enough above room temperature to be useful for growth-rate and directional-solidification experiments. The high volatility of toluene makes it unsuitable for experiments above 70 °C, where it vaporizes rapidly, reducing the toluene concentration in the mixture.

The SN/cyclohexanol experiments gave results in fair agreement with earlier experiments, except in the regions of low minority-phase concentration. The discrepancies are attributed to the fact that the cloud point cannot be observed visually until the materials are cooled well into the temperature/composition region of immiscibility.

The SN/(H_2O/D_2O) mixtures are of special interest because with the addition of a suitable amount of D_2O it is possible to achieve mutual buoyancy. The monotectic temperature and composition were 20.67 °C and 9.38 weight percent, respectively, for D_2O. The values for H_2O differed slightly, being 18.82 °C and 9.41 weight percent, respectively. These and other equilibrium properties changed with the relative D_2O and H_2O concentrations in a manner consistent with the previously known differences between D_2O and H_2O.

Of particular interest is a mixture of SN with 13.44 weight percent D_2O and 85.56 weight percent H_2O, in which the constituents are mutually buoyant at 20 °C. The mixture behaves more like SN/D_2O when rich in SN and more like SN/H_2O when rich in the water solution. This problem is attributed to a preferential interaction of SN with D_2O, causing a rejection of H_2O and a redistribution of SN from the SN-rich phase.

This work was done by, Donald O. Frazier of **Marshall Space Flight Center** *and James E. Smith, Jr., of the University of Alabama. To obtain a copy of the report, "Experimental Determination of Systems Suitable for Study as Monotectic Binary Metallic Alloy Solidification Models," Circle 143 on the TSP Request Card.*

MFS-27109

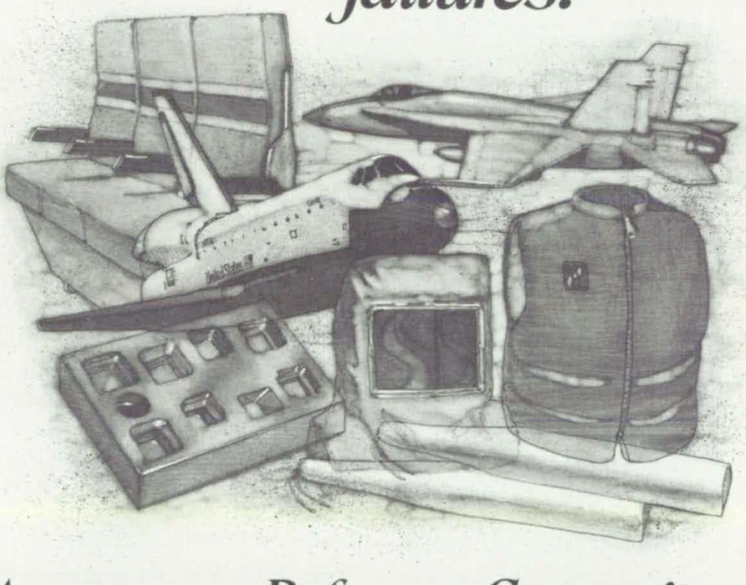

Computer Programs

56 Computer Simulation of Ablator Charring
58 Calculating Sonic-Boom Propagation
58 Predicting Spacecraft Trajectories
58 Computing Jet-Exhaust/Crossflow Interactions

COSMIC: Transferring NASA Software

COSMIC, NASA's Computer Software Management and Information Center, is the one central office established to distribute software that is developed with NASA funding. COSMIC's role as part of NASA's Technology Utilization Network is to ensure that NASA's advanced software technology is made available to industry, other government agencies, and academic institutions.

Because NASA's software development efforts are dynamic and ongoing, new programs and updates to programs are added to COSMIC's inventory on a regular basis. *Tech Briefs* will continue to report information on new programs. In addition, the 1986 edition of the *COSMIC Software Catalog* is available with descriptions and ordering information for available software. Several new programs for control systems/robotics, expert systems, thermal analysis, turbomachinery design, structural analysis, and computer graphics are offered.

For additional information on any programs described in this issue of *Tech Briefs*, circle the appropriate number on the TSP card at the back of the publication. If you don't find a program in this issue that meets your needs, you can call COSMIC directly at (404) 542-3265 and request a review of programs in your area of interest. There is no charge for this information review.

COSMIC®
Computer Services Annex, University of Georgia, Athens, GA 30602; Phone (404) 542-3265
John A. Gibson, Director

Computer Programs

These programs may be obtained at a very reasonable cost from COSMIC, a facility sponsored by NASA to provide tested and reliable software to the public. For information on program price, size and availability, circle the reference number on the TSP and COSMIC Request Card in this issue.

Materials

Computer Simulation of Ablator Charring

Pyrolysis effects in spacecraft re-entry shielding are calculated.

The transient response of a thermal-protection material to heat applied to its surface can be calculated using the CHAP III computer program. CHAP III can be used to analyze the chemical kinetics of pyrolysis gas in detail and examine pyrolysis reactions-in-depth. The analysis includes the deposition of solid products produced by chemical reactions in the gas phase. CHAP III uses a modeling technique that can approximate a wide range of ablation problems.

The energy equation used in CHAP III incorporates pyrolysis (both solid and gas reactions), convection, conduction, storage, work, kinetic energy, and viscous dissipation. The chemically reacting components of the solid are allowed to vary as a function of position and time. CHAP III employs a finite-difference method to approximate the energy equations. Input values include the specific heat, thermal conductivity, thermocouple locations, enthalpy, heating rates, and a description of the chemical reactions expected. The output tabulates the temperature at locations throughout the ablator, the gas flow within the solid, the density of the solid, the weight of pyrolysis gases, and the rate of carbon deposition. A sample case analyzes several pyrolysis reactions in an ablative material subjected to an environment typical of entry at lunar-return velocity.

CHAP III is written in FORTRAN IV for batch execution and has been implemented on a CDC CYBER 170-series computer operating under NOS with a central-memory requirement of approximately 102K (octal) of 60-bit words. This program was made available to the public in 1985.

This program was written by Columbus W. Stroud, Lona M. Howser, and Kay L. Brinkley of **Langley Research Center**. *For further information, Circle 73 on the TSP Request Card.*
LAR-13502

Mechanics

Calculating Sonic-Boom Propagation

Nonlinear effects are included, enabling more-realistic modeling.

The Modified Method of Characteristics Sonic Boom Extrapolation Program (MMOC) is a computer program for sonic-boom propagation that includes shock coalescence and incorporates the effects of asymmetries due to volume and lift. MMOC numerically integrates the nonlinear governing equations using data on an initial data line approximately one body length from the aircraft and yields the sonic-boom pressure at the ground as a function of time or of position at a given time.

Variations in entropy, enthalpy, and gravitational effects are accounted for in the governing equations, and because nonlinear terms are retained in the equations, extrapolation can begin nearer the body, where nonlinear effects are strong. This feature of MMOC allows wind-tunnel sonic-boom models to be built up to 3 ft (0.9 m) in length and thus enables more detailed, realistic models than did the previous 6-in. (15-cm) sizes.

The method of solution is based on an extension of the axisymmetric solution. A second set of governing equations is developed by taking the circumferential derivatives of the standard governing equations, and asymmetries are felt by an iterative solution between the two sets of equations. Initial flow-field data, circumferential derivatives of flow-field data, and shock locations are required on the initial data line approximately one body length from the aircraft. These data may be supplied from numerical methods or from experimental methods. The method-of-characteristics approach used in MMOC allows large computational steps to be taken in the radial direction without loss of accuracy.

The data required by MMOC include the mach number, shock angle, flow angles, and temperature. When the calculations reach the ground level, the overpressure and locations are printed, allowing the user to plot the pressure as a function of time or of position at a given time. The MMOC package contains a uniform-atmosphere pressure-field program and interpolation routines, which were used to generate required input for the sample cases.

MMOC is written in FORTRAN IV for batch execution and has been implemented on a CDC 170-series computer operating under NOS with a central-memory requirement of approximately 223K of 60-bit words. This program was developed in 1983.

This program was written by Christine M. Darden of **Langley Research Center** *and Lu Ting of New York University. For further information, Circle 141 on the TSP Request Card.*
LAR-13473

Predicting Spacecraft Trajectories

Calculations include drag, nonsphericity, and other perturbations.

The Artificial Satellite Analysis Program (ASAP) is a general orbit-prediction program that incorporates sufficient orbit-modeling accuracy for mission design, maneuver analysis, and mission planning. ASAP is suitable for studying planetary orbit missions with spacecraft trajectories of exploratory (mapping) nature. Sample data are included for the study of the drift cycle of a geosynchronous station, a strategy for mapping Venus by radar, a frozen orbit about Mars, and a repeat-ground-trace orbit.

ASAP uses Cowell's method in the numerical integration of the equations of motion. The orbital-mechanics calculation contains perturbations due to nonsphericity of the planet, lunar and solar effects, and drag. The input includes the classical osculating elements, orbital elements of the sun relative to the planet, reference time and dates, drag coefficient, gravitational constants, and planet radius, rotation rate, etc.

The printed output contains Cartesian coordinates, velocity, equinoctial elements, and classical elements for each time step or event step. At each step, selected output is added to a plot file. The ASAP package includes a program for sorting this plot file. LOTUS 1-2-3 is used in the supplied examples to graph the results, but any graphics software package could be used to process the plot file.

ASAP is written in FORTRAN 77 for batch execution and has been implemented on an IBM PC computer operating under DOS. The ASAP package requires the 8087 math-coprocessor. This program was developed in 1985.

This program was written by Johnny Kwok of Caltech for **NASA's Jet Propulsion Laboratory**. *For further information, Circle 61 on the TSP Request Card.*
NPO-16731

Machinery

Computing Jet-Exhaust/Crossflow Interactions

Outputs include velocity and pressure fields, forces, and moments.

The JETPLT and JETBOD programs were developed to predict the velocity and pressures induced by subsonic jets exhausting into a subsonic free stream. JETPLT predicts pressures induced on an infinite flat plate by a jet exhausting at angles to the plate. JETBOD, in conjunction with a panel code, predicts pressures induced on a body of revolution by a jet exhausting perpendicularly to the surface. These programs have been used to investigate the interactions between jet exhausts and crossflows in vertical/short-takeoff-and-landing aircraft shifting from hover to forward flight, where the induced-pressure loading can lead to a reduction in lift.

Both programs use a potential model of the jet and adjacent surface with empirical corrections for viscous or nonpotential effects. The analytical method can optionally include models for the blockage and entrainment properties of the jet. Input variables include the ratio of the jet-exhaust speed to free-stream speed, the size and shape of the jet, the body-control points, and the inclination of the jet. The JETBOD input requires the body-of-revolution shape from a modified potential-flow program, which is included in this package. Output from JETPLT/JETBOD consists of induced-velocity fields, pressures, and coefficients for the normal force and the pitching moments.

JETPLT/JETBOD is written in FORTRAN 77 for batch execution and has been implemented on a DEC VAX series computer operating under VMS with a central-memory requirement of approximately 359K of 8-bit bytes. This program was developed in 1984.

This program was written by S. C. Perkins, Jr., and M. R. Mendenhall of Nielsen Engineering and Research, Inc., for **Ames Research Center**. *For further information, Circle 80 on the TSP Request Card.*

Inquiries concerning rights for the commercial use of this invention should be addressed to the Patent Counsel, Ames Research Center [see page 17]. Refer to ARC-11597.

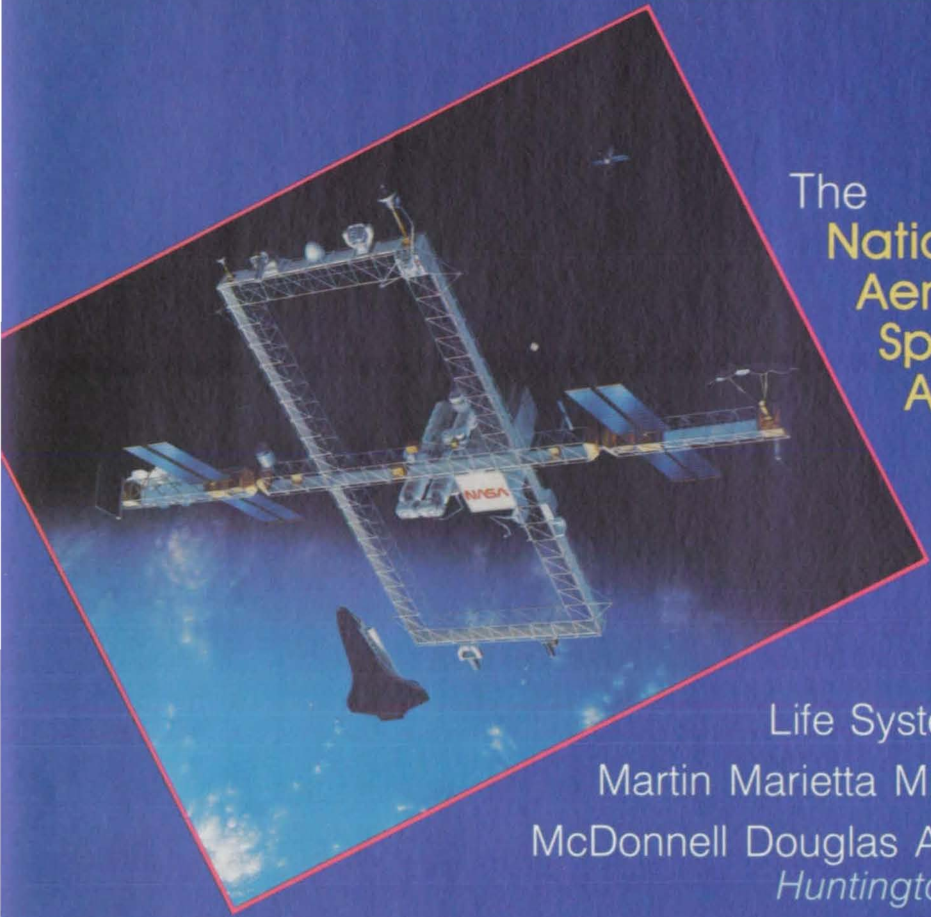
NASA

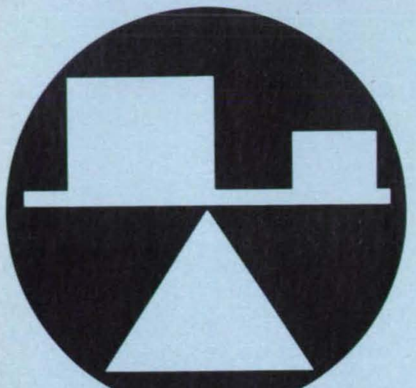

Hardware, Techniques, and Processes

60 Portable, Controlled-Load-Rate Tension Tester
61 Active-Control Bearings For Rotor Shafts
63 Noncontacting Measurement of Shaft Angle
63 Measuring Leakage From Large, Complicated Machinery
64 Reducing Fatigue in a Rotary Flowmeter

Books & Reports

64 On-Orbit System Indentification
65 Deployable Brake for Spacecraft

Computer Programs

58 Calculating Sonic-Boom Propagation
58 Predicting Spacecraft Trajectories

Portable, Controlled-Load-Rate Tension Tester

Damaging mechanical shocks are suppressed.

Marshall Space Flight Center, Alabama

A tensile-testing machine for ceramic and foam materials has a self-contained air supply with a built-in airflow controller. Unlike machines that rely on external air from a fixed source, the new machine can easily be moved to the point of use, and loads are applied automatically at a constant rate of increase, without fluctuations caused by manual control of the supply pressure. In addition, the new machine eliminates impact after failure of a specimen so that it does not damage itself.

The machine tests cylindrical plug specimens. First, a sheet of the specimen material is bonded to an aluminum

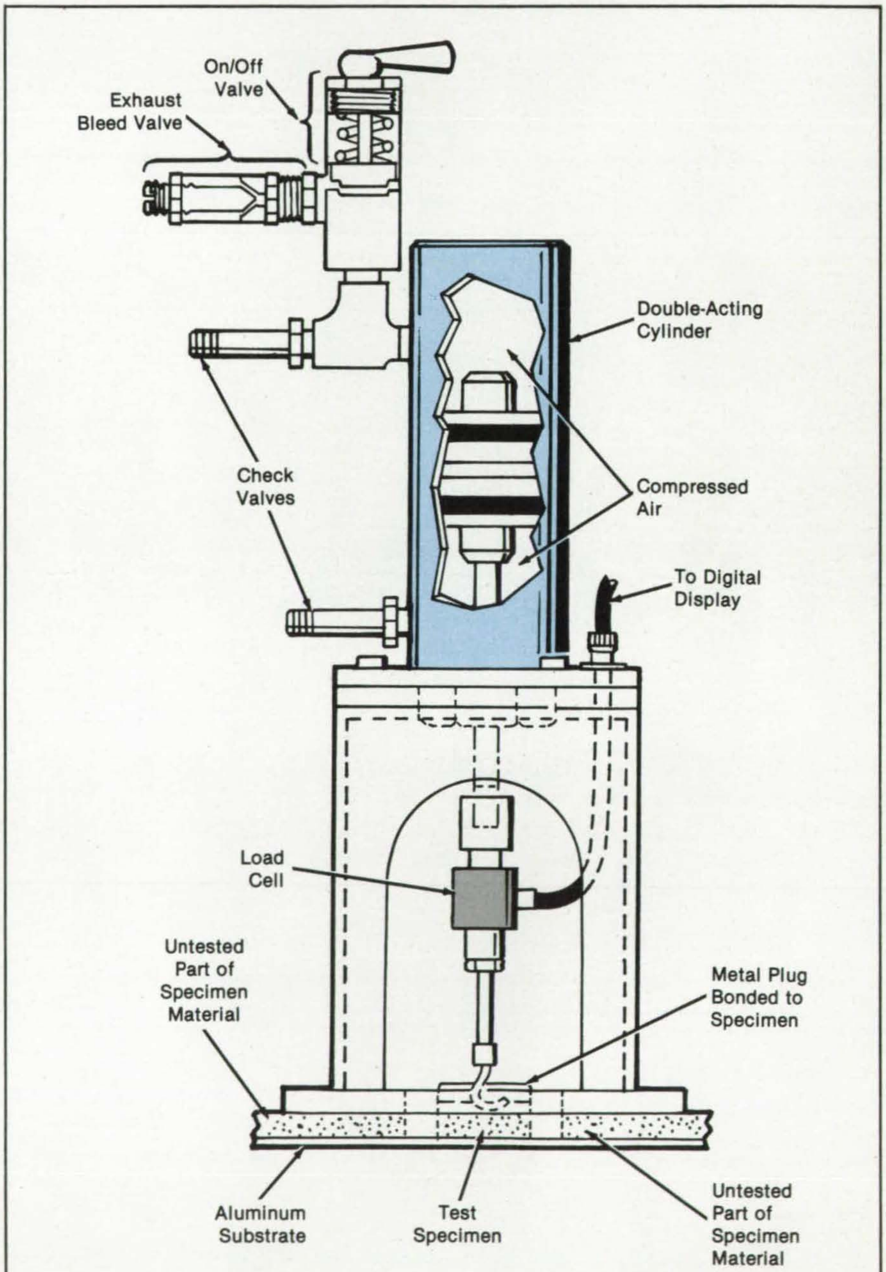

As the Exhaust-Control Valve Bleeds Air from the upper chamber, pressure in the lower chamber forces the piston upward. Tension is thereby created in the test plug. The check valves permit the two chambers to be charged with high-pressure air before a test.

substrate. Then a fly cutter, hole saw, or trepanning tool cuts through the sheet to the substrate so that a core or plug is isolated from the sheet by a cylindrical gap. A metal button is bonded to the top of the plug. The substrate and sheet are mounted in the test machine, and the tension hook of a load cell is attached to the button (see figure).

The tester employs a double-acting pneumatic cylinder with an exhaust-speed control unit to apply tension to the plug. The bottom and top chambers of the cylinder are precharged with compressed air. An operator opens a valve on the top chamber, releasing air to the exhaust-control unit, which allows air to flow through it at a preset rate that increases the tension on the specimen at the rate specified in the testing standards.

The prechargeable cylinder chambers make it unnecessary to attach the machine to an air line. The machine is therefore mobile and more convenient for users. The exhaust-speed control unit ensures a consistent loading rate. The control unit also prevents the piston from flying upward when a specimen breaks; the air remaining in the top cylinder brakes the piston so that it does not strike the cylinder head and damage the load cell.

In the previous version of the machine, an operator regulated a valve to admit compressed air to the chamber of a single-acting cylinder. The increasing pressure applied increasing tension to the specimen, but there was nothing to restrain the piston when the specimen fractured and failed.

Other potential applications of the machine include tensile tests of large composite parts that may contain localized defects and adhesion tests of virtually any bonded structure. The machine can be modified to accommodate standard tensile-test specimens instead of plugs. Strain gauges could then be used to determine a variety of material properties, including the strain at failure, the modulus of elasticity, and Poisson's ratio, in addition to the tensile strength. The machine can be adapted to compression testing simply by attaching the exhaust-control valve to the bottom cylinder instead of the top.

This work was done by Robert S. Jamieson of Martin Marietta Corp. for **Marshall Space Flight Center**. *For further information, Circle 147 on the TSP Request Card.*

Inquiries concerning rights for the commercial use of this invention should be addressed to the Patent Counsel, Marshall Space Flight Center [see page 17]. Refer to MFS-28075.

Active-Control Bearings for Rotor Shafts

Vibrations are suppressed by feedback control.

Lewis Research Center, Cleveland, Ohio

It is well known that a damped flexible support system can suppress the vibrations of a rotating-shaft system. However, it is very difficult for this method to supply proper damping in practical equipment or to be able to change the damping coefficient to respond to system variations.

Flexural forced vibrations or self-excited vibrations of a rotating system can also be suppressed by active elements. Instead of dissipating vibration forces through damped supports, these active elements apply forces, through the bearing housing, that cancel the vibration displacements. Bearing systems incorporating such devices are appropriately named active-control bearings.

In a practical system with a high-speed rotating shaft, the cancelling forces are best applied to the nonrotating bearing housings. Sensors transmit shaft-vibration displacements to a control device, which integrates these inputs and issues appropriate signals to the devices applying variable loads to the bearing housings.

Active-control-bearing systems are effective not only for imbalance forces but also for unstable forces or external forces transmitted from a foundation. The damping ratios of the system can be easily changed by modifying the state-feedback control system.

This concept has been proof tested at Lewis Research Center using a simple rotor system having one disk mounted on a slender shaft supported at its ends on flexible support bearings (see Figure 1). Each bearing housing was supported by four actuators made from modified electrodynamic transducers (see Figure 2). In the uncontrolled case, the system had two critical speeds at about 750 and 1,000 rpm.

The system was operated using two feedback control concepts: an optimal regulator method and a quasi-model control method. The active-control bearings reduced the maximum displacement amplitude at the lower critical speed to

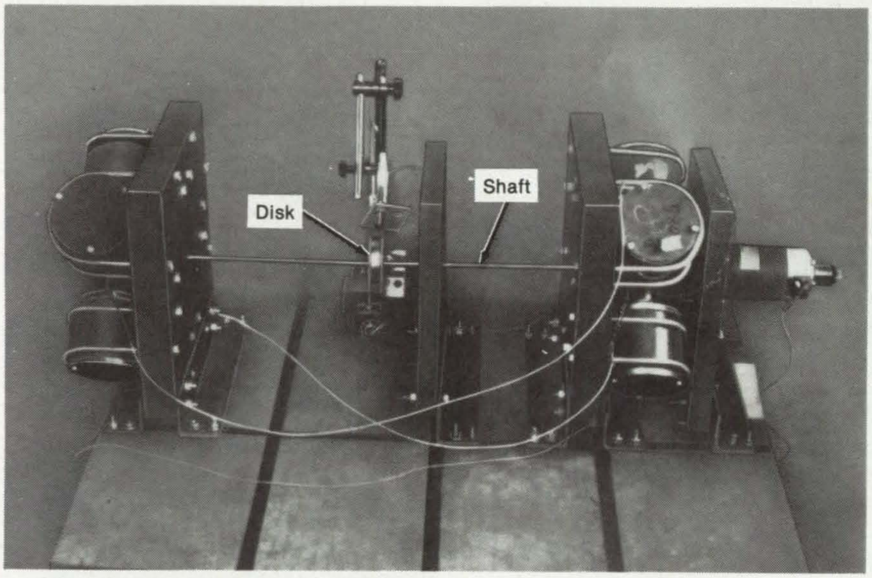

Figure 1. This **Test Rig With a Simple One-Disk Rotor** on a thin shaft was used to test the active-control-bearing concept.

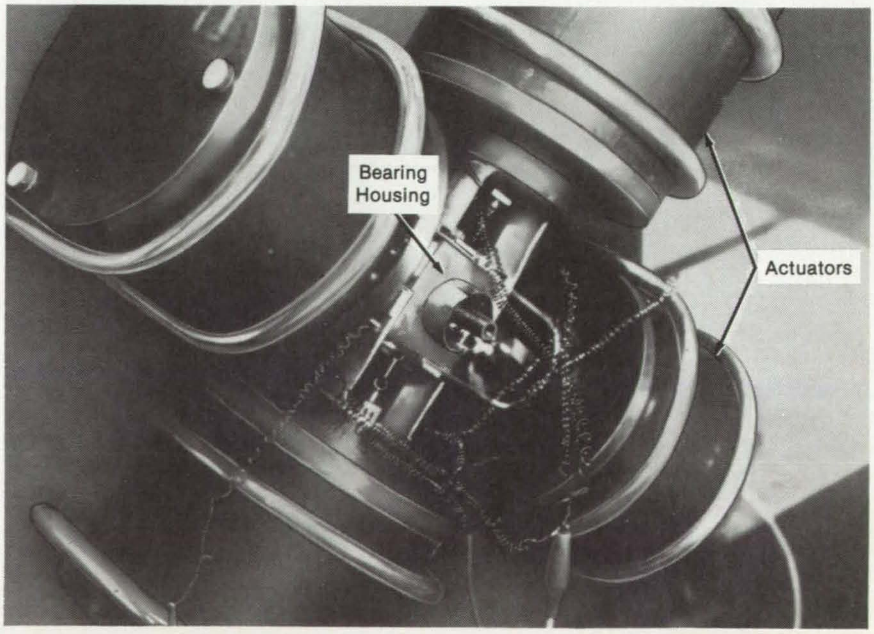

Figure 2. **Four Actuators** support the bearing housing at each end of the rotor shaft and exert the control forces on the housing.

about one-sixth the uncontrolled amplitude.

This work was done by Kenzou Nonami of **Lewis Research Center**. *Further information may be found in NASA TM-87053 [N85-29292/NSP], "Vibration Control of Rotor Shaft Systems by Active Control Bearings."*

Copies may be purchased [prepayment required] from the National Technical Information Service, Springfield, Virginia 22161, Telephone No. (703) 487-4650. Rush orders may be placed for an extra fee by calling (800) 336-4700.
LEW-14319

Noncontacting Measurement of Shaft Angle

A fiber-optic transducer offers several advantages over mechanical linkages.

Marshall Space Flight Center, Alabama

The angular position of a rotary valve is measured by a pair of optical-fiber deflectometers. The measurement device is sensitive, immune to electromagnetic interference, and does not wear out since the fibers do not make contact with the valve. The device is more rugged than are the linear or rotary variable-differential transformers it replaces.

Two gap-measuring fiber-optic probes are installed at the slanted end of the valve shaft. As the shaft rotates, the gaps vary, and the differential electrical output of the fiber-optic transducer changes accordingly. A 10-mil (0.25-mm) increase in the gap produces a 5-V change in output. Gap changes as small as 0.2 μin. (5 nm) are discernible.

The two-probe, differential-gap-measurement technique eliminates errors from radial and axial shaft play. Moreover, since there is no mechanical contact, the position sensor is not subject to mechanical fatigue or chattering.

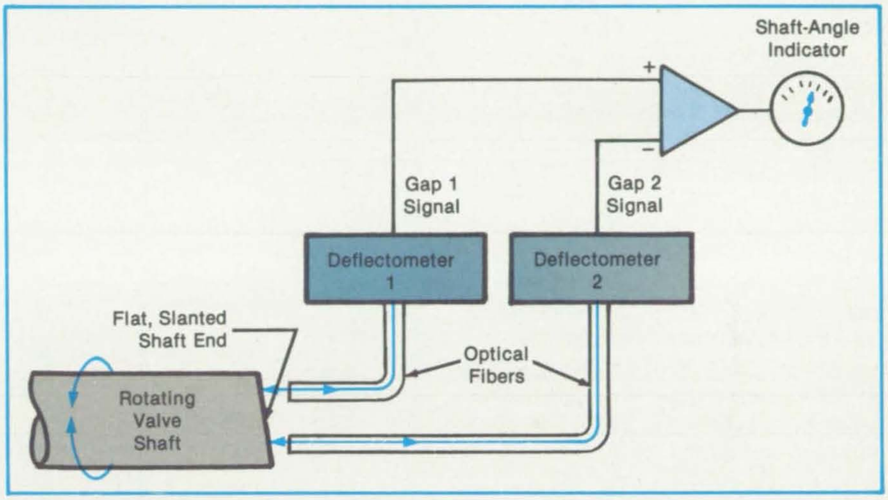

The **Difference in Gaps** between the slanted surface and the fiber-optic probes indicates the angular position of the valve shaft. A small difference in gaps creates a large difference in deflectometer signals.

This work was done by Sarkis Barkhoudarian of Rockwell International Corp. for **Marshall Space Flight Center**. *No further documentation is available.*
MFS-19810

Measuring Leakage From Large, Complicated Machinery

A test chamber is improvised from a large bag.

Marshall Space Flight Center, Alabama

The cumulative sizes of leaks in large, complicated machinery can be measured with a relatively simple variation of the helium leak-checking technique. When used to check the Space Shuttle main engine, the new technique gave repeatable and correct results within 0.5 stdin.^{3}/min (1.4×10^{-7} stdm^3/s).

A test chamber is improvised by enclosing the system or the portion of the system to be checked in a large bag of metallized shipping material. The bag material is a good barrier against helium diffusion. The bag does not have to be sealed tightly or totally free of leaks as long as the bag is purged of helium between tests to keep the helium concentration low.

Fans are enclosed in the bag with the system to be tested, because the technique relies on thorough mixing of the enclosed gases. The fans are turned on, and the whole system or the affected portion is pressurized with helium. The rate of increase of helium concentration in the bag is measured with a gas analyzer. Using this measurement and an estimate of the bag volume (the bag volume cannot be measured), an appropriate helium leak rate is estimated.

Next, without pressurizing the tested assembly, helium is injected through a calibrated flowmeter into the bag at the estimated rate. The rate of increase of helium concentration in the bag is measured during this injection. This measurement is used to calibrate the bag and to correct the previous estimate of the leak rate.

This work was done by S. L. Bottemiller of Rockwell International Corp. for **Marshall Space Flight Center.** *No further documentation is available.*
MFS-19945

Reducing Fatigue in a Rotary Flowmeter

Vanes are repositioned to reduce cyclic buffeting of rotor blades.

Marshall Space Flight Center, Alabama

The redesign of the vanes that straighten the flow of liquid in a rotary flowmeter increases the fatigue lives of the vanes and rotor. The purpose of the vanes is to eliminate turbulence so that the proportionality between the flow and the rotor speed is constant.

Originally, the vanes of the straightener were arranged in a hexagonal pattern reminiscent of a honeycomb or a distorted eggcrate. A radial/azimuthal distorted-eggcrate pattern was also tried. These configurations yielded accurate measurements, but the full length of the wakes of the vanes impinged on the blades every time they aligned — 12 times per blade per revolution. This repeated buffeting and the blade/vane interactions via the wakes eventually caused fatigue failure in the blades and vanes. Spiral vanes were substituted. As expected, they reduced buffeting, but turbulence increased and accuracy suffered.

Finally, the designers of the instrument resorted to a rectangular eggcrate arrangement (see figure). Now the rotors and vanes never align. The lifetimes of the rotor blades and the vanes are prolonged as a result. The nonuniform spacing of the vanes does not reduce accuracy.

This work was done by G. V. R. Rao of Rockwell International Corp. for **Marshall Space Flight Center**. *No further documentation is available. MFS-29038*

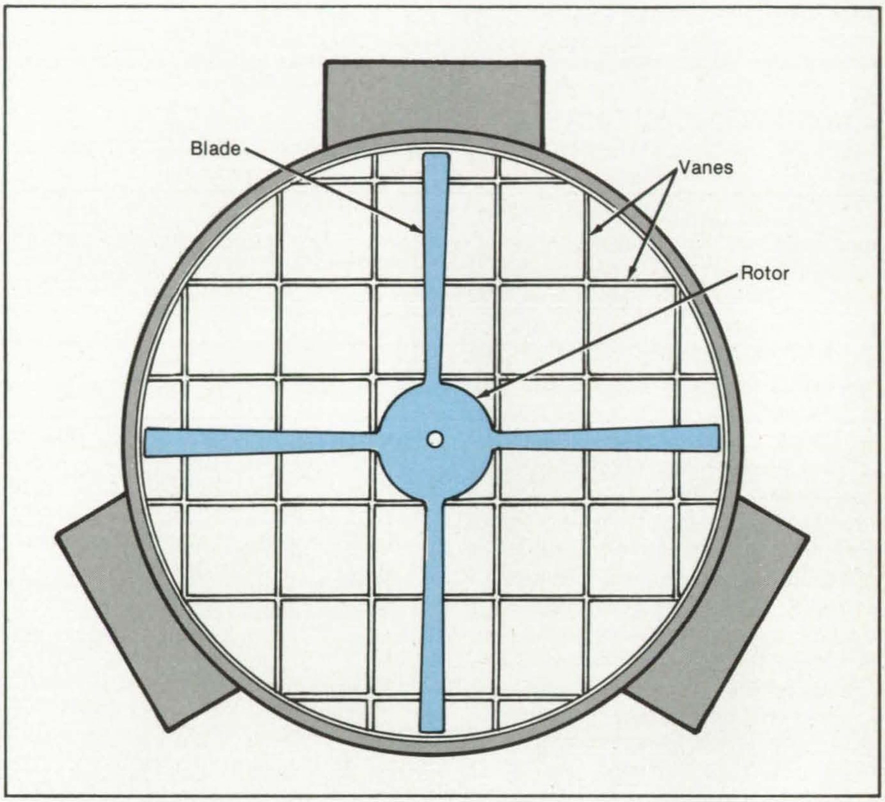

Nonuniform but Symmetrical, the new spacing of straightener vanes prevents the flow wake from strongly interacting with the rotor blades. At the same time, the vanes ensure accurate flow-rate measurement.

Books and Reports

These reports, studies, and handbooks are available from NASA as Technical Support Packages (TSP's) when a Request Card number is cited; otherwise they are available from the National Technical Information Service.

On-Orbit System Identification

Information derived from accelerometer readings would benefit important engineering and control functions.

A 15-page report discusses methodology for the detection, identification, and analysis of motions within a space station. Techniques of vibration and rotation analyses, control theory, statistics, filter theory, and transform methods are integrated to form a system for generating models and model parameters that characterize the total motion of a complicated space station, with respect to both control-induced and random mechanical disturbances.

The system identification process encompasses the entire flow of information from vibrations, rotations, rocket thrusts, crew motions, and the like; through inertial and relative motion sensors to onboard preprocessing and flight-dynamic data-processing systems; and finally, to generation of mathematical models, parameters, and other highly processed data. These data have numerous uses for such purposes as disturbance analysis, fault detection calibration, payload monitoring, attitude control, and management of momentum and vibration.

Potentially, the number of parameters and events of interest is so large that telemetry and data-processing equipment would be overwhelmed if all the parameters were monitored continuously. Therefore, the methodology includes detection algorithms to decide whether to perform a full analysis of a specific parameter, based on a global assessment of the data coming in from sensors all over the space station. With the help of the preprocessors, the detection algorithms thus provide a form of data compression. They enable unscheduled parameter updates by imposing data tests that signal parameter changes or other disturbances.

One of the important objectives is to reconstruct the time histories and power spectra of transients and stochastic disturbing forces and torques. In a test of the ability to do this, a computer simulation was performed on a conceptual space station in which an astronaut pushes off a compartment wall, travels along the compartment, and comes to a stop at the opposite wall. At the same time another astronaut is operating a work station console and generating a strong stochastic background disturbance. The simulated accelerometer data at various points around the station were processed according to the detection and identification algorithms. Both the pushoff/landing as well as the console disturbance were recovered from these data. Extrapolating from this success, the authors anticipate the ability to recover dynamic inputs deeply embedded in other signals, much in the manner of the highly-developed signal-processing techniques of geophysics, radar, and sonar.

This work was done by Edward Mettler, Mark H. Milman, David Bayard, and Daniel B. Eldred of Caltech for **NASA's Jet Propulsion Laboratory.** *To obtain a copy of the report "Space Station On-Orbit Identification and Performance Monitor," Circle 74 on the TSP Request Card. NPO-16588*

Deployable Brake for Spacecraft

An aerodynamic shield that could be opened and closed is proposed.

A report presents concepts for a deployable aerodynamic brake. The brake would be used by a spacecraft returning from a high orbit to a low orbit around the Earth. The spacecraft would make grazing passes through the atmosphere to slow down by the drag of the brake.

The brake would be a flexible shield made of woven metal or ceramic that could withstand the high temperature created by air friction. It would be stored until needed, then would be deployed by a set of struts. With its convex surface directed into the airstream, the shield would reduce the space-vehicle velocity and protect the vehicle from the pressure and heat of reentry. The shield would also provide life so that the depth of penetration into the atmosphere could be controlled during grazing maneuvers. When the maneuvers are finished, the shield would be retractred and stored for later use.

The report describes three alternative deployment concepts:

- Struts would unfold like the ribs of an umbrella to spread the shield.
- Petals would unfurl from a hub.
- A helically wound tube would uncoil and spread out the fabric.

The shield thickness would vary, being heaviest where the air pressure and heat are greatest. Small tubes could be woven into the fabric to carry coolant around the surface. The shield could also be cooled by using an ablative coating.

The deployable shield would be much lighter than the retrorockets needed to effect a similar braking. It would be larger and therefore more protective than a fixed shield. Unlike inflatable drag devices, it would not be subject to collapse when it developed small local leaks.

This work was done by John R. Rausch and John W. Maloney of General Dynamics Corp. for **Marshall Space Flight Center.** *To obtain a copy of the report, "Deployable Aerodynamic Lifting Brake for Space Vehicles and Hypersonic Entry Vehicles," Circle 24 on the TSP Request Card.*
MFS-25702 and MFS-25722

Machinery

Hardware, Techniques, and Processes

66 Heat-Exchanger/Heat-Pipe Interface
67 Changes in Blade Configuration Improve Turbopump
67 One-Dimensional Simulation of Isotropic Radiation
68 Translating Canard
70 Array of Shaped Heat Pipes
71 Braking System for Wind Turbines

Books & Reports

71 Mechanism for Retrieving Satellites From Orbit

Computer Programs

58 Computing Jet-Exhaust/Crossflow Interactions

Heat-Exchanger/Heat-Pipe Interface

A monolithic assembly would be reliable and light in weight.

NASA's Jet Propulsion Laboratory, Pasadena, California

An interface assembly would connect the heat exchanger of a furnace, reactor, or other power source with the heat pipes that carry the heat to the radiator or power-consuming system. One of several concepts proposed for nuclear-power supplies aboard spacecraft, the proposed interface may be useful on Earth in solar thermal power systems, heat engines, and lightweight cooling systems.

The assembly would be made from two monolithic halves, each of which would be hogged out of plate stock and finished by electrical-discharge machining. As shown in the figure, the conceptual assembly integrates the heat exchanger and the heat-pipe ends. Each heat-pipe end shares a common wall with the heat exchanger. After machining and inspection, the assembly halves would be seam-welded together, then the evaporator and other heat-pipe internal parts would be installed and the outer heat-pipe halves welded in place.

Because it minimizes the number of liquid/solid and solid/solid interfaces across which heat must be transferred,

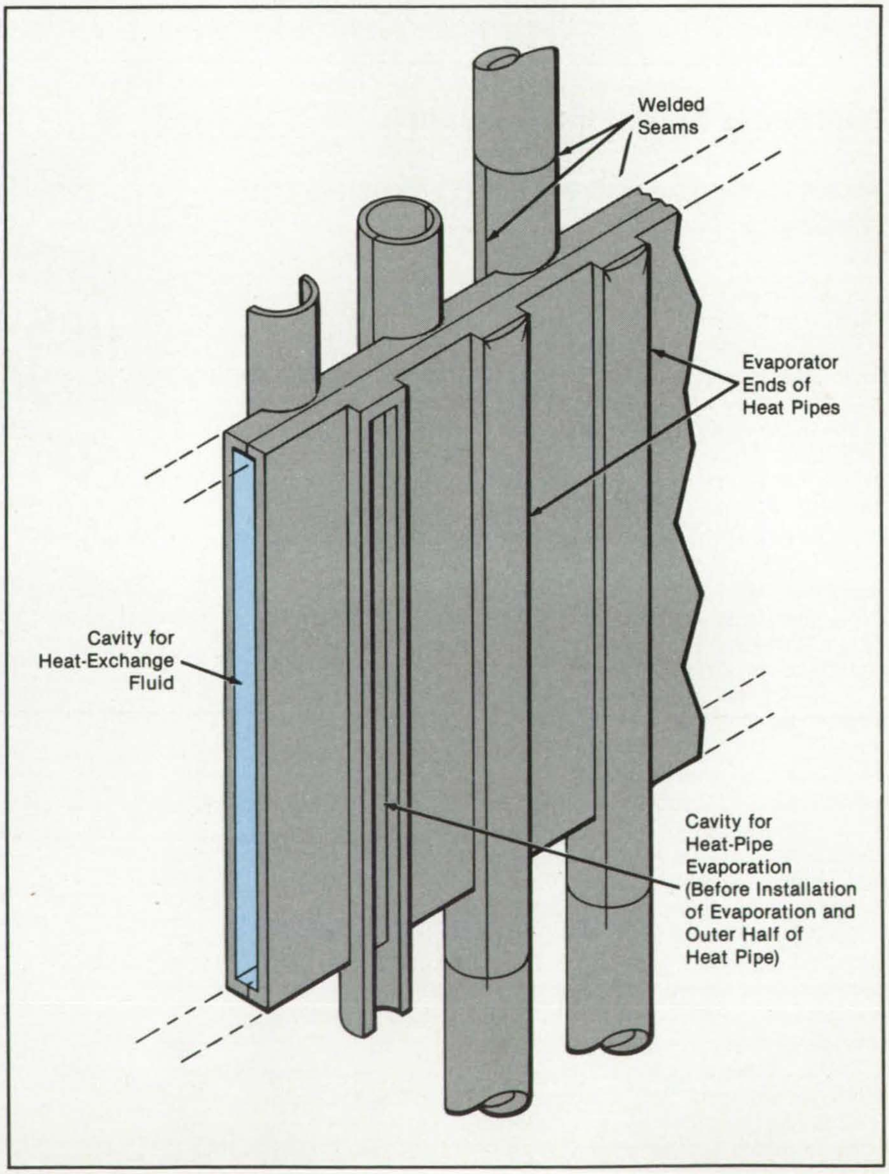

A **Heat Exhanger and the Evaporator Ends of Heat Pipes** are integrated in monolithic halves that are welded together.

the monolithic-assembly design provides low thermal resistance without adding excessive weight. While immersion of the heat pipes in the heat-exchange liquid would also result in low thermal resistance, it would require joints where the heat pipes enter the heat exchanger and would be highly susceptible to mechanical failures of the pipes and the joints. Since there are no such joints in the monolithic assembly, it should be more reliable.

Other advantages of the monolithic-assembly concept include the following:

- It can be inspected and repaired readily;
- It is replaceable;
- Graded thick-to-thin material transitions and ample fillet sections can be provided during machining;
- The heat pipes add stiffness to the heat exchanger;
- There is sufficient room for precise, full-penetration electron-beam welding; and
- All welding is done from the outside.

This work was done by Harold J. Snyder and Thomas H. Van Hagan of GA Technologies, Inc., for **NASA's Jet Propulsion Laboratory.** *For further information, Circle 6 on the TSP Request Card.*
NPO-16456

Changes in Blade Configuration Improve Turbopump

Cavitation is reduced while suction is increased.

Marshall Space Flight Center, Alabama

Tests conducted with a model liquid-oxygen turbopump using water as the pumped fluid confirm that performance is improved by a new "tandem" arrangement of the blades (see figure). The findings are also expected to apply to other pumps having two adjacent rotor rows.

The relative position of the inducer and impeller blades can be optimized to improve pump performance by (1) minimizing the cavitation occurring on the impeller leading edges and (2) reducing losses through better boundary-layer control. The overall length of the pump can also be reduced, thereby improving rotor dynamics. In the tests, the pressure-rise coefficient and the efficiency were increased by about 3 percent by a suitable choice of the "clocking" angle, a measure of the angular orientation of the impeller relative to the inducer.

Further gains can be expected if axial clearance is also optimized. Fluid-dynamic equations suggest that a smaller axial clearance between the impeller leading edge and the inducer trailing edge — possibly even a negative clearance (an intermeshing of the two sets of blades) — would increase the cavitation number by reducing the local relative velocity. In the optimal location, the impeller leading edge would be in a region of higher static pressure, which improves suction performance, an advantage not previously noted in tandem-pump studies.

This work was done by Sen Y. Meng and George E. Bache of Rockwell International Corp. for **Marshall Space Flight Center.** *For further information, Circle 19 on the TSP Request Card.*
MFS-29176

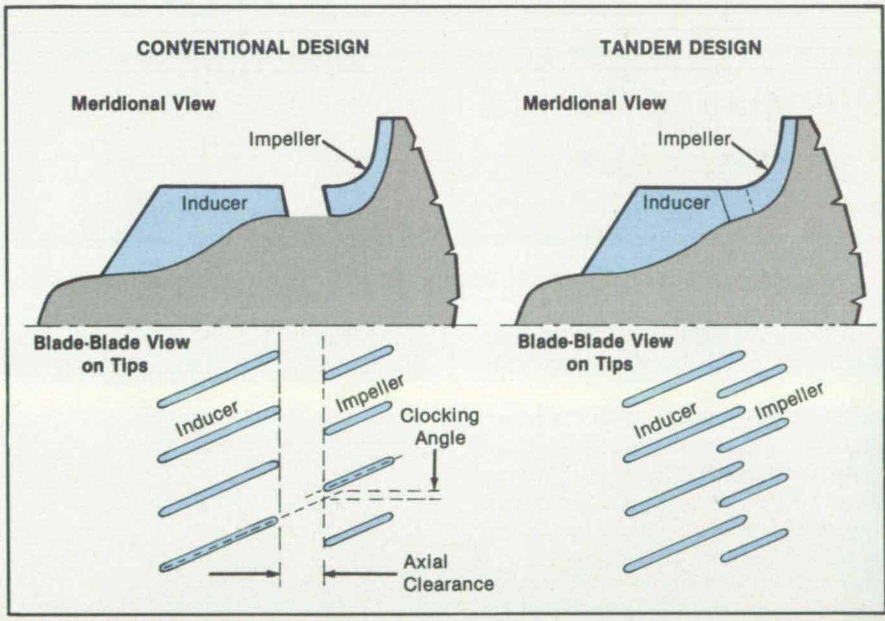

The **Conventional and Tandem Designs** differ in the axial spacings and relative circumferential positions (clocking angle) of the two sets of blades. The choice of clocking angle is critical: in the tests, an angle of 60° improved the performance, whereas an angle of 30° did not.

One-Dimensional Simulation of Isotropic Radiation

Solar cells are tested for effects of radiation in a unidirectional beam.

NASA's Jet Propulsion Laboratory, Pasadena, California

A test setup (see figure) exposes solar cells to the time-average equivalent of isotropic electron and proton radiation, even though the particles come from a single direction. A motor-driven cam rotates a target plate back and forth at a speed proportional to the cosecant of the angle of the incident radiation beam.

In isotropic irradiation, the frequency distribution of the incident particles is proportional to the sine of the angle of incidence. Therefore, to simulate isotropic irradiation of a sample by a unidirectional source of constant intensity, the sample is irradiated at each angle of incidence, with an exposure time inversely proportional to the sine of the angle; in other words, directly proportional to the cosecant. This will ensure that in the average over time, the radiation produces a dose-versus-depth profile that duplicates that from isotropic irradiation.

The motor rotates the cam continuously in one direction. The cam follower slides a carriage back and forth on rails. A rack at the rear of the carriage turns a pinion gear at the lower end of the shaft that holds the solar cells. The rack rotates the shaft back and forth to expose the sample at all angles of incidence between +90° and −90°. The cam groove is shaped to drive the cam follower in a pattern that makes the shaft rotational speed proportional to the cosecant of the angle. The beam is fairly large, encompassing the reciprocating cell specimens as well as stationary cells mounted above for comparison.

This work was done by Bruce E. Anspaugh and R. Gil Downing of Caltech for **NASA's Jet Propulsion Laboratory**. *For further information, Circle 13 on the TSP Request Card.* *NPO-16412*

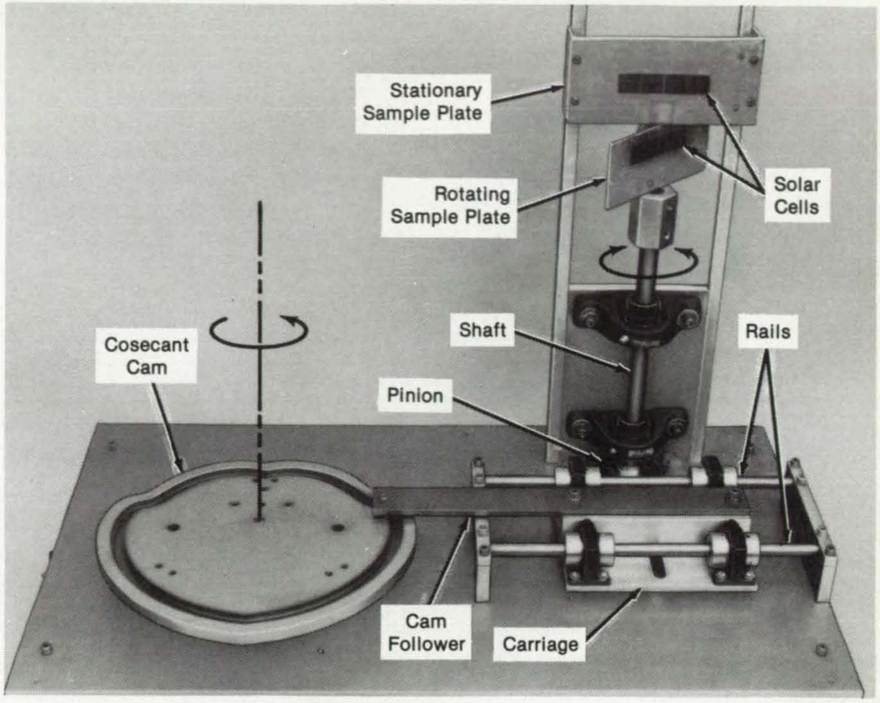

The **Cam Groove Imparts a Cosecant-Function** velocity to solar cells on a rotating target plate. The cells on the stationary plate above the rotating one absorb steady perpendicular radiation from a test source.

Translating Canard

Longitudinal trim control is augmented when landing flaps are deployed.

Langley Research Center, Hampton, Virginia

A translating canard provides automatic pitch trim when the wing flaps of an airplane are deployed. Heretofore, a general disadvantage of nontranslating canard configurations has been the inability to use wing flaps to achieve high lift (and therefore slower stalling speeds) for landing approaches. To achieve a longitudinally stable canard configuration, it is necessary to locate the center of gravity between the canard and the wing. This placement causes a significant moment to be associated with the lift centers of the canard and the wing. Therefore, large nosedown pitching moments associated with lift increments due to the use of wing flaps would require equivalent noseup pitching-moment contributions from the canard to provide pitch trim. In a stable canard arrangement, the canard must have a lift coefficient higher than that of the wing to provide pitch trim. Because of this requirement, the canard cannot provide pitch trim when the wing trailing-edge flaps are deflected.

The translating-canard concept is shown in the figure. The translating canard would be mechanized by a worm-screw system with a set of tracks to guide the movement of the canard. In addition, the movement of the canard would be geared to the movement of the wing flap since canard translation would be needed only

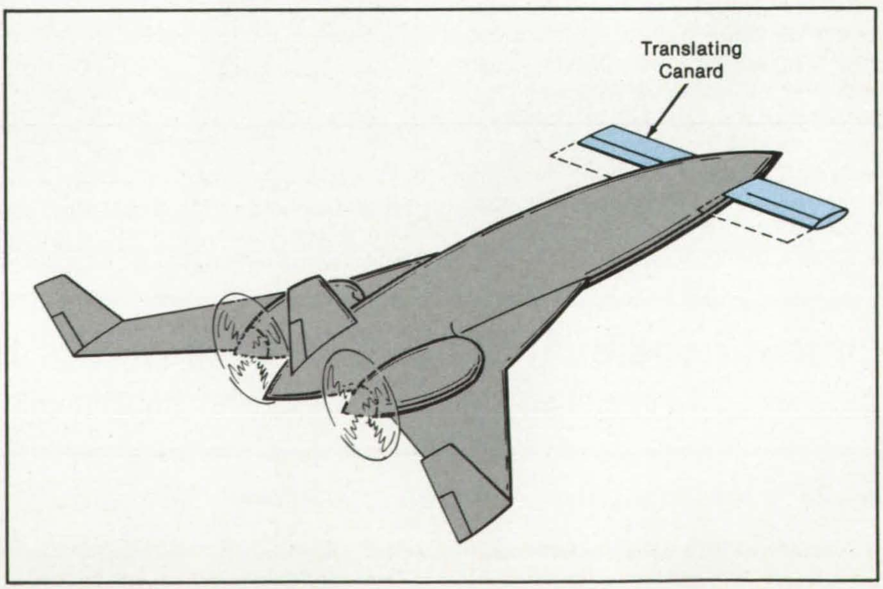

The **Translating Canard** provides automatic pitch trim for the wing-flap system while maintaining a stable pitch break.

when the wing flap is deployed.

Besides providing the automatic pitch adjustment required for trim when landing flaps on the main wing are deployed, this system maintains the stable pitch break inherent in the canard design. Test data indicate that a significant improvement in pitch-trim capability can be achieved with the translating canard concept. Additionally, the lift effectiveness of the translating canard does not change with the distance translated.

This work was done by Long P. Yip, Richard D. Robinson, and Joseph L. Johnson of **Langley Research Center.** *No further documentation is available.*

Inquiries concerning rights for the commercial use of this invention should be addressed to the Patent Counsel, Langley Research Center [see page 17]. Refer to LAR-13498.

Mechanized Polishing of Optical Rod and Fiber Ends

With a new mounting fixture, the job can be done by a standard machine instead of by hand.

Goddard Space Flight Center, Greenbelt, Maryland

A workpiece holder for a standard grinding and polishing machine makes it easier to produce an optical finish and shape on the end of a metal or glass rod or bundle of optical fibers. Previously, the glass parts had to be lapped and polished manually, a time-consuming procedure that called for considerable skill.

The holder is a pivoting, rotating eccentric head that keeps the rod or bundle end centered on the axis of the machine as it is ground and polished. The holder consists of a ball-and-socket joint, at the center of which is a ball-type bearing equipped to secure a brass mount at its center. The ball-type bearing allows the rod to spin easily. The ball-and-socket joint accommodates lap runout during spinning.

The end of the rod to be polished is placed in a closely fitting hole in the center of a blank of the same or a similar material. The rod is secured in the blank with wax. The blank and rod assembly are also waxed onto a brass mount with the rod passing through its central hole. Once the rod and eccentric head are mounted on the grinding machine, normal grinding and polishing procedures can be used.

This work was done by Jeffery S. Gum of **Goddard Space Flight Center.** *No further documentation is available.*
GSC-12917

Array of Shaped Heat Pipes

Heat would be distributed evenly over a cone.

NASA's Jet Propulsion Laboratory, Pasadena, California

A conceptual array of specially shaped heat pipes would distribute heat from a small source near the apex of a cone to an array of receptors on the conical surface. Intended originally for evenly spreading out the heat from a small nuclear reactor to an array of thermoelectric converters on a spacecraft, the shaped-heat-pipe concept may be applicable to solar-energy and other terrestrial systems requiring the spatially controlled distribution of large heat fluxes.

In the case of the small reactor, the heat pipes are coupled radiatively to the thermoelectric elements, which are mounted on the inside of an outer radiating conical surface, just outside the conical heat-pipe array. Near the apex and the reactor heat exchangers, the heat pipes are spaced close together. As the pipes spread out toward the base of the cone, the spacing increases by a factor of 2.4. It is estimated that the decreased heat-flux density at the widest separation would reduce the thermoelectric temperature drop by about 100 °C if conventional heat pipes were to be used.

In the new heat-pipe concept, the width of the radiating face would increase, and the cross-sectional area of the pipe (looking along its length) would decrease toward the base of the cone. By compensating for the increase of distance between pipe center lines, this feature would increase the average radiated power per unit area in the conical-base region.

The choice of heat-pipe shape and size is determined in part by the requirements of heat transfer. For example, a pair of simple parabolic equations incorporating these requirements gives the required and available cross-sectional areas for a tapered pipe with a rectangular cross section, the aspect ratio of which changes along the length of the pipe (see figure).

The fabrication process for a tapered pipe like that of the figure has not been developed. However, in an experiment, an ordinary ½-in. (13-cm) copper tube was easily forced into such a shape by pinching with C-clamps between rigid, flat metal bars. Inasmuch as this kind of shaping does not change the tube perimeter significantly, it may not do excessive damage to heat-pipe wicks and arteries inside. It may also be possible to install wicks and arteries after the wall has been shaped.

This work was done by Aaron Kirpich of General Electric Co. for **NASA's Jet Propulsion Laboratory.** *For further information, Circle 1 on the TSP Request Card.*
NPO-16445

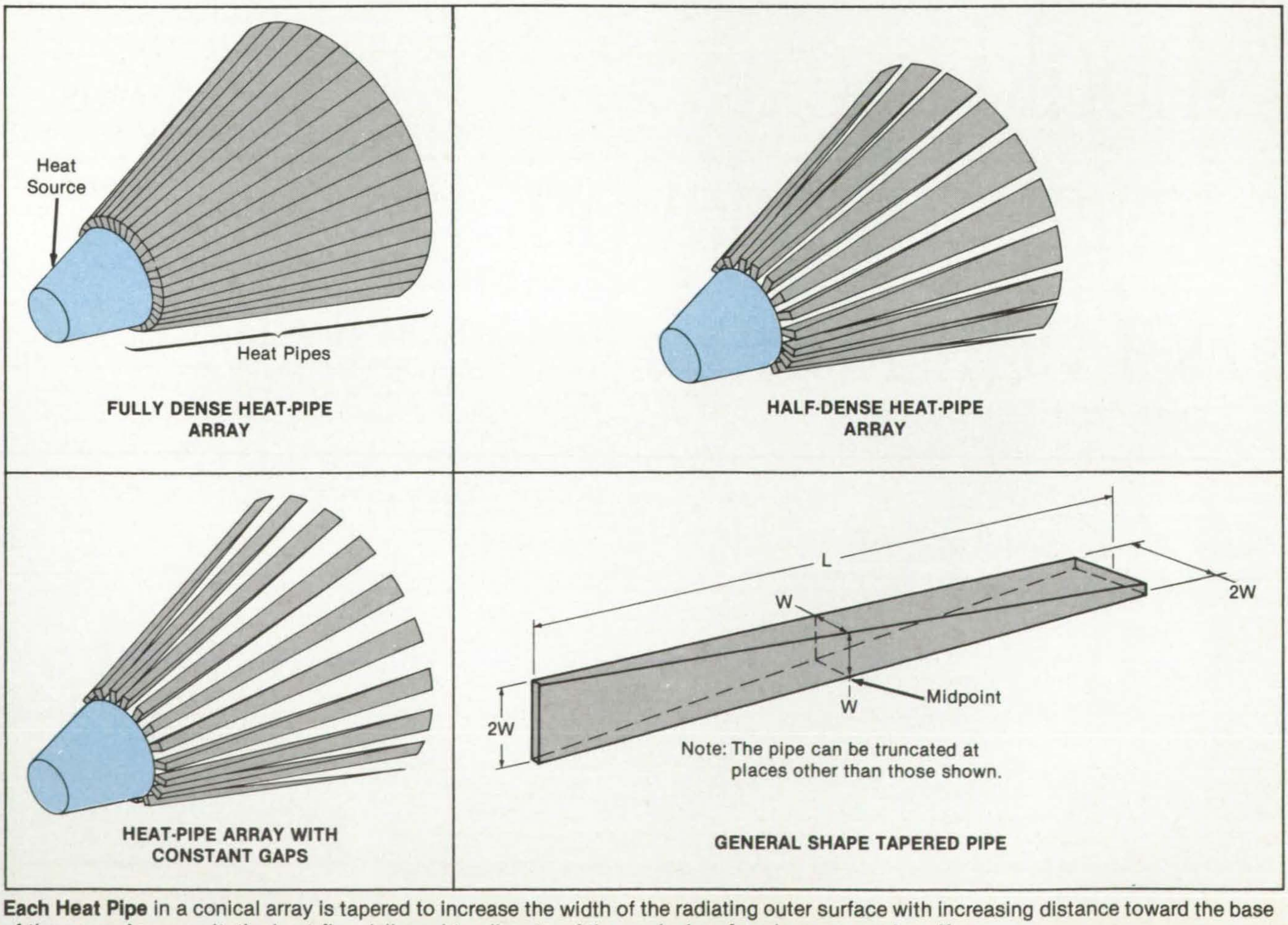

Each Heat Pipe in a conical array is tapered to increase the width of the radiating outer surface with increasing distance toward the base of the cone. As a result, the heat flux delivered to all parts of the conical surface is more nearly uniform.

Braking System for Wind Turbines

An operating turbine would be stopped smoothly by a fail-safe mechanism.

Lewis Research Center, Cleveland, Ohio

Present braking systems for wind-turbine generators are inadequate for future wind-turbine requirements. These braking systems are so small and so deficient in capability and reliability that they almost appear to be afterthoughts of the wind-turbine designs. The material selection of these braking systems (low-carbon steel) contributes to their inability to stop anything other than a slowly-rotating, low-power wind turbine and to act as a "parking" brake during shutdown.

The capability and reliability of wind-turbine braking systems can be improved by a braking system that consists of two large steel-alloy disks mounted on the high-speed shaft of the gear box, and a brake-pad assembly mounted on a bracket fastened to the top of the gear box. Lever arms (with brake pads) are actuated by spring-powered, pneumatic cylinders connected to these arms. The springs give a specific spring-loading constant and exert a predetermined load onto the brake pads through the lever arms.

The pneumatic cylinders are actuated positively to compress the springs and disengage the brake pads from the disks. During a power failure, the brakes automatically lock onto the disks, thereby producing highly reliable, fail-safe stops. Thus, the system can double as a stopping brake and a "parking" brake.

The commercial brake-pad material used in this system is a high-temperature, high-friction material. The brake pads have large face areas in order to ensure a more uniform distribution of the absorbed energy by the disks.

The braking system can stop a normally running wind-turbine generator smoothly and uniformly without any vibration or chattering that would damage the bearings and gears of the gearbox. Because the system is capable of absorbing 300 kW of constantly generating power for 90 seconds from an overspeeding wind-turbine generator, it allows the operators to yaw the wind turbine generator sufficiently out of the wind and thereby stop the overspeeding of the wind-turbine generator.

This work was done by Joseph E. Krysiak and Frank E. Webb for **Lewis Research Center**. *No further documentation is available.*

Inquiries concerning rights for the commercial use of this invention should be addressed to the Patent Counsel, Lewis Research Center *[see page 17].* *Refer to LEW-14337.*

Books and Reports

These reports, studies, and handbooks are available from NASA as Technical Support Packages (TSP's) when a Request Card number is cited; otherwise they are available from the National Technical Information Service.

Mechanism for Retrieving Satellites From Orbit

A probe locks inside a rocket motor of a satellite.

A pair of documents describes a mechanism that allows an astronaut to capture in extravehicular activity a small artificial satellite for retrieval and return to Earth. The mechanism operates by the insertion of a probe in the nozzle of a rocket motor on the satellite, followed by the expansion of the inserted probe end to grasp the motor inside the nozzle and thereby capture the satellite. The mechanism is designed for a specific satellite, but the operating principle can be adapted to almost any satellite equipped with a rocket motor or possibly be used in the retrieval of hollow-shaped objects in marine and other salvage operations.

The documents are generously illustrated and describe the tool and the method of operation in detail. Briefly, the astronaut travels to the satellite from a nearby Space Shuttle orbiter with the aid of a backpack rocket unit. Once at the satellite, the astronaut inserts the rodlike probe into the satellite rocket nozzle. When the probe has penetrated to a sufficient depth, as indicated by marks on the outside of the probe, the astronaut actuates a lever that releases a spring-loaded rod. The rod moves axially along the probe, removing a sleeve to expose three spring-loaded toggle fingers. The fingers pivot open radially to engage the wall of the nozzle.

The astronaut turns a screw on the probe handle to press the fingers against the inside of the nozzle and to press a stop on the probe firmly against the end of the nozzle, thereby locking the mechanism in the nozzle. The astronaut then returns to the Space Shuttle. Another member of the crew uses the Space Shuttle remote manipulator to grasp a fixture on the mechanism and tow the satellite into the Space Shuttle cargo bay.

The mechanism will still work even if one of its fingers should break. If the probe mechanism should jam while it is opening, the astronaut can usually unjam it by exerting more force.

This work was done by William D. Harwell and Dale A. Gardner of **Johnson Space Center**. *To obtain copies of the reports, "Apparatus and Method of Capturing on Orbiting Spacecraft" and "Technical Description of AKM Captive Device," Circle 108 on the TSP Request Card.*

This invention is owned by NASA, and a patent application has been filed. Inquiries concerning nonexclusive or exclusive license for its commercial development should be addressed to the Patent Counsel, Johnson Space Center *[see page 17].* *Refer to MSC-20979.*

Fabrication Technology

Hardware, Techniques, and Processes

72 Quick-Change Anode for Plating
72 Improved Stud Designs for Wood/Metal Joints
73 Preventing Oxidation Near Gas/Tungsten-Arc Welds
73 Surgical Borescopes Remove Contaminants
74 Spring-Loaded Inscribing Tool
74 Wet Winding Improves Coil Encapsulation
75 Making Fillets by Electrical-Discharge Machining

Quick-Change Anode for Plating

Removal and replacement would be faster.

Marshall Space Flight Center, Alabama

A proposed fastener for attaching an electroplating anode would improve the quality of plating and increase productivity. At present, when it comes time to change from anodic etching to cathodic etching in a plating process, it is necessary to remove a screw that holds the anode in place, replace the anode, and secure a new anode by replacing the screw. This procedure is not merely time consuming; in the case of copper plating, the delay between etching operations is sometimes sufficient to cause the newly plated copper to become detached.

A snap-on or twist-lock fastener is proposed as a replacement for the screw. The present anode could readily be modified to fit the new fastener (see figure). The plating operator would be able to grasp an installed anode quickly, pull it or twist it to disengage it from the fastener, insert a new anode by similar simple motions, and resume plating.

This work was done by John L. Beasley of Rockwell International Corp. for **Marshall Space Flight Center**. *No further documentation is available.*
MFS-19820

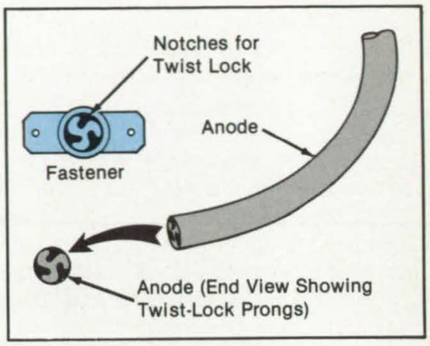

Notches in a Twist-Lock Fastener would mate with projections on the end of an anode bar. The fastener would be made of titanium for compatibility with a copper-plating solution. The fastener could also be constructed in a snap-on, snap-off configuration.

Improved Stud Designs for Wood/Metal Joints

Load-transfer capacities and resistances to fatigue are increased.

Lewis Research Center, Cleveland, Ohio

A series of high-strength bonded-stud designs have been developed for joining laminated wood to metal. Test results for the bonded-stud designs demonstrated that joint strengths approaching 10,000 to 12,000 psi (69 to 83 MPa) in ultimate strength and 5,000 psi (34 MPa) in high cycle fatigue strength of the wood/epoxy composite could be achieved.

Laminated wood that is manufactured by bonding 1/10-in. (2.5-mm) thick veneers (plies) together with epoxy resin is low in cost and maintenance, and, in the grain direction, has high specific strength (strength-to-density ratio) and high specific stiffness (modulus-to-density ratio). These qualities make it an attractive candidate material for such items as the blades for a large horizontal-axis wind turbine.

One major engineering problem for this application was connecting the laminated wood blades to a steel hub. The best solution employed a series of bonded steel studs.

The program started with a baseline stud design consisting of a threaded cylindrical body embedded in the wood by casting in place in a constant-diameter hole. The casting material was a filled and thickened epoxy. The maximum stud loads achieved from these early stud concepts were equivalent to wood strengths of about 5,000 psi (34 MPa) statically and 1,750 psi (12 MPa) in high cycle fatigue. These strengths were well below the laboratory-demonstrated strength of the wood/epoxy composite. It was believed that the stud design could be reconfigured to provide greater load-transfer capacity and achieve a 50- to 100-percent improvement in the structural capability of the bonded-stud joint.

This program resulted in improved

stud designs that provided significant increases in both static and fatigue strengths. Bonded steel studs achieved ultimate strengths on the order of 100,000 lbs (440 kN) in a 3-in. (7.6-cm) square block. It was possible to develop joint efficiencies in fatigue on the order of 100 percent of the capability of the parent wood.

Among the features of the improved stud designs were the following:

1. The shear planes in the wood at the interface between the epoxy and the wood were broken up by using a tapered hole. Step-taper, linear-taper, and nonlinear-taper designs were all developed.
2. The hollowing of the tip end of the stud provided a "softer" load transition and reduced the local shear stress.
3. The stud modulus was properly matched to the wood modulus.
4. Carbon-fiber filler in the resin improved the fatigue capability of the stud joint, compared to that of the baseline asbestos fiber filler. The carbon filler was also environmentally safer.

This work was done by James R. Faddoul of **Lewis Research Center,** *Michael Zuteck of Gougeon Brothers, Inc., and Greg Skaper of IIT Research Institute. Further information may be found in NASA TM-87109 [N86-10582/NSP], "Improved Stud Configurations for Attaching Laminated Woodwind Turbine Blades."*

Copies may be purchased [prepayment required] from the National Technical Information Service, Springfield, Virginia 22161, Telephone No. (703) 487-4650. Rush orders may be placed for an extra fee by calling (800) 336-4700.
LEW-14365

Preventing Oxidation Near Gas/Tungsten-Arc Welds

Auxiliary argon jets create a more nearly complete nonoxidizing atmosphere.

Marshall Space Flight Center, Alabama

An accessory for a gas/tungsten-arc welding machine prevents oxidation and microfissures at the edges of the weld bead. Although a gas/tungsten-arc welding machine delivers argon to the work during welding to minimize oxidation, the flow is usually directed to the top of the work. The hot material at edges of the weld may be exposed to the normal atmosphere, which causes oxidation and the development of microfissures. The reaction is severe even when only small quantities of oxygen are present.

To provide a better shield against oxidation, auxiliary cups are attached to the machine to direct additional gaseous argon to critical areas (see figure). The cups localize and trap the inert gas where it is needed.

The cups are made from stainless-steel sheet, tubing, and screen. They drastically reduce oxidation and microfissure defects and produce a clean, bright weld that can be easily inspected.

This work was done by Kenneth J. Reed of Rockwell International Corp. for **Marshall Space Flight Center.** *No further documentation is available.*
MFS-29162

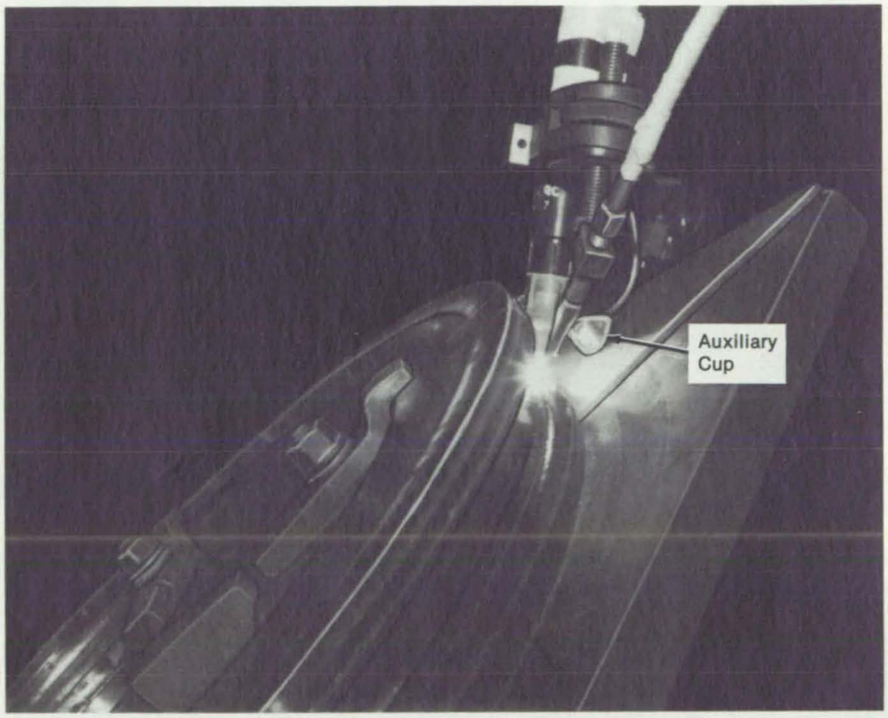

A **Pyramid-Shaped Cup** directs a stream of additional argon over a weld. The gas supplements that provided by the automatic welding machine so that oxidation is more completely suppressed.

Surgical Borescopes Remove Contaminants

Borescope instruments are put to use in extracting hard-to-reach particles.

Marshall Space Flight Center, Alabama

Surgical instruments in flexible borescopes are being used for a new purpose: removing contaminant particles from normally inaccessible places within equipment. The instruments readily enter small openings, turn corners, and reach far.

Previously, the equipment to be cleaned often had to be shaken, otherwise manipulated, or flushed with gas; sometimes makeshift tools had to be used. The surgical borescope instruments offer an easier, quicker, and more effective answer to the contamination problem.

The instruments are about 0.070 in. (1.8 mm) thick and up to 6 ft (1.8 m) long. They can be used by themselves or through the borescope channel. One type of instrument has a claw at its end, another has a retractable loop, and a third has forceps — a variety of end effectors that can grasp many different forms of contaminants.

This work was done by Karen Vallow of Rockwell International Corp. for **Marshall Space Flight Center**. *No further documentation is available. MFS-29156*

Spring-Loaded Inscribing Tool

Wavy surfaces can be marked.

Marshall Space Flight Center, Alabama

A spring-loaded, roller-type inscribing tool (see figure) marks flat or nearly flat panels. The tool was devised to apply grid lines to gore panels; the panels are then stress-tested by forming or stretching, followed by measurement of the grid-system movement to determine the distortion.

The gore panels were marked on a skin mill under numerical control. The tool can also be used to mark plastics, soft metals, and the like under numerical or manual control in a conventional machine or other convenient translation stage or used manually in situations that do not require precision. Because the inscribing roller is spring loaded, it follows the surface variations on the workpiece. Consequently, the workpiece does not have to be clampled extremely flat.

This work was done by Joseph P. Johnson of **Marshall Space Flight Center**. *No further documentation is available.*
MFS-28104

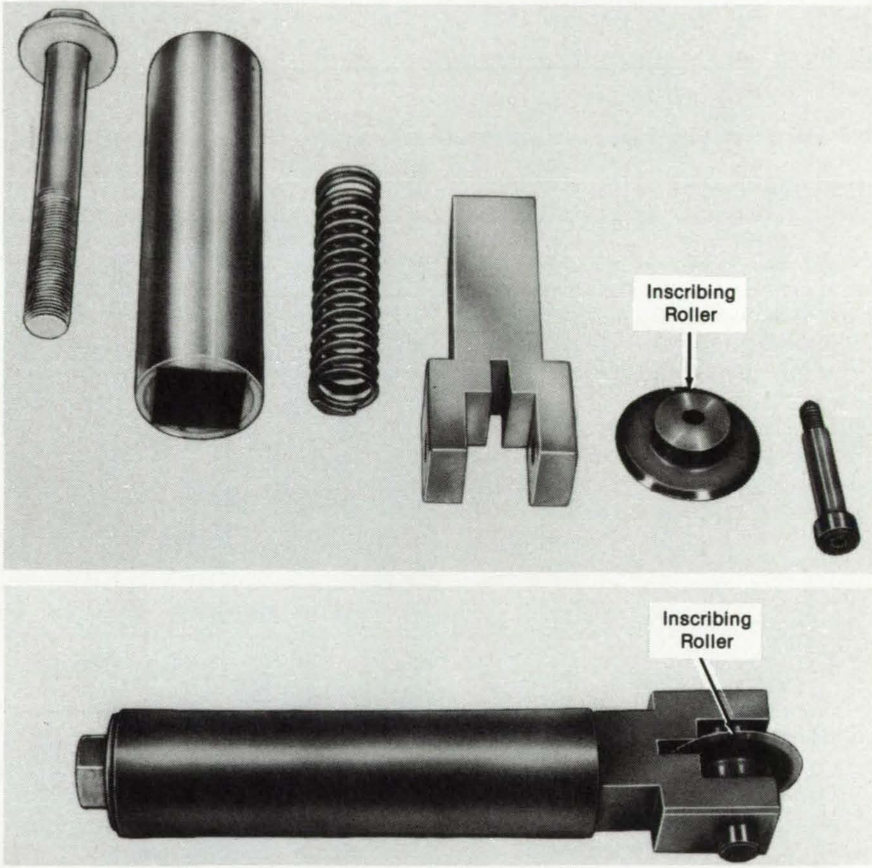

The Inscribing Tool is spring loaded against the workpiece. Otherwise, it resembles the scribing rollers on such tools as pipe cutters.

Wet Winding Improves Coil Encapsulation

Voids are eliminated without special vacuum processing.

Marshall Space Flight Center, Alabama

A wet-winding process encapsulates electrical coils more uniformly than do conventional processes. The process requires no vacuum pump and can be adapted easily to existing winding machines.

Encapsulation of electrical coils prevents electrical failures by protecting the coil wires against vibration and distortions due to temperature changes. Conventional methods of forcing potting materials into coil windings have often resulted in voids. Even impregnation in a vacuum does not completly eliminate the voids. The discontinuities resulting from these voids may degrade the coil performance or cause its failure under environmental loading. Coil wires, lead wires, wire-to-wire joints, and wire-to-pin joints can all break because of the inadequate support during vibration or because of cracking in conventional varnish coatings subjected to thermal cycling.

In wet winding (see figure) a brush or other suitable applicator is used to coat each layer of wire with the potting compound as soon as the layer is added to the coil. The coil is fully impregnated, and the joints between the coil wire and lead wires are encapsulated with the potting compound. In the original wet-winding application used on flow and speed sensors for fuel and oxygen turbopumps on the Space Shuttle, the potting compound was Hysol (or equivalent) epoxy.

This work was done by Arthur J. Hill of Rockwell International Corp. for **Marshall Space Flight Center**. *No further documentation is available.*

Inquiries concerning rights for the commercial use of this invention should be addressed to the Patent Counsel, Marshall Space Flight Center [see page 17]. *Refer to MFS-29174.*

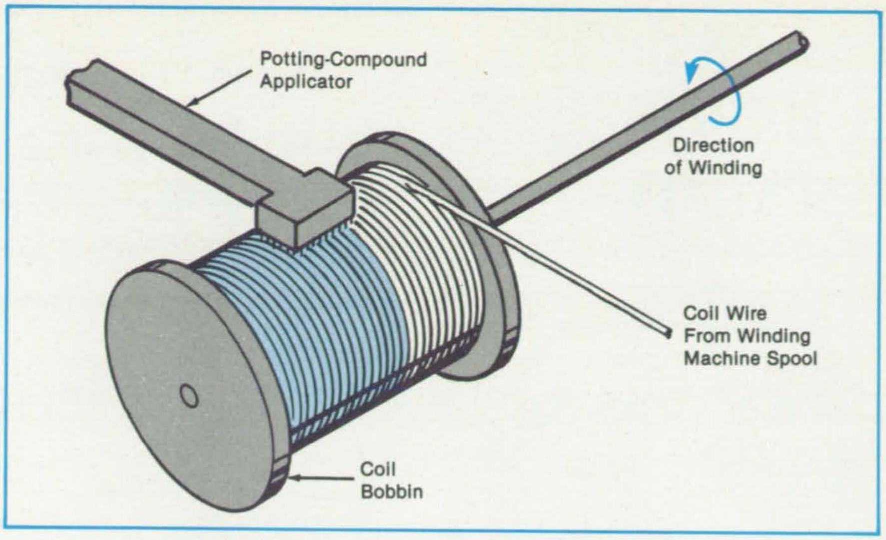

The **Encapsulant Is Applied** to each layer of wire as soon as it is added to the coil. This wet-winding process eliminates voids, giving a more uniformly encapsulated coil.

Making Fillets by Electrical-Discharge Machining

A shaped graphite electrode eliminates many hours of hand work.

Marshall Space Flight Center, Alabama

Fillets between tubes and a baseplate can be rounded to a small radius with a shaped electrode by electrical-discharge machining (EDM). The electrode was developed for finishing the base of the 600 injector posts in the Space Shuttle main engine. Previously, the hollow posts were finished manually with hand tools and a radius gauge. The procedure was time consuming, taking about 120 hours for one engine. With the new EDM electrode, all the posts are given fillets of 50-mil (1.27-mm) radius at their bases in only 10 hours.

The electrode is made by shaping it with a hardened-steel tool. The tool has a collar with the fillet that is to be impressed onto the corresponding internal lip of the electrode (see figure). The tool is brought to bear on the tip of the tubular graphite electrode and vibrated against it to produce the required fillet.

This work was done by R. K. Burley of Rockwell International Corp. for **Marshall Space Flight Center**. *No further documentation is available.*
MFS-19929

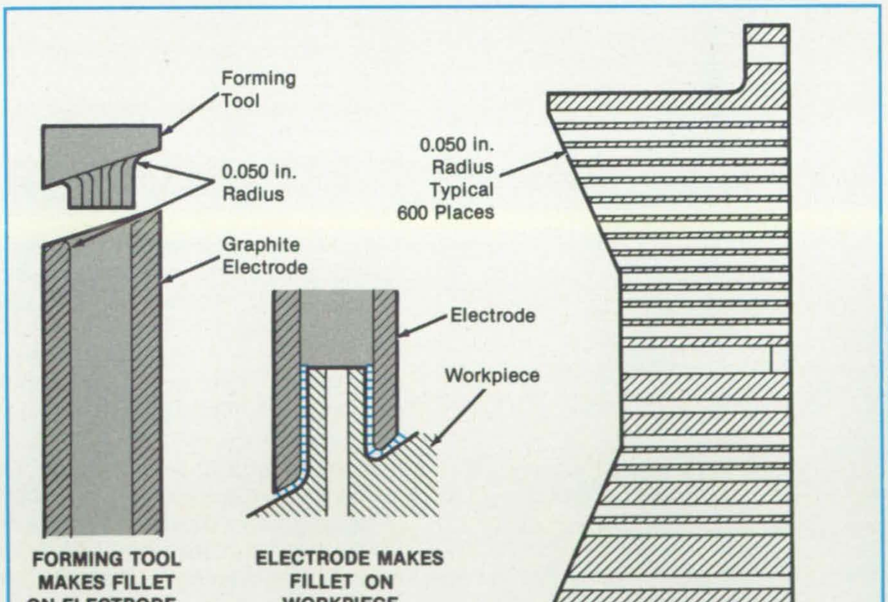

A **Hardened-Steel Forming Tool Transfers Its Fillet Shape** to the internal lip of an electrode. The lip shape is then transferred to the base of a post in the EDM procedure to form a fillet. An array of electrodes (right) can produce many fillets simultaneously.

Mathematics & Information Services

Hardware, Techniques, and Processes

76 Real-Time "Garbage Collection" for List Processing
78 Parallel Algorithm Solves Coupled Differential Equations

Real-Time "Garbage Collection" for List Processing

Two proposed techniques could reduce the memory requirements in list processors.

Lyndon B. Johnson Space Center, Houston, Texas

Two proposed algorithmic techniques for list processing enable the immediate identification of computer memory cells that have become inactive through their disconnection from active cells, together with the addition of these inactive cells to the pool of reusable cells. These two "garbage collection" techniques can reduce the memory requirements of list processors or increase their speed or both. With both techniques, processing continuity would be maintained, enabling real-time list processing.

Traditional "garbage collection" methods generally fall into two categories: The first category includes the marking strategies, sometimes called classical garbage collection. The second category includes reference-count strategies. A marking strategy involves a separate memory-scanning operation that marks all currently used cells and then reclaims the unmarked ones. The simplest versions require that list processing halt while this takes place; this is unsuitable for applications requiring real-time response.

In the reference-count approach, a counter is attached to each cell to record the number of references to that cell. When the count decreases to zero, the cell is no longer in use and can be reclaimed. Unfortunately, because reference counters must be large enough to accommodate the largest number of references that might be attempted, the memory required is increased by about 50 percent. Other disadvantages include the overhead of incrementing and decrementing the counters and the inability to reclaim cyclic structures.

The two newly proposed techniques are modified reference-count strategies that avoid the need for supplemental classical garbage collection. In the first of these techniques, arbitrarily small counters are used; when a reference is added that would make a given counter overflow, a copy is made of the memory cell, and the reference is made to the copy.

Because this process can be straightforwardly implemented in hardware, it would be very efficient. All "garbage" would be identified and added back to the free-cell list upon creation, giving performance far superior to that of any current technique. This method would incur a small penalty (negligible in most applications) because of the presence of extra copies of some memory cells. Moreover, certain list-splicing and cell-address comparison could not be reliably used in such a system.

This latter disadvantage is avoided in the second proposed technique, which would allow all "garbage" (except cyclic structures) to be collected accurately without copying or otherwise changing the form of the list so that the list-splicing operations could be used. This technique is to expand dynamically a small reference counter whenever it overflows. A normal cell would contain a small reference counter and two pointers. When the reference counter overflows, the pointers are moved into an available second cell. The room made in the first cell by moving out the pointers is used to hold the extended reference counter and the link to the second cell.

There then would be two representations of a cell: one with a small reference counter, and one with a large one. This method would require that the internal logic of the list processor be able to recognize and handle the two alternative forms of cell representation in a transparent manner. All references to the new "supercell" would be to the first cell to preserve compatibility with earlier references to the unexpanded cell.

This work was done by Robert L. Shuler, Jr., of **Johnson Space Center**. *For further information, Circle 16 on the TSP Request Card.*

This invention is owned by NASA, and a patent application has been filed. Inquiries concerning nonexclusive or exclusive license for its commercial development should be addressed to the Patent Counsel, Johnson Space Center [see page 17]. Refer to MSC-20964.

Capture the Glory!

Now you can own this collector's print, commemorating Columbia's exploits, at an exceptional introductory price.

Noted aviation artist Ken Kotik has captured *Columbia* in all its glory to commemorate the completion of four test flights and the first operational mission, STS-5. This fine print—truly a collector's item—depicts the orbiter in full color, side view, with every feature crisply detailed.

Arranged beneath the ship, also in full color, are the five distinctive mission patches. But what makes Ken Kotik's work most unique is his method of creating a 'historical panorama' via individual vignettes surrounding the side view of *Columbia*.

Educational as well as eye-appealing, these scenes, which are expertly rendered in a wash technique, include such subjects as the orbiter under construction at Rockwell, on the launch pad, at touch-down and during transit on its 747 carrier. Concise copy, hand-written by the artist, accompanies each vignette. (*Important:* The greatly reduced print reproduced here is intended only to show style—at the full 32" by 24" size, all copy is clearly readable.)

About the artist.

Ken Kotik, a 37-year old Colorado native, has been a professional commercial artist for the past 14 years. In his own words, he "eats, drinks and sleeps flying." It shows in the obvious care and attention he brings to each print or mural. When not at his drawing board creating artworks for such prestigious institutions as the Air Force Academy, Ken can be found at the controls of his Schweitzer sailplane, in which he competes nationally. A self-taught artist, he specializes in airbrush-applied acrylic techniques. *Space Shuttle Columbia: The Pathfinder* is his first work on the space program, and the original art has been accepted by the Smithsonian Air and Space Museum for its permanent collection.

About the artwork.

Space Shuttle Columbia: The Pathfinder was printed in five colors, after individual press proving, on exhibit-quality 80 lb text 'Hopper Feltweave' textured paper. The feltweave texture yields properties most desirable for framing and display.

About ordering.

Each *Columbia* print comes packed in a sturdy mailing tube and will be shipped upon receipt of your order at the introductory price of $9.95. Please allow two to three weeks for delivery. There is a one-time *first class* postage and handling charge of $2.50 for each order. (If you order three prints, for example, you still include only $2.50 for postage and handling to cover the entire order.) To ensure that you receive your prints without delay, fill out and mail the coupon today, *including check or money order only* and local tax where applicable. If coupon has been clipped, mail your order to: NASA Tech Briefs, Columbia Print Offer, 41 E. 42nd St., New York, N.Y. 10017.

Actual size: 32" wide by 24" high–In full color!

($17.95 for two; $26.95 for three; $7.95 each additional plus postage and handling.)

ONLY $9.95 EACH

MONEY BACK GUARANTEE
If not completely satisfied, return undamaged print, in wrapper, within 10 days for a full refund of print purchase price.

Mail to: NASA Tech Briefs
Columbia Print Offer
41 East 42nd St.
New York, N.Y. 10017

Note: One print $9.95; two $17.95; three $26.95; each additional $7.95, plus $2.50 postage and handling per order.

Please rush ________ Columbia prints.
I have enclosed $__________ plus $2.50 for *first class* postage and handling.
Total enclosed: $__________.

Name ______________________________

Address ______________________________

City ______________ State ______ Zip ________

New York State residents add 7% sales tax.
New York City residents add 8.75% sales tax.

☐ Please add my name to your mailing list for future print offerings. SS-1

Parallel Algorithm Solves Coupled Differential Equations

Numerical methods are adapted to concurrent processing.

NASA's Jet Propulsion Laboratory, Pasadena, California

An algorithm solves a set of coupled partial differential equations by numerical integration. Adapted to run on a hypercube computer, the algorithm separates the problem into smaller problems that are solved concurrently. The increase in computing speed with concurrent processing over that achievable with conventional sequential processing can be appreciable, especially for large problems.

The hypercube computer contains $N = 2^n$ processors connected as though each were at the corner of an n-dimensional cube, each communicating with its nearest neighbors along the cube edges. The total computational problem is therefore broken into N subproblems of equal (or nearly equal) complexity, each of which is processed at a separate node. In most problems, the solutions of the subproblems must be exchanged among the nodes, and an important consideration in the development of this and all algorithms is the minimization of communication time to achieve the maximum speedup.

The algorithm solves a set of second-order differential equations of the form that could describe a vibrating structure; namely, $\mathbf{M}\ddot{\mathbf{x}} + \mathbf{Kx} = \mathbf{F}(t)$, where $\mathbf{x}$ is an m-dimensional displacement vector for m degrees of freedom, $\mathbf{M}$ is a mass matrix, $\mathbf{K}$ is a stiffness matrix, $\mathbf{F}(t)$ represents the forcing function, and t = time. First, the equations are converted to 2m first-order differential equations by making each second derivative into an additional component of the first-derivative vector. The first-order equations are solved by direct numerical integration, using the Runge-Kutta method to obtain initial values, followed by Hamming's predictor/correlator method (which requires half as much internode broadcasting of results) to obtain subsequent values.

An intermediate host computer serves as the communication link between the hypercube processors and the outside world. Only node 0 has a direct link with the host. The broadcasting technique used in this algorithm reduces the hypercube to a two-dimensional ring (see Figure 1). When each node is ready, it passes its portion of **x** to its neighbor on the right and simultaneously receives from its neighbor on the left. This process repeats $N - 1$ times until all nodes contain the complete vector **x**.

The algorithm has been tested on finite-element models of a vibrating antenna dish with 48 and 192 degrees of freedom. As shown in Figure 2, the efficiency of the algorithm (defined as the actual speedup factor divided by the number of nodes) decreases with the number of nodes. This is expected, since the communication time increases with the number of nodes.

This work was done by Akiko Hayashi of Caltech for **NASA's Jet Propulsion Laboratory**. *For further information, Circle 113 on the TSP Request Card. NPO-16148*

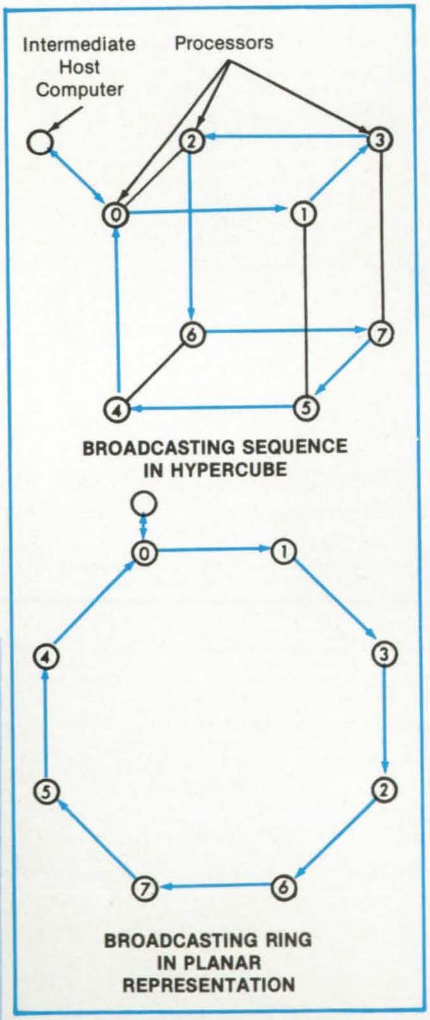

Figure 1. A **Ring Is Formed** in the hypercube (in this case, a 3-dimensional cube) by connecting the corners in a sequence.

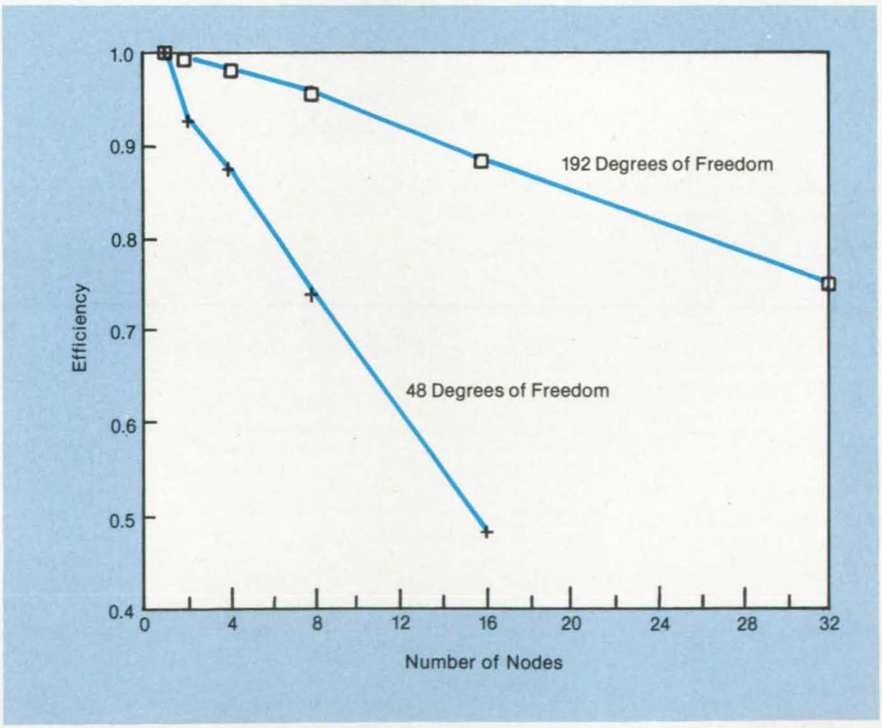

Figure 2. The **Efficiency at the Algorithm** is particularly high for complicated problems, as in the 192-degree-of-freedom vibrating-antenna problem. In general, the efficiency decreases with the number of nodes because of increased internode communication.

MARTIN MARIETTA BALTIMORE AEROSPACE

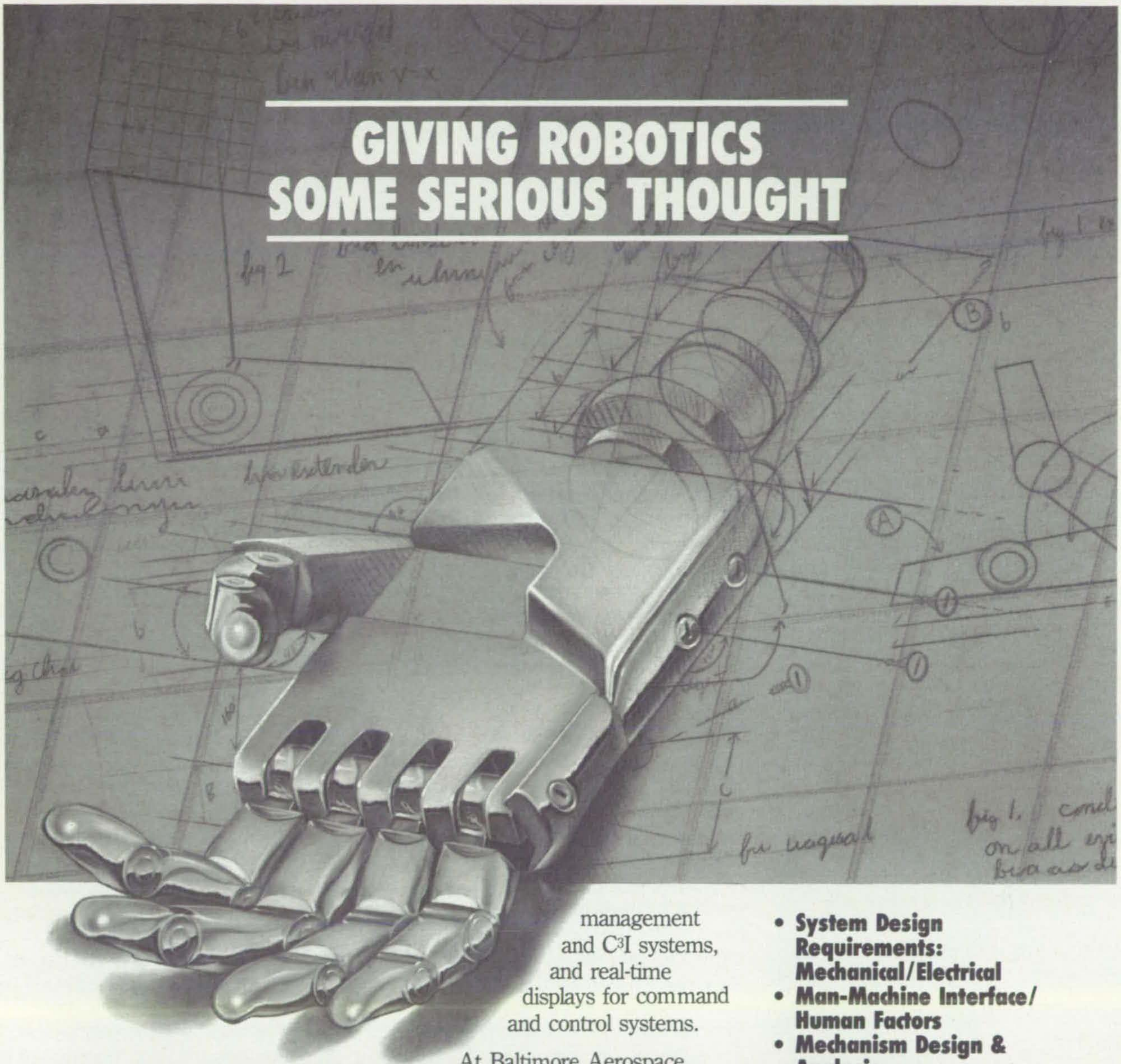

GIVING ROBOTICS SOME SERIOUS THOUGHT

Imagine a robotic device that will allow the operator to see and feel what the robot is seeing and feeling. A device controlled easily and reliably, in much the same way as a human hand. This is "telepresence." And it's a technology being advanced at Martin Marietta Baltimore Aerospace.

Telepresence is just part of the work being performed in military automation and robotics at Baltimore Aerospace. There's also on-going research in autonomous underwater vehicle systems, supervised control of remote vehicles, military robotics, expert systems for battle management and C^3I systems, and real-time displays for command and control systems.

At Baltimore Aerospace, we're giving robotics some serious thought. In fact, we're investing millions for research, equipment and facilities to further advance these technologies.

We invite you to be a part of this effort. If you have experience in robotics or artificial intelligence, give some serious thought to a career at Baltimore Aerospace. We have opportunities available in the following areas:

- **Servo Control Analysis & Simulation**
- **Sensor System Design & Applications**
- **System Design Requirements: Mechanical/Electrical**
- **Man-Machine Interface/ Human Factors**
- **Mechanism Design & Analysis**
- **Real-Time Hierarchical Control Systems**
- **Real-Time Computer Graphics for Animation**
- **AI Programming**
- **Operation Analysis**
- **C^3I**
- **Biomedical Engineering**

If interested please send your resume to: Martin Marietta Baltimore Aerospace, Employment Dept. NTB187, 103 Chesapeake Park Plaza, Baltimore, Maryland 21220. U.S. Citizenship Required. An Equal Opportunity Employer m/f/h/v.

MARTIN MARIETTA

Life Sciences

Hardware, Techniques, and Processes

80 Measurement of Human Blood and Plasma Volumes

Books and Reports

These reports, studies, and handbooks are available from NASA as Technical Support Packages (TSP's) when a Request Card number is cited; otherwise they are available from the National Technical Information Service.

Measurement of Human Blood and Plasma Volumes

The use of radioiodine can be avoided.

A report reviews techniques for measuring the blood-plasma volume in humans. According to the authors, the common technique of using a radioactive iodine isotope to label the plasma albumin may involve unwarranted risks from the low-level radiation. Consequently, they emphasize techniques using Evans-blue-dye (T-1824) labeling of albumin, hematocrit or hemoglobin/hematocrit measurements, or blood densitometry.

In the Evans-blue-dye technique, the plasma volume is determined from the decrease in dye concentration occurring after a small amount of dye solution has been injected into the circulatory system; the dye concentrations are determined from the spectrophotometric absorbance at 615 nm, and a correction factor (1.03) corrects for the slow uptake of dye by nonblood tissue. The use of a column-chromatographic purification procedure has reduced the variability of this technique — by removing interfering substances from the dyed plasma samples. The subjection of Evans blue dye to the Ames test for carcinogenicity gave negative results.

The accuracy and reliability of this dye technique depends upon the stability of the plasma albumin content over the period of measurement. This content can be lowered by as much as 8 percent by 10 min of strenuous exercise. The accuracy and reliability also depend upon the kinetics of the bond between the dye molecule and albumin molecule. The results obtained using this technique agree closely with those in which the albumin is labeled with radioiodine (I-131).

Repeated dye injections result in the saturation of the albumin-binding sites, creating such high preinfusion plasma concentrations that the injection of additional dye cannot be measured accurately. As a result, the short-term (hourly) changes in plasma volume have been calculated from sequential measurements of the hematocrit (Hct) and the hemoglobin (Hb) concentrations or from the Hct alone. (The Hct is the ratio of the packed-cell volume to the cell volume plus the plasma volume.) The percent change of the plasma volume (PV) at times a and b is given by the equation:

$$\%\ \Delta PV = 100\left(\frac{Hb_b}{Hb_a} \times \frac{1 - Hct_a}{1 - Hct_b}\right) - 100$$

If the red-cell volume and the ratio of the volumes of red and white blood cells remain constant, changes in the Hct alone can be used to calculate the changes in the PV.

Errors in the Hct and Hct/Hb techniques include errors in the measurement of these parameters and the probable error in using antecubital (i.e., inner forearm) venous blood values as representative of total blood volume levels. Moreover, the act of drawing blood samples through a catheter may cause a change in vascular hemodynamics and change the Hct and the Hb concentrations: neither technique can be used to estimate changes in PV continuously.

Such continuous estimates can be made by blood densitometry. With the mechanical-oscillator technique, densities of small blood samples ($\geqslant 50\ \mu L$) can be determined with high accuracy (to 10^{-6} g/ml) by measuring the resonant frequency of an oscillating U-shaped glass tube containing the fluid sample. Variations in plasma density, which are influenced by lipid, glucose, and urea concentrations, may diminish the accuracy of densitometry for the determination of the protein concentration and Hct, although the technique remains effective for screening. However, in a single experiment, in which confounding factors can be assumed constant, density alterations are a precise measure of shifts in plasma-protein and Hb concentrations and can be used for measurement of vascular fluid shifts.

This work was done by John E. Greenleaf and Helmut G. Hinghofer Szalkay of **Ames Research Center**. *To obtain a copy of the report, "Plasma Volume Methodology: Evans Blue, Hb-Hct, and Mass Density Transformations," Circle 87 on the TSP Request Card.*

Inquiries concerning rights for the commercial use of this invention should be addressed to the Patent Counsel, Ames Research Center [see page 17] Refer to ARC-11686.

Subject Index

A

ABLATIVE MATERIALS
Computer simulation of ablator charring
page 56 LAR-13502

ADDITION RESINS
Semi-interpenetrating polymer networks
page 44 LAR-13450

AERODYNAMIC BRAKES
Deployable brake for spacecraft
page 65 MFS-25722

AIRCRAFT NOISE
Calculating sonic-boom propagation
page 58 LAR-13473

AIRCRAFT STRUCTURES
Translating canard
page 68 LAR-13498

ALGORITHMS
Real-time "garbage collection" for list processing
page 76 MSC-20964

ALLOYS
Transparent analogs for alloy phase studies
page 48 MFS-27109

ANALOG TO DIGITAL CONVERTERS
Parallel analog-to-digital image processor
page 28 GSC-12898

ANODES
Quick-change anode for plating
page 72 MFS-19820

ANTENNA RADIATION PATTERNS
Calculating effects of reflector-antenna distortions
page 24 NPO-16641

APPROACH CONTROL
Optoelectronic docking system
page 30 MSC-21159

ARTIFICIAL SATELLITES
Mechanism for retrieving satellites from orbit
page 71 MSC-20979

ASTRONOMICAL TELESCOPES
Versatile x-ray telescope
page 32 MFS-28013
Wide-angle, flat-field telescope
page 36 GSC-12825

ATMOSPHERIC ENTRY SIMULATION
Computer simulation of ablator charring
page 56 LAR-13502

B

BEARINGS
Active-control bearings for rotor shafts
page 61 LEW-14319

BIREFRINGENCE
Determining optical axes of uniaxial crystals
page 35 LEW-14452

BLOOD VOLUME
Measurement of human blood and plasma volumes
page 80 ARC-11686

BRAKES (FOR ARRESTING MOTION)
Braking system for wind turbines
page 71 LEW-14337

C

CANARD CONFIGURATIONS
Translating canard
page 68 LAR-13498

CARDIOVASCULAR SYSTEM
Measurement of human blood and plasma volumes
page 80 ARC-11686

CATALYSTS
Negative-electrode catalysts for Fe/Cr redox cells
page 42 LEW-14028

CENTRAL PROCESSING UNITS
Real-time "garbage collection" for list processing
page 76 MSC-20964

CERAMICS
Portable, controlled-load-rate tension tester
page 60 MFS-28075

COAL UTILIZATION
Desulfurizing coal with an alkali treatment
page 43 NPO-16366

COMPUTERIZED SIMULATION
Computer simulation of ablator charring
page 56 LAR-13502

CONCURRENT PROCESSING
Parallel algorithm solves coupled differential equations
page 78 NPO-16148

CONTROL SURFACES
Translating canard
page 68 LAR-13498

CONTROLLERS
Controller for fast-acting furnaces
page 27 MSC-20624

CROSSFLOW
Computing jet-exhaust/crossflow interactions
page 58 ARC-11597

CRYOGENICS
Calibration of germanium resistance thermometers
page 38 MFS-27107

D

DATA PROCESSING
Local data processing for a robot hand
page 29 NPO-16695

DECONTAMINATION
Surgical borescopes remove contaminants
page 73 MFS-29156

DESULFURIZING
Desulfurizing coal with an alkali treatment
page 43 NPO-16366

DIFFERENTIAL EQUATIONS
Parallel algorithm solves coupled differential equations
page 78 NPO-16148

DIRECTIONAL SOLIDIFICATION (CRYSTALS)
Progress toward monolithic peritectic solidification
page 45 MFS-28079

DISPLACEMENT MEASUREMENT
Sliding capacitive displacement transducer
page 20 MFS-28017

DYNAMIC RESPONSE
On-orbit system identification
page 64 NPO-16588

E

ELECTRIC COILS
Wet winding improves coil encapsulation
page 74 MFS-29174

ELECTRIC FURNACES
Controller for fast-acting furnaces
page 27 MSC-20624

ELECTRODES
Negative-electrode catalysts for Fe/Cr redox cells
page 42 LEW-14028

ELECTRON IRRADIATION
One-dimensional simulation of isotropic radiation
page 67 NPO-16412

ELECTRONIC TRANSDUCERS
Sliding capacitive displacement transducer
page 20 MFS-28017

ELECTROPLATING
Quick-change anode for plating
page 72 MFS-19820

ENCAPSULATING
Wet winding improves coil encapsulation
page 74 MFS-29174

ENDOSCOPES
Surgical borescopes remove contaminants
page 73 MFS-29156

ENERGY CONVERSION EFFICIENCY
A surface-controlled solar cell
page 22 NPO-16430

F

FATIGUE LIFE
Reducing fatigue in a rotary flowmeter
page 64 MFS-29038

FIBER OPTICS
Mechanized polishing of optical rod and fiber ends
page 69 GSC-12917
Noncontacting measurement of shaft angle
page 63 MFS-19810

FILLETS
Making fillets by electrical-discharge machining
page 75 MFS-19929

FLOWMETERS
Reducing fatigue in a rotary flowmeter
page 64 MFS-29038

FLUID DYNAMICS
Changes in blade configuration improve turbopump
page 67 MFS-29176

FLUIDIZED BED PROCESSORS
Desulfurizing coal with an alkali treatment
page 43 NPO-16366

FREQUENCY STABILITY
Monolithic isolated single-mode ring laser
page 22 LAR-13191

G

GAS TUNGSTEN ARC WELDING
Preventing oxidation near gas/tungsten-arc welds
page 73 MFS-29162

GLASS
High-strength glass for solar applications
page 48 NPO-16536

GRAPHITE-POLYIMIDE COMPOSITES
Polyimide prepegs with improved tack
page 40 LEW-14198

H

HEAT EXCHANGERS
Heat-exchanger/heat-pipe interface
page 66 NPO-16456

HEAT PIPES
Array of shaped heat pipes
page 70 NPO-16445
Heat-exchanger/heat-pipe interface
page 66 NPO-16456

HEAT STORAGE
More efficient thermal-energy receiver
page 37 LEW-14309

HELIUM
Measuring leakage from large, complicated machinery
page 63 MFS-19945

HEMODYNAMICS
Measurement of human blood and plasma volumes
page 80 ARC-11686

HYDROGEN EMBRITTLEMENT
Noble metals would prevent hydrogen embrittlement
page 45 MFS-29114

I

IMAGE PROCESSING
Parallel analog-to-digital image processor
page 28 GSC-12898

INERT ATMOSPHERE
Preventing oxidation near gas/tungsten-arc welds
page 73 MFS-29162

INTERFACES
Heat-exchanger/heat-pipe interface
page 66 NPO-16456

IRON ALLOYS
Noble metals would prevent hydrogen embrittlement
page 45 MFS-29114

J

JET EXHAUST
Computing jet-exhaust/crossflow interactions
page 58 ARC-11597

JOINTS (JUNCTIONS)
Improved stud designs for wood/metal joints
page 72 LEW-14365

K

KEVLAR (TRADEMARK)
Flexural properties of aramid-reinforced pultrusions
page 46 LAR-13442

L

LASER RANGEFINDERS
Optoelectronic docking system
page 30 MSC-21159

LASER STABILITY
Monolithic isolated single-mode ring laser
page 22 LAR-13191

LASERS
Monolithic isolated single-mode ring laser
page 22 LAR-13191

LEAKAGE
Measuring leakage from large, complicated machinery
page 63 MFS-19945

LISTS
Real-time "garbage collection" for list processing
page 76 MSC-20964

LOADING RATE
Portable, controlled-load-rate tension tester
page 60 MFS-28075

M

MACHINING
Making fillets by electrical-discharge machining
page 75 MFS-19929

MARKING
Spring-loaded inscribing tool
page 74 MFS-28104

METALLIZING
Quick-change anode for plating
page 72 MFS-19820

MOUNTING
Mechanized polishing of optical rod and fiber ends
page 69 GSC-12917

N

NICKEL ALLOYS
Noble metals would prevent hydrogen embrittlement
page 45 MFS-29114

NOBLE METALS
Noble metals would prevent hydrogen embrittlement
page 45 MFS-29114

NUMERICAL INTEGRATION
Parallel algorithm solves coupled differential equations
page 78 NPO-16148

O

OPEN CIRCUIT VOLTAGE
A surface-controlled solar cell
page 22 NPO-16430

OPTICAL PROPERTIES
Determining optical axes of uniaxial crystals
page 35 LEW-14452

ORBIT CALCULATION
Predicting spacecraft trajectories
page 58 NPO-16731

P

PARABOLIC REFLECTORS
Calculating effects of reflector-antenna distortions
page 24 NPO-16641

PHASE TRANSFORMATIONS
Progress toward monolithic peritectic solidification
page 45 MFS-28079
Transparent analogs for alloy phase studies
page 48 MFS-27109

PHOTOMETERS
Parallel analog-to-digital image processor
page 28 GSC-12898

POLARIZED LIGHT
Determining optical axes of uniaxial crystals
page 35 LEW-14452

POLISHING
Mechanized polishing of optical rod and fiber ends
page 69 GSC-12917

POLYAMIDE RESINS
Flexural properties of aramid-reinforced pultrusions
page 46 LAR-13442
Polyimide prepegs with improved tack
page 40 LEW-14198

POLYIMIDES
Semi-interpenetrating polymer networks
page 44 LAR-13450

PREPEGS
Polyimide prepegs with improved tack
page 40 LEW-14198

PROTECTIVE COATINGS
Wet winding improves coil encapsulation
page 74 MFS-29174

PROTON IRRADIATION
One-dimensional simulation of isotropic radiation
page 67 NPO-16412

R

RADIATION EFFECTS
One-dimensional simulation of isotropic radiation
page 67 NPO-16412

REDOX CELLS
Negative-electrode catalysts for Fe/Cr redox cells
page 42 LEW-14028

REENTRY SHIEDLING
Deployable brake for spacecraft
page 65 MFS-25722

REFLECTING TELESCOPES
Wide-angle, flat-field telescope
page 36 GSC-12825

REFLECTORS
Calculating effects of reflector-antenna distortions
page 24 NPO-16641

REMOTE MANIPULATOR SYSTEM
Local data processing for a robot hand
page 29 NPO-16695

RESIN MATRIX COMPOSITES
Flexural properties of aramid-reinforced pultrusions
page 46 LAR-13442

RESISTANCE THERMOMETERS
Calibration of germanium resistance thermometers
page 38 MFS-27107

RING LASERS
Monolithic isolated single-mode ring laser
page 22 LAR-13191

ROBOTICS
Local data processing for a robot hand
page 29 NPO-16695

ROTOR BLADES (TURBOMACHINERY)
Changes in blade configuration improve turbopump
page 67 MFS-29176

S

SATELLITE ORBITS
Predicting spacecraft trajectories
page 58 NPO-16731

SATELLITES
Mechanism for retrieving satellites from orbit
page 71 MSC-20979

SCORING
Spring-loaded inscribing tool
page 74 MFS-28104

SHAFTS (MACHINE ELEMENTS)
Active-control bearings for rotor shafts
page 61 LEW-14319
Noncontacting measurement of shaft angle
page 63 MFS-19810

SHOCK WAVES
Calculating sonic-boom propagation
page 58 LAR-13473

SOLAR CELLS
A surface-controlled solar cell
page 22 NPO-16430
One-dimensional simulation of isotropic radiation
page 67 NPO-16412

SOLAR COLLECTORS
High-strength glass for solar applications
page 48 NPO-16536

SOLAR ENERGY CONVERSION
Array of shaped heat pipes
page 70 NPO-16445
More efficient thermal-energy receiver
page 37 LEW-14309

SOLIDIFICATION
Progress toward monolithic peritectic solidification
page 45 MFS-28079
Transparent analogs for alloy phase studies
page 48 MFS-27109

SONIC BOOMS
Calculating sonic-boom propagation
page 58 LAR-13473

SPACE STATIONS
On-orbit system identification
page 64 NPO-16588

SPACECRAFT DOCKING
Optoelectronic docking system
page 30 MSC-21159

SPACECRAFT RECOVERY
Mechanism for retrieving satellites from orbit
page 71 MSC-20979

SPACECRAFT REENTRY
Deployable brake for spacecraft
page 65 MFS-25722

SPACECRAFT TRAJECTORIES
Predicting spacecraft trajectories
page 58 NPO-16731

SPARK MACHINING
Making fillets by electrical-discharge machining
page 75 MFS-19929

STUDS (STRUCTURAL MEMBERS)
Improved stud designs for wood/metal joints
page 72 LEW-14365

SURFACE PROPERTIES
High-strength glass for solar applications
page 48 NPO-16536

SURGICAL INSTRUMENTS
Surgical borescopes remove contaminants
page 73 MFS-29156

SYSTEM IDENTIFICATION
On-orbit system identification
page 64 NPO-16588

T

TELESCOPES
Wide-angle, flat-field telescope
page 36 GSC-12825

TEMPERATURE CONTROL
Controller for fast-acting furnaces
page 27 MSC-20624

TENSILE TESTS
Portable, controlled-load-rate tension tester
page 60 MFS-28075

TEST CHAMBERS
Measuring leakage from large, complicated machinery
page 63 MFS-19945

THERMAL CONTROL COATINGS
Computer simulation of ablator charring
page 56 LAR-13502

THERMAL ENERGY
More efficient thermal-energy receiver
page 37 LEW-14309

THERMAL RESISTANCE
Semi-interpenetrating polymer networks
page 44 LAR-13450

THERMOELECTRIC POWER GENERATION
Array of shaped heat pipes
page 70 NPO-16445

THERMOMETERS
Calibration of germanium resistance thermometers
page 38 MFS-27107

TOOL
Spring-loaded inscribing tool
page 74 MFS-28104

TRANSDUCERS
Noncontacting measurement of shaft angle
page 63 MFS-19810
Sliding capacitive displacement transducer
page 20 MFS-28017

TURBINE PUMPS
Changes in blade configuration improve turbopump
page 67 MFS-29176

TURBOGENERATORS
Braking system for wind turbines
page 71 LEW-14337

U

ULTRAVIOLET TELESCOPES
Versatile x-ray telescope
page 32 MFS-28013

UNIONS (CONNECTORS)
Improved stud designs for wood/metal joints
page 72 LEW-14365

V

VANES
Reducing fatigue in a rotary flowmeter
page 64 MFS-29038

VERTICAL TAKEOFF AIRCRAFT
Computing jet-exhaust/crossflow interactions
page 58 ARC-11597

VIBRATION DAMPING
Active-control bearings for rotor shafts
page 61 LEW-14319

W

WELDING
Preventing oxidation near gas/tungsten-arc welds
page 73 MFS-29162

WIND TURBINES
Braking system for wind turbines
page 71 LEW-14337

X

X RAY TELESCOPES
Versatile x-ray telescope
page 32 MFS-28013

NASA TECH BRIEF INDEXES 1981, 1982, 1983

$10.00 per copy

Please send me ______ copy(ies) of the □1981, ______ copy(ies) of the □1982, and ______ cop(ies) of the □1983 Tech Brief Indexes. A check in the amount of $________ is enclosed.

Subscription ID Number (if appropriate):

T______________________________

Name ______________________

Company ______________________

Division ______________________

Mail Stop ______________________

Address ______________________

____

Make checks payable to: "RMS Associates," (NASA STI Facility, P.O. Box 8757 Baltimore, MD 21240)

Mission Accomplished

Through the technology transfer process, many of the systems, methods and products pioneered by NASA are reapplied in the private sector, obviating duplicate research and making a broad range of new products and services available to the public.

Micro Focus view of cyanide laced capsule (black) inside a Tylenol bottle. Inset:The portable Lixiscope

From an astrophysicist's goal to the Super Bowl, a portable x-ray imaging machine called the Lixiscope has displayed diverse applications, earning the most royalties of any NASA technology spinoff.

The Lixiscope is a version of an invention by Dr. Lo I Yin, an astrophysicist at the Goddard Space Flight Center. Dr. Yin was seeking a method of imaging x-rays in astronomy when he discovered the device's earthly potential.

"We were looking for a sensitive detector for imaging at extremely low x-ray intensity," explained Dr. Yin. "To test the detector, we had to use a radioactive source. I started fooling with different things, like looking at the shadow of a razor blade. This naturally led to other applications."

NASA granted a license in 1982 to Lixi, Inc., a midwestern high technology firm, to manufacture Dr. Yin's imaging device. The resulting Lixi Imaging Scope is a completely self-contained and portable battery-powered unit weighing only 6-½ pounds. It uses a small amount of radioactive isotope to produce an image instantly at up to 27X magnification. The scope is safe, too, requiring less than one percent of the radiation of conventional x-ray machines. Lead aprons or other shields are unnecessary.

Originally designed for emergency medical use, the Lixiscope has become a handy tool in a wide range of fields. Because the scope doesn't require a still patient to produce a viable image, veterinarians can examine animals without sedation. Parcel services use the scope to verify the contents of packages insured for large amounts, minimizing the risk of insurance fraud. Manufacturers improve quality and process control with the instrument. Lixiscope can penetrate high-density materials, a feature standard machine vision systems lack. It can also check PC boards for inner layer registration at about $80,000 less than most cabinet type x-ray systems.

Since the Lixiscope doesn't process x-ray images, but produces them immediately, the device is ideal for sporting events. The portable unit served at both the 1984 Olympics and the 1985 Super Bowl, determining the condition of injured athletes while still on the playing field.

Lixiscope has also proven to be a vital tool in assessing product safety. When Tylenol capsules were suspected of being laced with cyanide in 1986, the FDA, rather than subjecting each capsule to a time-consuming chemical analysis, screened entire bottles with the Lixiscope. The scope, which showed the tampered capsules as black images against a green background, detected eight capsules containing potassium cyanide.

Since 1982, sales of the portable x-ray have reached $4 million worldwide, translating into NASA royalties of more than $100,000. Though its origin is in the stars, the Lixiscope's success is due to its many down-to-earth applications. □

Feedback

The Feedback column is designed to encourage a wide exchange of ideas among *NASA Tech Briefs* readers. To contribute a request for information or to respond to such a request, use the feedback cards in this issue, or write or call: Manager/Technology Transfer Division, P.O. Box 8757, Baltimore/Washington International Airport, MD 21240; (301) 859-5300. While we can print only a small number of letters, we will endeavor to select those that are of varied and wide interest.

SPECIAL ISSUES

I have enjoyed receiving and reading NASA Tech Briefs *for years now. I like the special issue idea (to cover specialized topics) as reflected in the Special Edition—NASA Computer Previews '87.*

May I recommend a reader reply forum section where an exchange of ideas, thoughts and testimonials can further benefit the objective of NASA Tech Briefs: *technology dissemination by NASA.*

Alfred L. Weisbrich
United Technologies
Windsor Locks, CT

THOUGHT STIMULANTS

It is always of interest to read through other engineers' solutions to various problems. It often stimulates thoughts of solutions for other problems. NASA Tech Briefs *is very helpful as a "thought process accelerator."*

James E. Swirczynski
Chief Engineer
JES Audio Design
Eugene, OR

I have been a reader of NASA Tech Briefs for a few months, and have found it interesting, inspiring and helpful. The article "Digital Fly-By-Wire" in your November/December Special Edition gave me some useful ideas about synchronizing CPUs in multiprocessor redundant control systems. I plan to use this information in my future projects.

Marek Nieliwodzki
Design Engineering
Custom Video Systems, Inc.
Rockaway, NY

A good share of my design work relates to proportion, control of DC and AC motors, brakes and heating equipment. An article such as the one by Rodney Clukey (Pulse-Width Proportional-Controller Circuit, NASA Tech Briefs *Volume 10, No. 5, page 43) is most interesting and useful. I have done much work already concerning this type of problem and would be interested in more information.*

Ronald W. Bauer
Design Engineer
SCR Controls
Matthews, NC

Erratum

We errantly published an incomplete graph with the brief titled "Noiseless Data Compression Algorithm," on page 93 of the November/December 1986 issue of *NASA Tech Briefs*. Here is the correct graph. We regret the error.

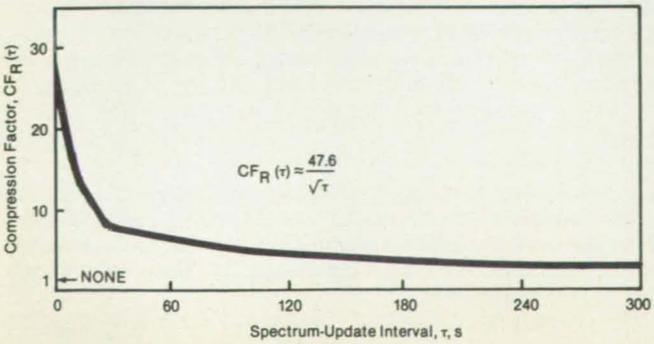

Advertiser's Index

AI '87 81
Alpha Galaxtic Design Systems .... (RAC* 483) 83
Alsys Inc. .... (RAC 341) 57
American Society For Quality Control .... (RAC 476) 59
Amoco Performance Products .... (RAC 336) 4-5
Automation Gages .... (RAC 453) 6
Ctrl-C .... (RAC 482) 69
Corning Glass Works .... (RAC 454) 15
Data-Control Systems .... (RAC 371) 25
Electronic Data Systems Corp. .... (RAC 334) 2
E G & G Photon Devices .... (RAC 431) 10
Fluoramics Inc. .... (RAC 455) 21
Greene, Tweed & Co. .... (RAC 328) 61
Hedland Products .... (RAC 480) 65
Howmet Turbine Components Corp. .... (RAC 335) 41
Klinger Scientific Corp. .... (RAC 368) 7
Marquardt Company .... (RAC 477) 77
Martin Marietta .... COV II-1
Martin Marietta/recruitment .... (RAC 40) 79
McDonnell Douglas Corp. .... (RAC 372) .... COV IV
Nicolet Test Instruments Div. .... (RAC 438) 47
NTS Testing .... (RAC 358) 35
Post Offers 85
Scientific Computer Systems Corp. .... (RAC 478) .... COV III
STAC .... (RAC 345) 31
TA Manufacturing Company .... (RAC 452) 48
Televac, Division of the Fredericks Co. .... (RAC 481) 29
Tektronix Inc., AI Marketing .... (RAC 462) 33
Tektronix Inc., Integrated Circuits Operation .... RAC 469) 13
Teledyne Taber .... (RAC 479) 26
Tex-Tech Industries Inc. .... (RAC 392) 55
3M Comtal .... (RAC 319) 11
Tycor Electric Products Ltd. .... (RAC 308-309) 84-85
Valcor Engineering Corp. .... (RAC 326) 39
Visionics Corporation .... (RAC 473) 19
Wyle Laboratories Scientific Services & Systems Group .... (RAC 396) 23
Yellow Springs Instrument Co. .... (RAC 448) 24

***RAC** stands for **Reader Action Card.** For further information on these advertisers, please circle the RAC number on the Reader Action Card elsewhere in this issue. This index has been compiled as a service to our readers and advertisers. Every precaution is taken to ensure its accuracy, but the publisher assumes no liability for errors or omissions.

ABOUT THE NASA TECHNOLOGY UTILIZATION PROGRAM

Thumb Index

NASA TU Services

New Product Ideas

Electronic Components and Circuits

Electronic Systems

Physical Sciences

Materials

Computer Programs

Mechanics

Machinery

Fabrication Technology

Mathematics and Information Sciences

Life Sciences

Subject Index

This document was prepared under the sponsorship of the National Aeronautics and Space Administration. NASA Tech Briefs is published ten times a year and is free to engineers in U.S. industry and to other domestic technology transfer agents. It is both a current-awareness medium and a problem-solving tool. Potential products...industrial processes...basic and applied research... shop and lab techniques...computer software...new sources of technical data...concepts...can be found here. The short section on New Product Ideas highlights a few of the potential new products contained in this issue. The remainder of the volume is organized by technical category to help you quickly review new developments in your areas of interest. Finally, a subject index makes each issue a convenient reference file.

Further information on innovations—Although some new technology announcements are complete in themselves, most are backed up by Technical Support Packages (TSP's). TSP's are available without charge and may be ordered by simply completing a TSP Request Card, found at the back of this volume. Further information on some innovations is available for a nominal fee from other sources, as indicated. In addition, Technology Utilization Officers at NASA Field Centers will often be able to lend necessary guidance and assistance.

Patent Licenses—Patents have been issued to NASA on some of the inventions described, and patent applications have been submitted on others. Each announcement indicates patent status and availability of patent licenses if applicable.

Other Technology Utilization Services—To assist engineers, industrial researchers, business executives, Government officials, and other potential users in applying space technology to their problems, NASA sponsors Industrial Applications Centers. Their services are described on pages 14-15. In addition, an extensive library of computer programs is available through COSMIC, the Technology Utilization Program's outlet for NASA-developed software. See special section on computer programs on page 56.

Applications Program—NASA conducts applications engineering projects to help solve public-sector problems in such areas as safety, health, transportation, and environmental protection. Two applications teams, staffed by professionals from a variety of disciplines, assist in this effort by working with Federal agencies and health organizations to identify critical problems amenable to solution by the application of existing NASA technology.

Reader Feedback—We hope you find the information in *NASA Tech Briefs* useful. A reader-feedback card has been included because we want your comments and suggestions on how we can further help you apply NASA innovations and technology to your needs. Please use it; or if you need more space, write to the Manager, Technology Transfer Division, P.O. Box 8757, Baltimore/Washington International Airport, Maryland 21240.

Advertising Reader Service—Reader Action Card (RAC): For further information on the advertisers, please circle the RAC number on the separate Reader Action Card in this issue.

Change of Address—If you wish to have *NASA Tech Briefs* forwarded to your new address, use the Subscription Card enclosed at the back of this volume of *NASA Tech Briefs*. Be sure to check the appropriate box indicating change of address, and also fill in your identification number (T number) in the space indicated.

CRAY COMPATIBILITY.

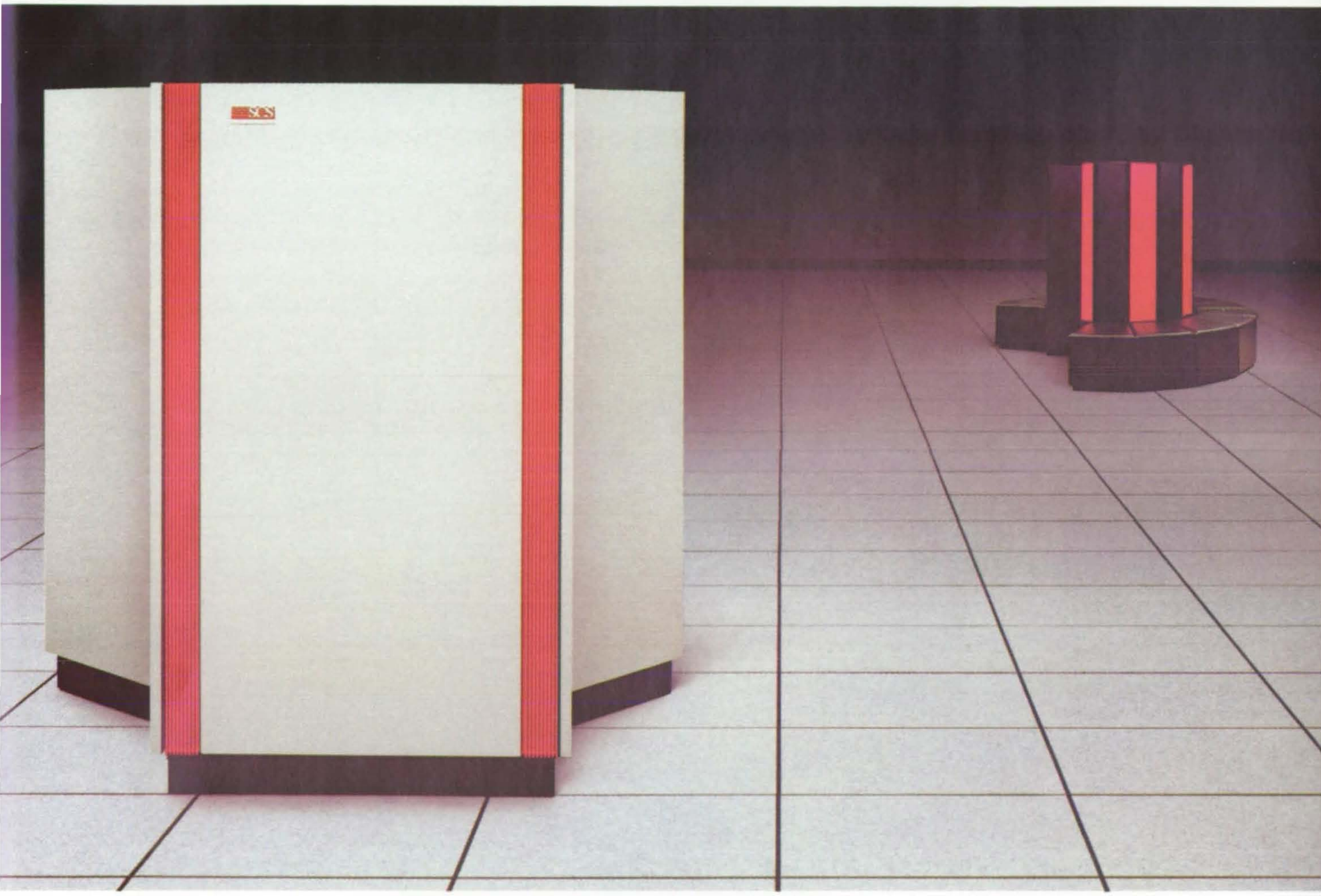

PERIOD.

Whenever scientists or engineers talk supercomputing, the word "CRAY" surfaces almost immediately.

And with good reason. CRAY supercomputers represent a performance standard that has led the industry for over a decade. However, the power of supercomputing comes with a price tag not everyone can afford.

So a lot of people have been offering more affordable products, like "near supercomputers" with "CRAY-like performance."

But no one offered true CRAY-compatibility. Until now. The SCS-40 from Scientific Computer Systems is a 64-bit general-purpose computer that runs the same software as the CRAY X-MP® supercomputers.

How? Through an architecture designed specifically to execute the CRAY instruction set. Which means you can immediately run a vast array of application packages developed and optimized over ten years for use on CRAY computers.

And if you're ultimately in the market for a CRAY supercomputer, the SCS-40 is the perfect stepping stone. Every bit of experience gained on the SCS-40 is directly applicable to the CRAY environment.

The SCS-40 runs at over 25% the speed of an X-MP/14 computer. 50-300% faster than competing "near-supercomputers," as demonstrated by numerous real benchmarks. That's fast enough to take on such compute-intensive applications as finite element analysis and fluid flow dynamics.

Cost? Less than 10% that of the CRAY X-MP/14 system. So you can start supercomputing right now.

Plus, you can enjoy the price/performance of the SCS-40 without leaving the comfort of your VAX™-based VMS™ environment.

And the SCS-40's CRAY compatibility and performance have been proven through over 1000 hours of CPU time by scientists at the San Diego Supercomputer Center.

So if you want true CRAY supercomputer compatibility, you want the SCS-40. Period. Contact us for more information.

SCS

Scientific Computer Systems Corporation

10180 Barnes Canyon Road
San Diego, California 92121
(619) 546-1212

The Super Compatible.

CRAY X/MP is a registered trademark of Cray Research, Inc. VAX and VMS are trademarks of Digital Equipment Corp.

Circle Reader Action No. 478


MCDONNELL DOUGLAS
c 1987 McDonnell Douglas Corporation